



3 1293 01571 1595

This is to certify that the

dissertation entitled

**Mechanisms of Ion Formation and Fragmentation by
Fast Atom Bombardment and Matrix Assisted Laser
Desorption Ionization Mass Spectrometry**
presented by

Gabriella Szekely

has been accepted towards fulfillment
of the requirements for

Ph.D. degree in Chemistry


Major professor

Date April 28, 1997

LIBRARY
Michigan State
University

PLACE IN RETURN BOX to remove this checkout from your record.
TO AVOID FINES return on or before date due.

DATE DUE	DATE DUE	DATE DUE
FEB 20 2000		
AUG 24 2002		

**MECHANISMS OF ION FORMATION AND FRAGMENTATION
BY FAST-ATOM BOMBARDMENT AND MATRIX-ASSISTED LASER
DESORPTION IONIZATION MASS SPECTROMETRY**

By

Gabriella Székely

A DISSERTATION

**Submitted to
Michigan State University
in partial fulfillment of the requirements
for the degree of**

DOCTOR OF PHILOSOPHY

Department of Chemistry

1997

ABSTRACT

MECHANISMS OF ION FORMATION AND FRAGMENTATION BY FAST-ATOM BOMBARDMENT AND MATRIX-ASSISTED LASER DESORPTION IONIZATION MASS SPECTROMETRY

By

Gabriella Székely

The evaporation in vacuo of the matrices and the particle-induced desorption of matrix molecules in fast-atom bombardment (FAB) contribute to a proposed high pressure region above the matrix known as the selvedge region. If the neutral number density is sufficiently high, ions formed upon bombardment may undergo collisions with molecules, yielding matrix-related cluster ions and, in cases when the analyte is desorbed in neutral form, protonated and deprotonated analyte molecules. Similarities with the chemical ionization (CI) experiment have been pointed out previously and are further developed here. If FAB is similar to CI, then the response depends on the structures of the reagent ions that react with gas phase analyte molecules. The time dependence of the positive and negative ion FAB spectra were considered to attempt to identify the reagent ions of FAB. A model is suggested for the FAB ion source which evaluates similarities to a CI source, as well as spatial aspects that are unique to desorption/ionization techniques.

The formation and fragmentation mechanisms of negative (even electron) ions formed by fast-atom bombardment were elucidated in the case

of cardiac glycosides as model compounds. Our studies strongly support a gas-phase ionization mechanism for these compounds. Deuterium exchange experiments and linked scan studies suggest that there is a distribution of deprotonated quasi-molecular ions, $[A-H]^-$, meaning that the analyte molecule can be deprotonated at various sites. The fragmentation pattern was found to be in good agreement with the negative OH/CI spectra reported in the literature. The observed fragmentation pattern is characteristic of the structure of the molecule and provides complete sequence information for the glycosidic linkages. A comparison of the spectra of isomeric compounds such as digoxin and gitoxin also reveals that the negative ion FAB spectrum contains unique characteristics, thus the two isomers can be distinguished based on their FAB spectra. The formation of the various fragment ions is explained by charge-induced as well as remote-site processes.

The mechanism of activation in matrix-assisted laser desorption ionization (MALDI) post-source decay (PSD) has been investigated using glycoalkaloids as model compounds. The high- and low-energy collisional activation spectra for these compounds have been previously reported, and they are considerably different. The MALDI-PSD spectra for these compounds are remarkably similar to the low energy collisional activation spectra, suggesting low-energy activation in the laser desorbed plume. Calculations on the energetics and the probabilities of collisional events in the MALDI source have been performed and the results are consistent with low-energy collisional activation for MALDI-PSD.

This dissertation is dedicated to my Parents and in memory of my late Grandfather. Without their love, guidance, encouragement and support I would not have been able to achieve this degree. My Grandfather passed away when I was finishing my third year of my undergraduate studies. He always wanted to study but could not in his time. He was a simple farmer but he could solve a quadratic equation in his head with his four year elementary schooling. I will never forget the fun we, grandkids had when he challenged us with his mathematical puzzles. Before he left this world, he waited for me to come home from the university to tell me how proud he was of me. Sometimes, when I felt weak to go on, I would remember his words, that I should appreciate the opportunities I have, educate myself and be strong then I will have all I need to face the difficulties my life may bring. This was a lesson accompanying me ever since.

Köszönöm Nagyapa.

ACKNOWLEDGMENT

I am very grateful to my advisor and mentor, Professor John Allison, for sharing his scientific knowledge and experience with me. I never really told you how much I appreciated your continuous support, even during the times when I felt despair, I would like to do so, now.

This dissertation would had been impossible to complete without the support of the MSU Mass Spectrometry Facility. I would like to express my gratitude for not only teaching me how to operate mass spectrometers, but also for providing a special working atmosphere. I thank all of you, in particular, Professors Douglas Gage and Z. Huang, Beverly Chamberlin, Mel Micke and Melinda Berning.

I want to thank my friends Peter and Nelli Tanev, Vladim and Yanina Smelyanskiy and John Asara for standing by my side, listening to me, trying to cheer me up, in other words, for being my friends.

I am also grateful to György Filep. It meant a lot to me that you could support me throughout this time.

Last, but not least, I want to show my appreciation to a very special person I met in the last year of my studies at MSU. Jens Klepser, thank you for making me dream and helping me believe in those dreams.

TABLE OF CONTENTS

LIST OF TABLES	ix
LIST OF FIGURES	x
LIST OF SCHEMES	xiii
LIST OF ABBREVIATIONS	xiv
CHAPTER ONE. INTRODUCTION	1
Overview of the Ionization Methods and Analytical Capabilities of Mass Spectrometry	1
The Objectives and Organization of the Dissertation	5
References	7
CHAPTER TWO. THEORY AND METHODS	9
Introduction to Fast Atom Bombardment Mass Spectrometry	9
Instrumentation	10
Tandem Mass Spectrometry (MS/MS) and Collision-Activated Dissociation (CAD)	16
High Resolution Mass Spectrometry - Peak Matching	20
Theories of Ion Formation in FAB	21
References	32

CHAPTER THREE. ELUCIDATION OF THE FRAGMENTATION MECHANISMS OF ORGANIC NEGATIVE IONS FORMED BY FAST ATOM BOMBARDMENT MASS SPECTROMETRY	34
Mass Spectrometric Analysis of Digoxin and Related Cardiac Glycosides	34
Experimental	36
Results and Discussion	37
Conclusions	87
References	89
CHAPTER FOUR. MATRIX-ASSISTED LASER DESORPTION IONIZATION MASS SPECTROMETRY	93
Introduction to Matrix Assisted Laser desorption Ionization Time-of-flight Mass Spectrometry (MALDI-TOF MS)	93
Practical Methods for MALDI Sample Preparation	95
Time-of-flight Mass Spectrometry	97
References	105
CHAPTER FIVE. MALDI/POST-SOURCE DECAY	
Do MALDI/PSD Spectra Suggests High- or Low-Energy Collisional Activation? The MALDI Spectra of Glycoalkaloids and their Use as Probes of the PSD Process	108
Fundamental Aspects of Collision-Activated Dissociation of Ions	111

The Use of Glycoalkaloids as Test Compounds for the Mechanisms of Activation in MALDI-PSD	116
Experimental	117
Results and Discussion	119
Conclusions	144
References	146
 APPENDIX ONE. If the Ionization Mechanism in Fast-Atom Bombardment Involves Ion/Molecule Reactions, What are the Reagent Ions?: The Time Dependence of Fast-Atom Bombardment Mass Spectra and Parallels to Chemical Ionization	 149

LIST OF TABLES

Table 1.1	Mass Spectrometry Sources for Molecular Studies.	4
Table 3.1	Relative intensity data from the CAD mass spectra of the digoxin fragment ions.	41
Table 3.2	Digoxin fragment ions, deuterium exchange results.	45
Table 3.3	Digoxin: Hydrogen-deuterium exchange experiments.	54
Table 4.1	Structures of the most commonly used MALDI matrices.	94
Table 5.1	The kinetic energy of an ion of m/z 1000 as a function of time and distance from the sample plate.	140

LIST OF FIGURES

Figure 2.1	Schematic diagram of a JEOL charge exchange fast atom bombardment gun.	12
Figure 2.2	Schematic diagram of a JEOL HX-110 double focusing mass spectrometer.	13
Figure 2.3	Fast atom bombardment mass spectra of lactosylceramide. The top two charts show the positive ion spectrum; the the bottom two charts the negative ion spectrum. Ions labeled nG +/- H are due to the glycerol matrix. Adapted from reference [6].	22
Figure 2.4	Spatial aspects and possible chemistry of the fast atom bombardment experiment.	26
Figure 3.1	Structures of the cardiac glycosides. The m/z values of the fragment ions are for the anions of digoxin.	39
Figure 3.2a	The negative ion FAB spectrum of digoxin in glycerol matrix.	40
Figure 3.2b	The linked-scan CAD spectrum of digoxin parent ion [M-H] ⁻ at m/z 779.	40
Figure 3.3	The extended structure of digoxin based on crystallographic data, showing the possible deprotonation sites.	47
Figure 3.4	Estimates of the gas phase acidities of the acidic sites in the digoxin structure, and the estimates of the acidities of the possible deprotonating agents from the glycerol [20].	48

Figure 3.5	Time dependence of the relative abundances of the ions from pure glycerol (A), and the ions from the glycerol matrix (B) containing digoxin (C).	50
Figure 3.6	The negative ion FAB spectrum of the deuterium exchanged digoxin-d ₆ .	55
Figure 3.7	The negative ion FAB spectrum of gitoxin.	64
Figure 3.8	The negative ion FAB spectrum of digoxigenin.	64
Figure 3.9	The negative ion FAB spectrum of digoxin-d ₉ .	67
Figure 3.10	The negative ion FAB spectrum of digoxin-d ₃ .	69
Figure 3.11	Possible structures from the digoxin fragment ions at m/z values 779, 777 and 759.	73
Figure 3.12	The negative ion FAB spectrum of digitoxin.	76
Figure 4.1	Curves of flight time <i>vs.</i> initial position used in discussion of time lag focusing. Adapted from reference [9].	99
Figure 4.2	Schematic diagram of the Voyager Elite Single-Stage Reflectron Time-of-Flight Mass Spectrometer.	101
Figure 5.1	Photochemical ionization processes for analyte ions in MALDI. M = Matrix; F = Fragment; A = Analyte	104
Figure 5.2a	(a) Low-energy and (b) high-energy CAD spectra of tomatidine adapted from reference [9].	121
Figure 5.2b	The FAB-CAD (top) and MALDI-PSD (bottom) spectra of tomatidine.	122

Figure 5.3	Low- and high-energy CAD fragmentations of the various aglycones (tomatidine, solasodine and solanidine) studied. Adapted from reference [9].	123
Figure 5.4a	(a) Low-energy and (b) high-energy CAD spectra of solasodine adapted from reference [9].	127
Figure 5.4b	The FAB-CAD (top) and MALDI-PSD (bottom) spectra of solasodine.	128
Figure 5.5a	(a) 10 eV and (b) 50 eV low- and (c) high-energy CAD spectra of solanidine adapted from reference [9].	129
Figure 5.5b	The FAB-CAD (top) and MALDI-PSD (bottom) spectra of solanidine.	130
Figure 5.6a	(a) Low-energy and (b) high-energy CAD spectra of tomatine adapted from reference [9].	132
Figure 5.6b	The FAB-CAD (top) and MALDI-PSD (bottom) spectra of tomatine.	133
Figure 5.7	Low- and high-energy fragmentations of tomatine and α -solanine adapted from reference [9].	134
Figure 5.8a	(a) Low-energy and (b) high-energy CAD spectra of α -solanine adapted from reference [9].	135
Figure 5.8b	The FAB-CAD (top) and MALDI-PSD (bottom) spectra of α -solanine.	136
Figure 5.9.	Schematic of the MALDI ion source. Assume that an ion formed at the sample plate has to travel through the dense cloud of neutrals ejected with a velocity of 350 m/s while it is accelerated out of the source.	138
Figure 5.10	Schematic showing the desorbed packet of neutrals and ions as it travels through the ion source towards the field free region.	141

LIST OF SCHEMES

Scheme 1	Eliminations from ring systems.	61
Scheme 2	Eliminations from the deprotonated digoxin.	63
Scheme 3	Thermochemistry of eliminations from cyclohexanol and cyclohexenol.	66
Scheme 4	Elimination of water and hydrogen from the deprotonated terminal digitoxose.	72
Scheme 5	Cleavage of the terminal glycosidic bond through an anion-dipole complex.	78
Scheme 6	Possible reactions for the glycosidic cleavage of deprotonated oligosaccharides.	82
Scheme 7	Charge induced cleavage of the glycosidic bond through hemiacetals.	83
Scheme 8	Remote site and inductive cleavage of the terminal glycosidic bond in digoxin.	86

LIST OF ABBREVIATIONS

A	Analyte molecule
B	Magnetic sector, magnetic field strength
CAD	Collision-activated dissociation
CID	Collision-induced dissociation
CI	Chemical ionization
DE	Delayed extraction
D/I	Desorption/ionization
DIP	Direct insertion probe
E	Electric sector, electric field strength
e⁻	electron
EE	even electron species
ESI	Electrospray ionization
eV	Electron volt
F⁺	Fragment ion
FAB	Fast-atom bombardment
FD	Field desorption
FI	Field ionization
G	Glycerol
GB	Gas phase basicity
G_F⁺	Glycerol fragment ions
K⁺IDS	Potassium ion ionization of desorbed species
KE	Kinetic energy
LC	Liquid chromatography
LD	Laser desorption
LSIMS	Liquid secondary ion mass spectrometry
M	Matrix molecule
[M+H]⁺	Protonated molecule
[M-H]⁻	Deprotonated molecule
MALDI	Matrix assisted laser desorption ionization
m/z	mass-to-charge ratio value
MS	Mass spectrometry
MS/MS	Tandem mass spectrometry
M.W.	Molecular weight
PA	Proton affinity
PD	Plasma desorption
PSD	Post-source decay
RA	Relative abundance
RI	Relative intensity

SIMS	Secondary ion mass spectrometry
TIC	Total ion current
TOF	Time-of-flight
r-TOF	Reflectron-time-of-flight

CHAPTER ONE. INTRODUCTION

Overview of the Ionization Methods and Analytical Capabilities of Mass Spectrometry

"We are coming to expect more and more of [mass spectrometry] and our demands seem to be satisfied... The big invasion into everyday chemistry came when fairly complex mixtures could be analyzed... Analysis of solid samples, or of high molecular weight compounds is now moving into the forefront." "The progress towards the satisfaction of more and more exacting technical demands is perhaps one of the major themes of the present conference and it is clear ... that [mass spectrometry] is still rapidly on the move." "But ... the accurate and detailed analyses which mass spectrometry provides are showing us that the things going in our own fields are often very much more complicated than we thought they were." (Cyril Hinshelwood, First International Mass Spectrometry Conference, London 1958.)

The above statements, which sound contemporaneous, are in fact to be found in the opening remarks of Cyril Hinshelwood at the first International Mass Spectrometry Conference, held in London in 1958. How true these same comments are today.

The first mass spectrometers were developed by J. J. Thompson around the turn of the century, but the technique was not applied extensively to the field of chemistry due to the lack of suitable vacuum systems which became available several decades later. At that time, mass spectrometry was principally used for the determination of exact masses and relative abundances of the elements and their isotopes [1, 2]. In the 1940s and 1950s, characterization of the mixtures encountered during petroleum refining launched the applications of mass spectrometry to organic compound identification. At the time of the first international conference, in 1958, mass

spectrometers had provided access to several rich veins of fundamental chemistry: prominent among them was the question of how dissociation of polyatomic ions occurs [3-6]. The relationship between the structure of a compound and its mass spectrum is still a lively subject today. The development of new mass analyzers and ionization techniques has resulted in the application of mass spectrometry to such diverse fields as biochemistry, medicine, and surface science. Thus, in 1997, the scientifically and economically most important driving force for mass spectrometry is provided by biotechnology. Today, mass spectrometry is recognized as a powerful tool for the analysis of organic and inorganic compounds. It is one of the most widely used methods of chemical analysis that is still expanding in scope as the limits of mass range, sensitivity and resolving power continued to be challenged by researchers. An overview of mass spectrometry sources for molecular studies is presented in Table 1.1.

Ionization of the sample has often hindered the utility of mass spectrometry in the past. In the early days, electron ionization (EI) was the only ionization method available. Chemical ionization (CI) [7] and field ionization (FI) [8] were the other two reliable ionization techniques prior to 1970s. All of these methods require thermal evaporation of the analyte, thereby limiting mass spectrometry to the analysis of low molecular weight and thermally stable compounds.

The extension of mass spectrometry for the identification and structural determination of large, biologically active compounds became possible with the development of desorption/ionization (D/I) techniques which are capable of producing ions directly from the condensed phase.

Field Desorption (FD) [9] was the first D/I technique amenable for the analysis of polar, high molecular weight (M.W.), thermally labile analytes.

From the end of a direct insertion probe (DIP), intact ionized analyte molecules and a few fragment ions are generated from thermally heating a microneedle-containing pyrolytic carbon emitter, on which a solid or liquid analyte resides, in the presence of a very high electric field.

In the late 1970s, particle bombardment techniques, such as plasma desorption (PD) [10] laser desorption (LD) [11], and secondary ion mass spectrometry (SIMS) [12] were developed as alternatives to FD.

In 1981, the advent of the D/I technique, fast-atom-bombardment (FAB) [13] changed mass spectrometry forever, because, for the first time fragile, high M.W., highly functionalized compounds could be analyzed routinely. In FAB a low intensity beam of keV Xe or Ar atoms impinges on the end of a DIP target, which is a nmolar solution of the analyte in a liquid matrix, most often glycerol, deposited on a stainless steel probe. These particle bombardment techniques are most appropriate for the analysis of molecules up to 10,000 Da.

Most recently, electrospray ionization (ESI) [14] and matrix assisted laser desorption ionization (MALDI) [15] have emerged as important ionization methods that are particularly well-suited for the characterization of high-mass compounds. Analysis of synthetic polymers with average molecular masses as high as ~ 400,000 Da became possible with MALDI [16]. Here, the solid analyte/matrix is routinely prepared by dissolving picomole amounts of analytes in a solution saturated in low M.W. UV-absorbing organic matrix molecules, and a portion of this solution is deposited and dried on a DIP target.

Table 1.1 Mass Spectrometry Sources for Molecular Studies. The dates correspond to the first sustained use.

Electron ionization (EI). 1920. Samples are introduced into the ion source as a gas where they are ionized by energetic electrons. Use is limited to volatile and thermally stable compounds. Extensive fragmentation is observed, thus molecular weight information is sometimes hard to obtain.

Chemical ionization (CI). 1965. The source is held at a relatively high pressure of 1 torr. Under such condition a reagent gas e.g. methane can yield CH_5^+ , which ionizes gas-phase sample molecules by exothermic proton transfer to form $[\text{M}+\text{H}]^+$. "Soft" ionization, provides molecular weight information.

Field desorption (FD). 1969. Samples are placed on microdendrites, usually carbon grown on a fine metal wire. Ions are desorbed by the combined action of heat and very high fields present in the source. Commercial sources are available, but the technique has a reputation for erratic performance, and ion currents are transient and not intense.

Plasma desorption (PD). 1974. Samples are supported on a thin foil and energized by the passage of high-energy fission fragments from ^{252}Cf , or ions from a particle accelerator. Mass analysis is normally performed on time-of-flight (TOF) instruments. No commercial source available.

Secondary ion mass spectrometry (SIMS). 1977. Samples, usually in solid form but often mixed with a solid matrix, are energized by ions of keV energy. Low fluxes of ions are used for molecular SIMS and high fluxes for inorganic analysis and depth profiling.

Electrohydrodynamic ionization (EHMS). 1978. Samples are dissolved in glycerol containing an electrolyte. Desorption takes place directly from solution under the influence of high fields.

Laser desorption (LD). 1978. Samples are prepared in various ways since both reflection and transmission experiments are performed. Applications in inorganic analysis predated the first organic studies in the late 1960's. High tendency toward thermal degradation. Mass analysis on TOF instruments.

Thermal desorption (TD). 1979. Samples are introduced on a direct insertion probe. Heating of the probe tip desorbs ion and neutrals: no ionization filament is used.

Fast atom bombardment (FAB). 1981. Samples, usually in solution (often glycerol), are energized by atoms of keV energy. Fluxes are higher than in SIMS.

Thermospray (Electrospray) ionization (ES). 1985. Analysis of liquid samples takes place by spraying them into high electric field. Multiply charged ions are produced.

Matrix assisted laser desorption (MALD). 1991. Samples are prepared by co-crystallization of the analyte (high molecular weight biologically active compounds) with a small M.W. UV absorbing organic matrix. Ionization by UV laser. Mass analysis by TOF instruments.

Electrospray ionization (ESI) have enabled the direct introduction of trace amounts of analytes in their native aqueous media by flow injection or from a liquid chromatography (LC) or capillary electrophoresis (CE) separation experiment for mass spectral analysis. In this technique, small highly charged droplets of the analyte solution are sprayed into a high electric field. As the droplets evaporate, their surface charge density increases until the Rayleigh limit is reached, and, at this point, a coulomb explosion occurs to produce an array of smaller charged droplets. Eventually, when solvents are fully evaporated, a distribution of multiply protonated analyte molecules emerges. Determination of the m/z values and the charged states enables the calculation of the molecular weight. The molecular weight limit of this technique is 100,000 Da.

The Objectives and Organization of the Dissertation

The power of mass spectrometry for analytical applications is the ability to provide molecular weight and structural information about the analyte through the interpretation of its mass spectrum. The correct interpretation of the mass spectra requires the knowledge of the ion formation and fragmentation mechanisms specific for the analyte under consideration. General interpretation rules and fragmentation mechanisms for mass spectrometry were developed in detail by analyzing small volatile molecules, containing no more than two functional groups, with EI and CI. This was possible because the ion formation and fragmentation mechanisms were well understood for both techniques. However, using the D/I techniques, FAB or MALDI, to elucidate the structure of polar, highly functionalized, higher

molecular weight molecules is not always straightforward because the ionization and fragmentation mechanisms are not known with the same certainty as in EI. Unfortunately, in FAB and MALDI the ion formation mechanisms are highly complex and even if some of their aspects are known, the structure of the (quasi)molecular ion cannot be determined unambiguously because of the high functionality of the analyte molecules. The many ionizable groups and the three dimensional structures that are capable of folding make the fragmentation mechanisms more complex to elucidate. The main objective of this dissertation is to study the fundamental aspects of the D/I techniques FAB and MALDI, with the goal of trying to improve the understanding of the ion formation and dissociation mechanisms for biologically active molecules in order to further improve the interpretation process.

Chapter two will discuss the instrumentation of the FAB experiment, introducing the reader to fundamental mass spectrometry principles: tandem mass spectrometry (MS/MS) scanning techniques, collisionally activated dissociation (CAD), and high resolution mass spectrometry. At the end of this Chapter the theories of the ion formation in FAB are summarized. In the published paper in Appendix One the results of my research considering the chemical aspects of the ion formation in FAB are presented. Chapter three evaluates and/or elucidates the fragmentation of organic negative ions formed by FAB. Chapter four describes the instrumentation involved in the MALDI experiment. Chapter five summarizes the results of research regarding the mechanisms of ion formation and fragmentation in MALDI/MS.

REFERENCES

1. Busch, K. L.; Glish, G. L.; McLuckey, S. A. *Mass Spectrometry/Mass Spectrometry: Techniques and Applications of Tandem Mass Spectrometry*; VCH: New York, 1988; pp 1-3.
2. Skoog, D. A. *Principles of Instrumental Analysis*, 3rd ed.; Saunders: Philadelphia, 1985; pp 523-524.
3. Beynon, J. H. *Mass Spectrometry and Its Applications to Organic Chemistry*; Elsevier: Amsterdam, 1960.
4. Biemann, K. *Mass Spectrometry, Organic Applications*; McGraw-Hill: New York, 1962.
5. McLafferty, F. W. *Mass Spectrometry of Organic Ions*; Academic: New York, 1963.
6. Budzikiewicz, H.; Djerrasi, C.; Williams, D. H. *Mass Spectrometry of Organic Compounds*; Holden-Day: San Francisco, 1967.
7. Munson, M. S. B.; Field, F. H. *J. Am. Chem. Soc.* **1966**, *88*, 2621.
8. Müller, E. W.; Bahadur, K. *Phys. Rev.* **1956**, *102*, 624.
9. Prókai, L. *Field Desorption Mass Spectrometry*; Marcel Dekker: New York, 1990; Vol. 2.
10. Torgerson, D. F.; Showronski, R.P.; Macfarlane, R. D. *Biochem. Biophys. Res. Commun.* **1974**, *60*, 616.
11. Posthumus, M. A.; Kistemaker, P. G.; Meuzelaar, H. L. C.; Ten Noever de Brauw, M. C. *Anal. Chem.* **1978**, *50*, 985.
12. Benninghoven, A.; Sichtermann, W. K. *Anal. Chem.* **1978**, *50*, 1180.

13. Barber, M.; Bordoli, R. S.; Sedgwick, R. D.; Tyler, A. N. *J. Chem. Soc., Chem. Commun.* **1981**, 325.
14. Fenn, J. B.; Mann, M.; Meng, C. K.; Wong, S. F.; Whitehouse, C. M. *Mass Spectrom. Rev.* **1990**, *9*, 37.
15. Hillenkamp, F.; Karas, M.; Beavis, R. C.; Chait, B. T. *Anal. Chem.* **1991**, *63*, 1193A.
16. Danis, P. O.; Karr, D. E.; Mayer, F.; Holle, A.; Watson, C. H. *Org. Mass Spectrom.* **1992**, *27*, 843.

CHAPTER TWO. THEORY AND METHODS

Introduction to Fast Atom Bombardment Mass Spectrometry

In the past twenty years a number of new desorption/ionization (D/I) methods for the analysis of large, often thermally labile molecules have been developed. Of these techniques, Fast Atom Bombardment (FAB) has become the most widely used. In FAB, the primary beam is composed of fast xenon, argon, or neon atoms with kinetic energies in the kiloelectron volt range. While solid samples may be analyzed directly by this method, it was found that the analyte solutions prepared in viscous solvents with low vapor pressures would generate signal for several hours when bombarded [1]. It was soon recognized that the viscous liquid matrix was the key parameter in FAB, and the charge on the particles in the primary beam had no effect on the desorption/ionization process [2]. Ion beams can be focused more than neutral beams therefore ionization efficiencies are slightly higher and lower detection limits can be achieved with liquid secondary ion mass spectrometry (LSIMS). The kinetic energy of the primary beam typically ranges from 2-8 keV. Solid samples are dissolved in a solvent which is miscible with the viscous matrix material. Most commonly used FAB matrices are glycerol, thioglycerol, diethanolamine, triethanolamine and nitrobenzyl alcohol. Aliquots of the sample solution are mixed with the matrix prior or after deposition on the end of the direct insertion probe. The volatile solvent is removed under reduced pressure in either the inlet port of the mass spectrometer or a separate vacuum apparatus. The FAB sample is inserted into the mass spectrometer and bombarded with the primary beam.

Secondary ions which are generated during this process are focused by a series of electrostatic lens elements, then accelerated out of the source and allowed to pass through the mass analyzer where they are filtered and detected.

The FAB technique has been applied to the analysis of a wide variety of inorganic, organic, and biologically important compounds. It is particularly well suited to the characterization of compounds up to 5,000 or 6,000 Da. FAB mass spectra frequently contain information about the molecular weight of the analyte in addition to structurally informative ions. The extent of fragmentation is small relative to EI, therefore the technique is considered to be "soft". Unfortunately, the chemical noise produced by the matrix and any impurities that are present in the FAB sample can obscure the analyte spectrum. Signals persist long enough for high resolution and tandem mass spectrometry (MS/MS) experiments to be completed.

INSTRUMENTATION

FAB Gun

The FAB gun used in this research was manufactured by JEOL (Peabody, MA). Its operation is based on a charge exchange process [3] to produce a beam of xenon atoms with 6 keV of kinetic energy. Initially, primary xenon ions (Xe^{+}) are generated in the ionization chamber. Xenon gas is introduced into the chamber which contains a rhenium filament (cathode) and a cylindrical wire mesh anode. Electrons are thermionically emitted from the cathode when current of 5-30 mA is passed through the rhenium wire. In this research the emission current was usually set to 5 mA. A potential difference of 200 V is set between the cathode and the anode, so

that the electrons are accelerated toward the wire mesh. Xenon atoms are ionized in the region near the wire mesh by the electron impact. The Xe^+ ions are extracted out of the ionization chamber and accelerated to 3 keV of kinetic energy. The ion beam is shaped and focused, before it is directed into the gas chamber which is pressurized with unionized xenon gas. Xe^+ ions passing through the gas chamber are accelerated to a final kinetic energy of 6 keV as they pass through the exit nozzle. In the gas chamber they undergo charge exchange reactions with the neutral xenon gas. The neutralized particles experience an insignificant change in kinetic energy and direction of travel during the charge exchange process. The beam that emerges from the exit nozzle is composed of fast ions and fast atoms, but the ions are deflected by the potential applied to the mass spectrometer ion source, and only the fast atoms hit the sample. A diagram of the JEOL FAB gun is shown in Figure 2.1.

Mass Spectrometer

All experiments for this research were performed on a JEOL HX-110 (Peabody, MA) double-focusing mass spectrometer of EB configuration (Nier-Johnson or forward geometry). The instrument is composed of an ion source, a mass analyzer, and a detector. Slits and quadrupole lenses are located between the major components to adjust the shape of the ion beam. A brief description of each component will be given here. Figure 2.2 shows the schematic diagram of the HX-110 mass spectrometer.

The FAB gun is mounted at an angle to the ion source of the mass spectrometer so that the beam of fast xenon atoms enters the ion volume and strikes the sample holder at an angle of 60-70°, to obtain maximum signal level. The FAB sample is introduced directly into the ion source via a direct

insertion probe. Secondary ions are generated from the FAB sample during the bombardment process. A repeller plate deflects the secondary ions away from

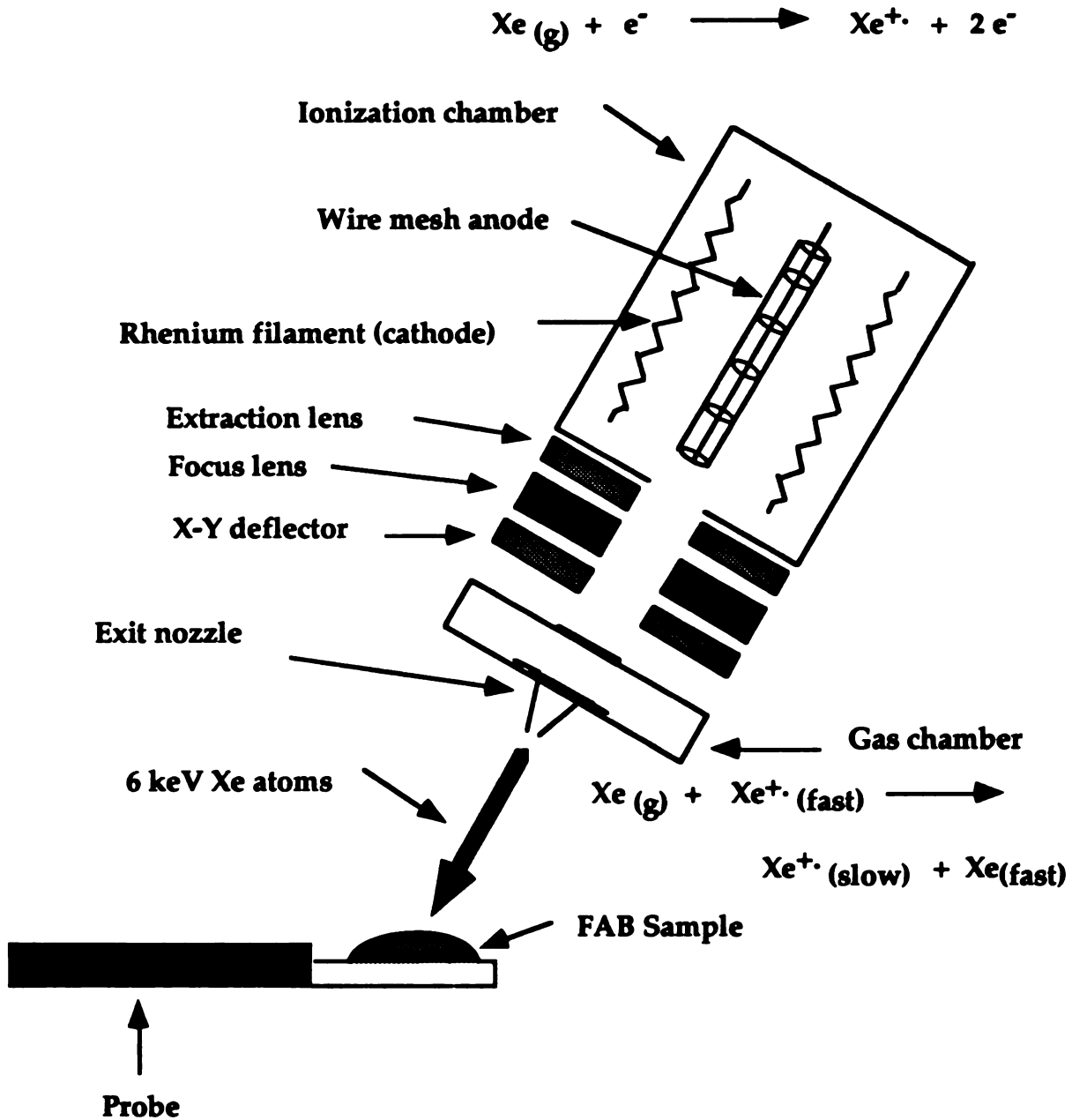


Figure 2.1 Schematic diagram of a JEOL charge exchange fast atom bombardment gun.

the insertion probe and out of the ion volume through the exit slit. The ions

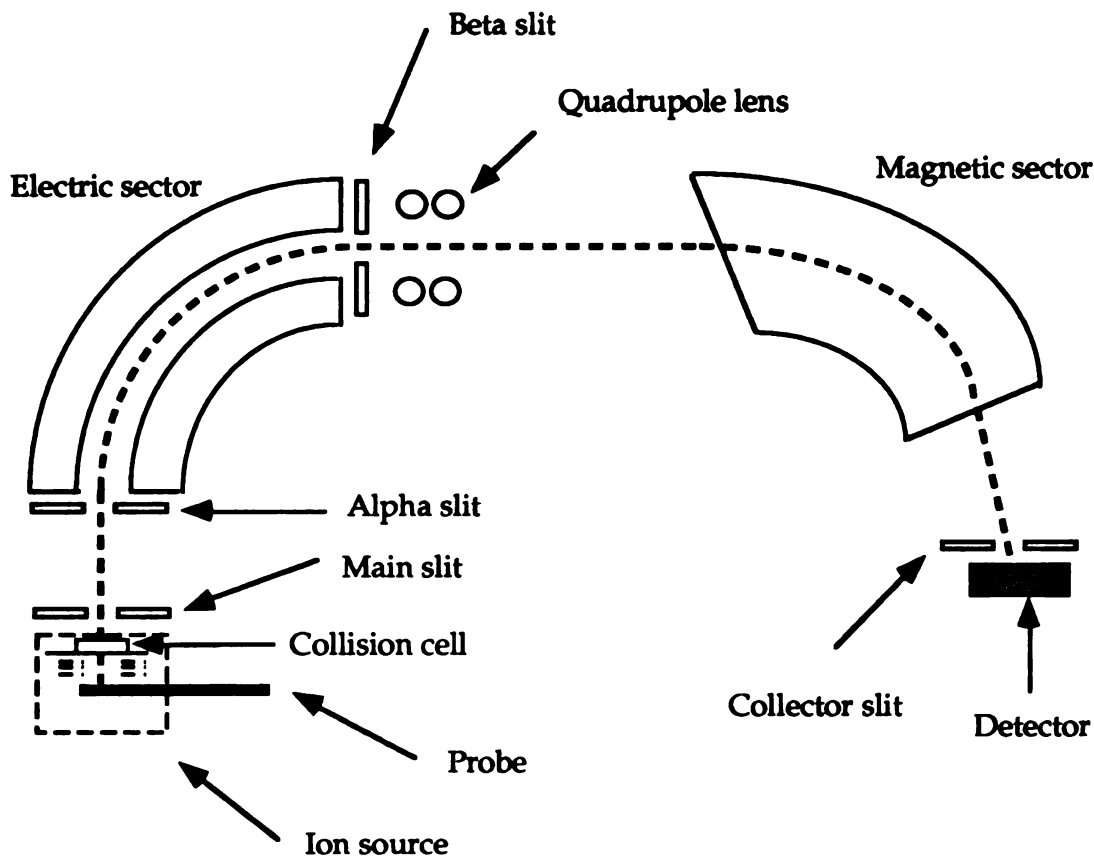


Figure 2.2 Schematic diagram of a JEOL HX-110 double focusing mass spectrometer.

are focused into a beam by a series of electrostatic lens elements, then accelerated to 10 keV of kinetic energy. The ions pass through the main slit which determines the horizontal dimension of the beam and, in conjunction with the collector slit the resolution of the mass spectrometer. In theory, all the ions emanating from the source have the same kinetic energy, but the velocity of each ion will be inversely proportional to the square root of the mass, according to the equation:

$$K. E. = zeV_{acc} = \frac{1}{2} m v^2 \quad \text{or} \quad v = \sqrt{\frac{2zeV_{acc}}{m}}$$

where $K. E.$ is the kinetic energy of the ion, z is the charge number, e is the elementary unit of charge, V_{acc} is the accelerating voltage, m is the mass, and v is the velocity.

Before entering the electrostatic analyzer, the ion beam is focused in the horizontal and vertical directions by a quadrupole lens, and the angular divergence of the beam is defined by the α slit. The electrostatic analyzer in the JEOL HX-110 consists of a positive and a negative cylindrical electrode aligned on coaxial circles. During routine operation, the potential difference between the two electrodes is held constant, creating a fixed electric field, E , that is linked to the accelerating voltage (10 keV). Ions traveling through the electrostatic field take a circular path of radius r according to the equation:

$$Ee = \frac{m v^2}{r}$$

The radius also depends on the kinetic energy of the ions as follows:

$$zeV_{acc} = \frac{1}{2} m v^2$$

$$\frac{2zeV_{acc}}{r} = \frac{m v^2}{r} = Ee \quad \text{then} \quad r = \frac{2zV_{acc}}{E}$$

The diverging ion beam is spatially focused by the electrostatic analyzer at the β slit, located between the electric sector and the magnetic sector. In this

configuration, the electrostatic analyzer does not separate the ions according to their m/z ratios.

The β slit defines the energy spread of the ions entering the magnetic sector, while a second quadrupole lens is used to maintain the shape of the beam. As the ions pass through the magnetic sector analyzer, the force exerted by the magnetic field causes the ions to change direction and follow a circular trajectory that is perpendicular to the direction of the field, according to the relationship:

$$R = \frac{m v}{B z e}$$

where R is the radius of the ion trajectory through the magnetic sector, and B is the magnetic field strength. For a given field strength B , ions with different momenta (mv) will follow paths of different radii. In the HX-110, the value of R is fixed and B is scanned or varied, so that ions of different momenta are focused at the collector slit as a function of time. Dispersion of the ions by the magnetic sector analyzer can be related to the mass-to-charge ratio using the equations for the kinetic energy and the radius of travel:

$$z e V_{acc} = \frac{1}{2} m v^2$$

$$R = \frac{m v}{B z e} \quad \text{or} \quad v^2 = \frac{R^2 B^2 z^2 e^2}{m^2}$$

then

$$\frac{2 z e V_{acc}}{m} = \frac{R^2 B^2 z^2 e^2}{m^2} \quad \text{or} \quad \frac{m}{z} = \frac{e R^2 B^2}{2 V_{acc}}$$

Thus, at constant accelerating voltage and a fixed value of R , ions with different m/z values will pass through the collector slit sequentially as the magnetic field strength is scanned over a short period of time.

Detector

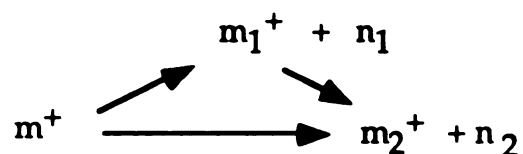
The detector consists of two parts: the post acceleration detector and the single channel electron multiplier. The post acceleration detector in the JEOL HX-110 is located slightly off axis to the ion beam. A potential of +20 kV is applied to this component in the negative ion mode. In case of positive ion mode, the applied potential is - 6 kV. Sample ions are accelerated toward the post acceleration detector, where they strike the surface and cause the ejection of secondary electrons and positive ions. The positive ions are accelerated toward the entrance of the electron multiplier, in which the cathode is maintained at a negative potential and the anode is at ground. Secondary electrons are emitted from the surface of the multiplier and accelerated into the channel where they strike the surface of the multiplier and cause the release of additional secondary electrons. The signal is amplified in this manner. Typical gains for a single channel electron multiplier are 10^4 to 10^5 .

Tandem Mass Spectrometry (MS/MS) and Collision-Activated Dissociation (CAD)

Until now, the mass analyzer discussion above has only considered scanning a single mass analyzer to separate, as a function of mass, the ions formed in the ion source volume. However, from the standpoint of stability there are three major types of ions produced in the source: (a) those that are

stable for about 100 μsec or longer thus reach the detector intact, (b) those that decompose immediately (less than 10^{-7} sec) after formation and are detected as fragment ions, and (c) those that decompose in 1 to 10 μsec after ion formation. This classification is based on a time scale defined by the instrumental parameters, the mechanics of ion acceleration and analysis by the mass spectrometer. The ions in the first group are called stable ions, those in the second group are described as unstable ions. Those in the third group, called metastable ions, are accelerated out of the ion source as one species (precursor ion) but decompose into another species (fragment ion) before reaching the magnetic field. The fragmentation pattern (stable or metastable) observed in the mass spectrum facilitates the structural analysis of the compound under investigation. Tandem mass spectrometry instrumentation is necessary for observing the fragmentation of intact ionized analyte molecules by inducing their decomposition, or for detection of fragment ions that are formed after their precursor ion has been accelerated. Instrumentally, true tandem mass spectrometry (MS/MS) involves interfacing two mass analyzers on either side of a field-free region that contains a collision cell for the activation technique called collisionally activated dissociation (CAD). To facilitate interpretation of a given mass spectrum, ions of any given mass to charge ratio can be selected by the first mass spectrometer as precursor ions for CAD. The precursor ions are directed to the collision cell, where their decomposition is induced by collisional activation using an inert gas, and a second mass spectrometer analyzes the fragment ions. In the case of FAB, CAD also provides a possibility to eliminate part of the chemical noise due to the application of the liquid matrix. Furthermore, in the case of mixture analysis the product-ion scan of each component coupled with CAD will yield structural information for each

individual component. Under special operating conditions a double focusing mass spectrometer can be used to detect metastable decomposition products and products of collisional activation, thus no second mass spectrometer is necessary. The operational mode is referred to as linked scan. There are two possible linked scan operations on the double focusing instruments with forward geometry, such as the JEOL HX-110. For each of these scans the accelerating voltage, V_{acc} , is held constant, while the electric and magnetic fields are "linked scanned" keeping either the ratio of B/E or B^2/E constant. (For double focusing mass spectrometers with reverse geometry, there is one additional mode of linked scanning, keeping B^2E constant.) Let m^+ represent an ion formed upon fast atom bombardment inside the ion source before acceleration, and consider the following fragmentation reactions producing fragment ions m_1^+ and m_2^+ and neutral species n_1 and n_2 :



Thus, a portion of the m_2^+ fragment ions are formed by a secondary fragmentation process from m_1^+ . Since all of these ions are produced before acceleration, they all are transmitted through the electric sector, held at a constant potential of E_0 . In the normal operational mode, these ions are mass-dispersed in the magnetic sector and individually focused on the detector during the scanning of B . Thus, all of these ions would appear in the normal mass spectrum. However, if m^+ decomposes after acceleration, in a metastable process, to form m_2^+ and n_2 in the first field free region, between the ion source and the electric sector, the fragment ion m_2^+ will most likely be

filtered out in the electric sector, since its kinetic energy is going to be less than that of the parent ion, because its mass is less than that of m^+ while their velocities are the same. To sample these ions from metastable transitions on an EB instrument, a product ion scan can be performed by a linked scan at constant B/E , in which both E and B are scanned simultaneously, under computer control, holding the ratio of the two fields constant. In this scan type only ions of predetermined m/z values are transmitted. These are the precursor or parent ions whose fragment-ion spectrum is required. The slope of the linked-scan line can be calculated from the B/E ratio for m^+ , where E is the potential at full accelerating voltage at which m^+ is transmitted through E , and B is the magnetic field strength required to detect this ion. Since m_2^+ has lower kinetic energy than m^+ , the electric potential is lowered from E to a value E_2 , in order to let this fragment ion pass through the electric sector. Likewise, the fragment ion has a lower momentum than the parent ion, but their velocities are the same, so B has to be lowered to B_2 so that m_2^+ can be detected.

$$E = mv^2/R \text{ and } E_2 = m_2v^2/R, \text{ so } E/E_2 = m/m_2 \Rightarrow E_2 = m_2E/m$$

$$B = mv/r \text{ and } B_2 = m_2v/r, \text{ so } B/B_2 = m/m_2 \Rightarrow B_2 = m_2B/m$$

B/E ratio = constant

Essentially, since the precursor ion and its fragments have the same velocity, keeping the B/E ratio constant while scanning, makes it possible to select the ions with the same velocity. (The electric sector is a kinetic energy filter, selecting ions with the same kinetic energy ($KE = 1/2 mv^2$). While the magnetic sector is a momentum filter, selecting ions with the same

momentum, mv . Thus, when B/E is constant, $B/E = \text{constant} = 2mv/mv^2 \sim 1/v$.)

A linked scan at constant B/E can be done on fragment ions, such as m_1^+ as well.

For the precursor ion scan on an EB instrument, a fragment ion, such as m_2^+ is user selected from the normal mass spectrum and a linked scan at constant B^2/E is performed to identify the various precursor ions of m_2^+ .

Besides the product ion and precursor ion spectra described above, a third type of spectrum can also be generated. This spectrum type is called constant neutral loss spectrum. In this spectrum, for the example used, all m^+ ions that decompose to give an m_2^+ ion by the loss of a specified n_2 will be represented. This linked-scan is performed by keeping B/E constant.

In order to produce good quality linked scan spectra the resolution for the parent ion selection has to be at least unit mass, otherwise a number of analyte isotopic peaks and possibly peaks from interfering analytes will also be selected.

High Resolution Mass Spectrometry - Peak Matching

There are at least three levels of resolution in mass spectrometry. Low resolution usually means unit resolution in the mass range of interest. In case of unit resolution two adjacent peaks in a mass spectrum are resolved sufficiently that the overlap between them is less than 10 to 20 % of their height. (10 % - 20 % valley definition). Numerical expression of the resolution can be obtained from the ratio of $m/\Delta m$, where m and $m + \Delta m$ are the m/z values of two adjacent peaks. Medium resolution implies a resolving power of 2,000 to 10,000 ($\Delta m = 0.010 m/z$ unit). For high resolution

$m/\Delta m$ is at least 10,000 or greater. Double focusing instruments, such as the JEOL HX-110 are designed to provide high resolution.

High resolution is essential for the determination of the elemental composition of ions. The technique called peak-matching is used to calculate exact masses. It involves the careful comparison of the two values of accelerating potentials that must be alternatively applied to the ion source to make two different ions (one of them with unknown, the other is with known mass to charge ratio value) to reach the detector at the same time. The reference ion should have an m/z value within 10% range of the unknown ion mass. Whichever ion has the lower mass is focused on the detector by adjusting the magnetic field at full accelerating voltage. Then the magnetic field is kept constant (thus the rotation radius of the two ions has to be the same) as the ion of higher mass is focused on the detector by decreasing the accelerating voltage through a high-precision voltage divider. (Since in a double focusing instrument the ratio between the acceleration voltage and the electric field potential is fixed, the electric field is also changed.) The ratio of the voltages necessary to bring the two ions alternatively into focus at the detector is directly proportional to the mass ratio of the unknown and the reference ion.

Theories of Ion Formation in FAB

Since the invention of the highly successful desorption/ionization methods the elucidation of the mechanism of the D/I process has been the subject of great attention. That the deposition of a large energy in a very small volume should result in the desorption of some intact (ionized) molecules is quite surprising, in particular since the molecules may be both

large and thermally labile. However, there is no widespread agreement in the literature with regard to the D/I mechanism. The most striking feature of D/I is that similar spectra are produced by ion impact, fission particle impact, laser irradiation, and other methods of energization of the sample [4, 5]. These similarities are explicable on the basis of a few dominant mechanisms for ion formation and a single mode of ion dissociation. In this Chapter a brief overview of the theories describing the ion formation in FAB will be presented. Figure 2.3 shows typical FAB mass spectrum of lactosylceramide

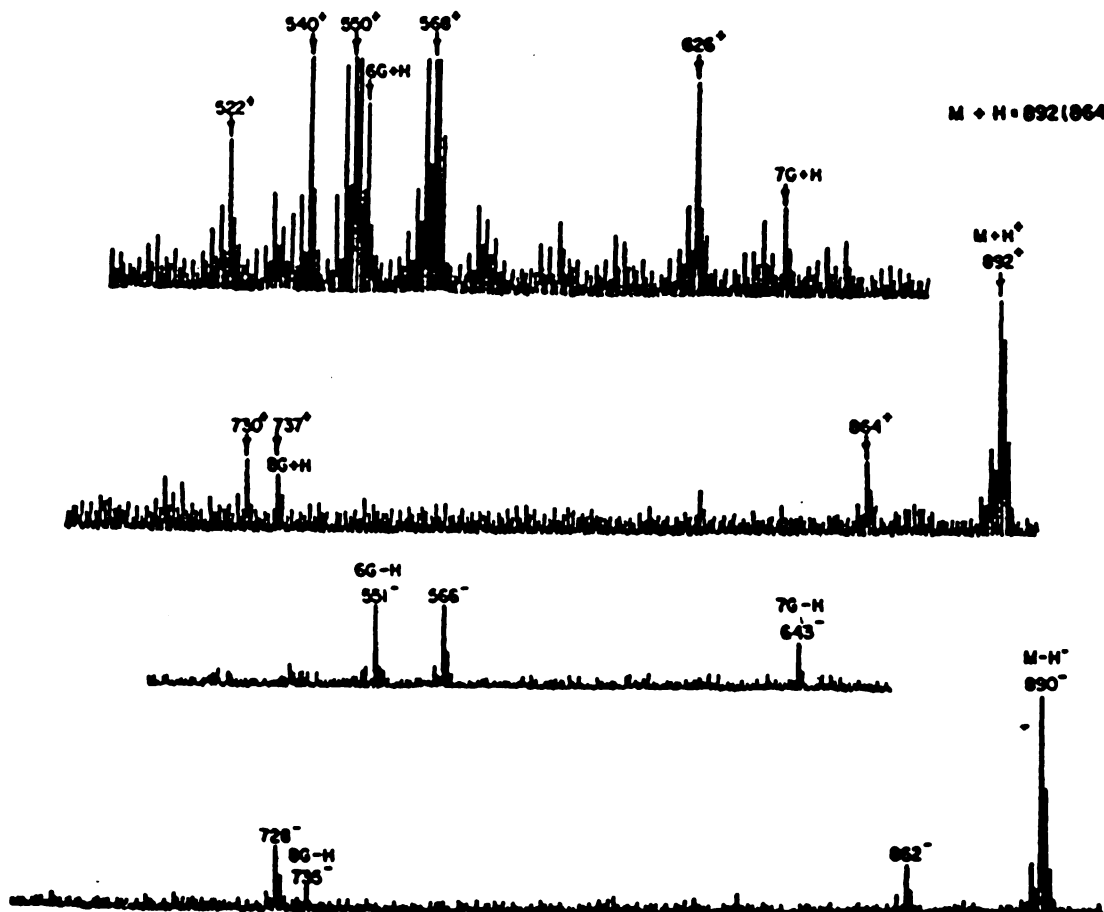


Figure 2.3 The FAB mass spectrum of lactosylceramide. The top two charts show the positive ion spectrum; the bottom two charts the negative ion spectrum. Ions labeled nG +/- H are due to the glycerol matrix. [Adapted from reference 6].

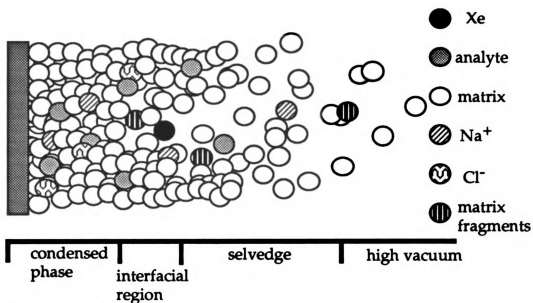
(M.W. 891 Da) published in one of the first papers which evaluated the technique and found it to be routinely applicable [6]. As can be seen, spectra can be obtained equally well for positive and negative ions and the two modes often compliment one another. A typical feature of the spectra is the occurrence of low intensity peaks at every mass-to-charge ratio value. In addition to those low-intensity peaks, there are much stronger peaks at m/z values corresponding to multiples of glycerol matrix molecules ($C_3H_8O_3$) plus some added cation. For example a series of ions appears at mass-to-charge ratio values 93, 185, 277... for $[(C_3H_8O_3)_n + H]^+$, another series at m/z 115, 207, 299,... for $[(C_3H_8O_3)_n + Na]^+$. A similar series, at m/z 91, 183, 275,... for $[(C_3H_8O_3)_n - H]^-$ is prominent in the negative ion FAB spectra. Analytes are usually detected as protonated molecules, $[M+H]^+$, in the positive ion mode and as deprotonated species, $[M-H]^-$, in the negative ion mode. Since the mass of these species differ by one mass unit from the molecular weight of the compound in consideration, they are called quasi-molecular ions.

In an early review of FAB [7], three mechanistic models were presented for ionization and/or desorption. These were desorption of ions preformed in solution by a localized non-equilibrium vibrational process analogous to that considered operational in Secondary Ion Mass Spectrometry (SIMS); evaporation of preformed ions from droplets analogous to proposals by Iribarne *et al.* [8] and Vestal *et al.* [9] for aerosols; and gas-phase ion/molecule reactions following neutral analyte desorption analogous to the thermalized processes in chemical ionization. The ideas which have been proposed by various authors regarding the ionization of compounds which are not present in ionic form (salts) in the matrix are especially contradictory. Thus, Clayton and Wakefield [10] postulate that by the interaction of the atom beam with the condensed phase an electron is abstracted from a substrate or from a

matrix molecule followed by an ionization cascade. According to MacFarlane [11], ionization occurs only a few nm below the surface of the liquid drop by excitation of translational, rotational and vibrational degrees of freedom. Other authors [12] assume ion sputtering from the surface. Each of these mechanisms has received some experimental support. It seems likely that multiple mechanisms exist in FAB, and their relative contributions vary with different kind of samples, liquid matrices and ionization chambers. Recently, a more coherent mechanistic picture has been developed trying to focus on the fundamentals of the desorption/ionization process [13]. According to this model, in D/I the term refers to all processes responsible for the formation of gas phase ions from condensed phase neutral species or ions. Three very different types of processes are involved: formation and destruction of charges (net ionization); desorption of ions; and ion-molecule reactions. A summary of the major theories accounting for these reactions will be presented here.

The collision cascade mechanism was one of the earliest models suggested [14, 15]. According to this theory, as the primary particle impacts the surface of the target and penetrates a short distance into the liquid sample its momentum is transferred to the sample in the form of vibrational energy. This process is sometimes referred as energy isomerization [16]. Emission or sputtering of atoms, molecules, and decomposition products occurs from the area near the impact site if the velocity vector of their vibrational motion is near normal to the surface and they acquire enough energy to overcome the binding energy of the surface. The collision cascade propagates randomly in the sample as the energy of the primary particle is dissipated. Some of the ions formed in the collision cascade remain in the condensed phase and are involved in subsequent reactions such as recombination [13]. Rapid

deposition of a large amount of energy in a small region of the sample results in a localized thermal spike. Temperatures in this region could be high enough to vaporize the sample and a deep narrow cavity of hot gas is created. The interface between the condensed phase and the vacuum breaks down during this process, forming an interfacial region and a region of high pressure, high density gas just above the sample called the selvedge [16]. The above-mentioned spatial aspects of the experiment are depicted in Figure 2.4. An ion or molecule ejected from the liquid traverses through the selvedge region and undergoes numerous collisions, which can be stabilizing or reactive. According to the collision cascade or thermal spike model the direct desorption of ions formed in the condensed phase produces the largest contribution to the ions detected in the mass spectrum and the ion/molecule reactions taking place in the selvedge region has little contribution. Measurements of the secondary ions yields in FAB are reported to be in the range of 0.1-1.5 ion per primary particle impact [17]. The estimated neutral yield is considerably higher, ~ 1000 glycerol molecules per primary atom [18]. Thus, the ratio of secondary ions to neutrals is $\sim 10^{-4}$. In neutral glycerol, the GH^+ concentration is about 10^{-7} [19] and the ion/neutral ratio is 10^{-8} . Ionization in the collision cascade explains why the ratio of ions to neutrals among the ejected species could be much larger than the same ratio in the liquid matrix. On the other hand, it has also been shown experimentally that the secondary ion current from alkali metal halide solutions in glycerol is nearly independent of the salt concentration from 0 to 1 M [20]. This can be explained by extensive ion-ion or ion-electron recombination taking place in the interfacial region during the desorption process. These processes could also account for the fact that multiply charged ions are rarely observed in



Reactions in the interfacial region:

For ionic analytes (M^{2-}) lowering their charged state.

- (1) Proton abstraction from matrix:



- (2) Ion/ion recombination:



Reactions in the selvedge region:

- (1) Cluster formation:



- (2) Protonation/Cationization:

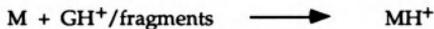


Figure 2.4 Spatial aspects and possible chemistry of the fast atom bombardment experiment.

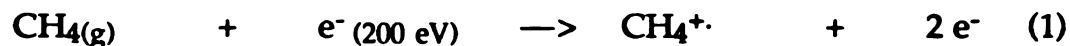
FAB. Instead, singly charged species are produced from multiply charged solvated ions by clustering with counter ions, by fragmentation or by reduction.

An alternative description of the desorption/ionization process was formulated in the gas phase collision model [20]. This model suggests that protonated/deprotonated molecules can be formed in ion/molecule proton transfer reactions in the selvedge region. Thereby, it accounts for the experimental observation that if two matrices with different gas-phase basicities (GB) are mixed on the target, with one having the typical concentration of an analyte, and analyzed by FAB, the matrix with lower GB will be suppressed by an amount relative to its concentration in comparison to the matrix with the higher GB. The GB ($-\Delta G_{\text{rxn}}$) is approximately equal to the proton affinity PA ($-\Delta H_{\text{rxn}}$) if the entropy change is negligible for the proton transfer reaction. Besides proton transfer, other types of ion/molecules reaction can also take place in the selvedge region such as cationization, cluster formation. The possible reactions taking place in the selvedge region are summarized in Figure 2.4. Since, the majority of the desorbed molecules are matrix or matrix-related species, they contribute to the greatest extent to the high pressure in the selvedge region where the above mentioned ion/molecule reactions can occur. Thus, the gas phase collision model portrays FAB essentially as a matrix (glycerol) chemical ionization experiment using protonated matrix molecules as the reagent ions for protonating the analyte molecules. The details of this model are going to be described below.

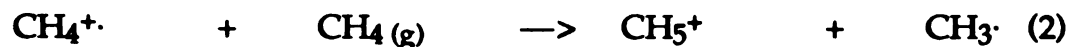
As was mentioned in the First Chapter before the 1970's chemical ionization (CI) was the only complementary ionization method to electron ionization for the analysis of gas phase analytes. Then, in the 1970's and

1980's the advent of desorption/ionization (D/I) methods extended the analytical capabilities of mass spectrometry. It was soon recognized that the mass spectra produced by the various D/I techniques (FAB, MALDI) are remarkably similar to CI mass spectra. In these techniques, in the positive ion mode, analytes are detected, almost exclusively, as protonated species, while the corresponding negative ion spectra contain deprotonated molecules [2]. Thus, the noted similarities between CI and D/I mass spectra urged the researchers investigating the mechanism of desorption/ionization to go back to the well known chemical ionization literature in order to find similarities between the mechanism of ion formation.

The essential reactions in chemical ionization are presented below. The initial ionization is usually by electron impact on the reagent gas which is present in large excess (99.9 %) over the sample molecules of interest. Ionization of the reagent gas is followed by ion/molecule reactions involving the primary ions and the reagent gas neutrals and produces the chemical ionization reagent ion(s). In the initial report of chemical ionization methane was used as the reagent gas [23]. When a 200 eV electron collides with methane molecules there is a high probability that the $\text{CH}_4^{+\cdot}$ radical cation is formed:



The CH_5^+ methane reagent ion is formed by an ion/molecule reaction from a bimolecular collision between a radical cation and another methane molecule:



The analyte, M, needs to be in the gas phase at a pressure of at least 10^{-4} Torr. If the proton affinity of M is greater than that of CH_4 , then an exothermic

proton transfer from CH_5^+ to M will occur to form the protonated analyte molecule:



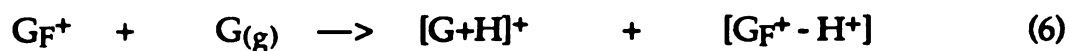
The proton affinity (PA) is defined as the exothermicity ($\text{PA} = -\Delta H_{\text{rxn}}$) of the proton attachment to a particular analyte, M , as shown below:



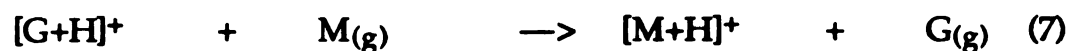
The extent of fragmentation in CI depends most on the amount of internal energy in $[\text{M}+\text{H}]^+$, deposited during protonation, and also on the types of fragmentation pathways available depending on the protonation site. Thus, if the proton affinity of the reagent gas is a lot smaller than that of the analyte, the proton transfer reaction will be more exothermic, therefore the extent of fragmentation is likely to be greater.

The experimental conditions in FAB, such as matrix to-analyte-ratios are similar to the relative pressure of the reagent gas to that of the analyte in CI. The two techniques produced very similar spectra [24]. Thus, it was logical to assume that FAB can be regarded as a matrix chemical ionization experiment in which the reagent ions are produced from the matrix and they undergo CI-like reactions in the high pressure, high temperature selvedge region [16]. This is the previously mentioned gas-phase collision or chemical ionization model for FAB proposed by Kebarle *et al.* [20]. In the selvedge region the high number density is mostly due to the desorbed glycerol matrix molecules (G). Also, analyte molecules (M) are desorbed and ionic fragment species G_F^+ that are related to glycerol are formed near the impact site of the keV Xe atom. The G_F^+ ionic species undergo many collisions with G and initially protonate the intact gas-phase glycerol molecules in the selvedge region by a process similar to that of CI as shown below.

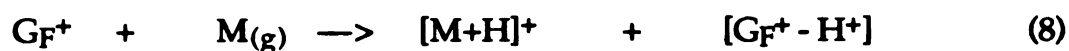




A protonated glycerol molecule may undergo a bimolecular collision with a gas-phase analyte molecule which will result in a proton transfer if the PA of the analyte is higher than that of glycerol.



Thus, according to this CI model for FAB the protonated glycerol molecules act as reagent ions in the proton transfer reaction to the analyte. However, if these were the only reagent ions only analytes with proton affinities higher than PA(glycerol) would be protonated. So it was proposed that the analyte may also be protonated by the ionic fragments of glycerol.



What are these G_F^+ reagents ions? Attempts to identify these have not been made. We have conducted a study to determine the possible reagent ions of FAB for the case of a glycerol matrix. The results are presented in the published article in Appendix I.

The formation of "cluster" ions in FAB represents another selvedge region reaction type in which protonated glycerol molecules collide with G to form a proton-bound dimer of glycerol.



The distribution of the cluster ions of glycerol matrix and the relative intensity of glycerol fragment ions changes with time as it was first shown by Field in 1982 [21]. According to him this is primarily due to the radiation damage of the sample caused by the fast atom beam. Later, the time dependence of the FAB spectra was studied for different analytes [22, 25]. Changes in the mass spectrum with time were related to the differences in the surface activities and diffusion rates of the sample components. However, no

model tried to incorporate the observed time dependence in the description of the desorption/ionization process. In our studies, we used the time dependence of the mass spectra to try to identify the reagent ions in FAB in case of glycerol matrix and refine the chemical ionization model for FAB.

Both the collision cascade/thermal spike and the gas phase collision/chemical ionization models emphasize the charge recombination, ion-pair formation during the desorption process. Preformed ions and ions formed deep in the interfacial cavities are more susceptible to recombination than ions formed in the selvedge. Consequently, the competition between ion/molecule reactions and charge recombination processes is reflected in the mass spectrum.

As we have seen so far no single description is able to account for all the experimental observations in FAB. While, a combination of the theories gives reasonable explanations for the desorption/ionization process, all models described so far are static models and do not take into consideration the observed time dependence of the FAB mass spectra [21, 22] We have extended the gas phase collision/glycerol chemical ionization model to include the dynamics of the FAB experiment. The refined model is published and included in the dissertation as Appendix I. This mechanism also accounts for the observed time dependence of the FAB mass spectra, and gives practical suggestions for the analysis of different analytes.

REFERENCES

1. Barber, M.; Bordoli, R. S.; Elliott, G. J.; Sedgwick, R. D.; Tyler, A. N. *Anal. Chem.* **1982**, *54*, 645A.
2. Harrison, A. G.; Cotter, R.J. In *Methods in Enzymology*; McCloskey, J. A., Ed.; Academic: San Diego, 1990; Vol. 193, pp 3-37.
3. Lew, H. In *Methods of Experimental Physics*; Hughes, V. W. and Schultz, H. L., Eds.; Academic: New York, 1967; Vol. 4, Part A, pp 187-190.
4. McNeal, C. J. *Anal. Chem.* **1982**, *54*, 43A.
5. Daves, G. D. Jr. *Acc. Chem. Res.* **1979**, *12*, 359.
6. Rinehart, K. L. Jr. *Science* **1982**, *218*, 254.
7. Fenselau, C. *Ion Formation from Organic Solids*; Benninghoven, A., Ed.: Springer-Verlag: Berlin, 1983, 90-100.
8. Iribarne, J.V.; Thompson, B.A. *J. Chem. Phys.*, **1976**, *64*, 2287.
9. Blakley, C.R.; Vestal, M.L. *Anal. Chem.* **1983**, *55*, 750-754.
10. Clayton, E.; Wakefield, A.J.C. *J. Chem. Soc. Chem. Commun.* **1984**, 969.
11. MacFarlane, R.D. *Acc. Chem. Res.*, **1982**, *15*, 268.
12. Hoogerbrugg, R.; Van der Zande, W. J.; Kistemaker, P. *Int. J. Mass Spectrom. Ion Process.* **1987**, *76*, 239.
13. Sunner, J. *Org. Mass Spectrom.* **1993**, *28*, 805-823.
14. Benninghoven, A.; Sichtermann, W.K. *Org. Mass Spectrom.* **1977**, *12*, 595-597.

15. Barber, M; Bordoli, R.S.; Elliot, G.J.; Sedgwick, R.D.; Tyler, A.A. *Anal. Chem.* **1982**, *54*, 645A-657A
16. Cooks, R.G. Bush, K.L. *Int. J. Mass Spectrom. Ion Phys.* **1983**, *53*, 111-124.
17. Wong, S. S.; Röllgen, F.W. *Nucl. Instrum. Methods Phys. Res.* **1986**, *B14*, 436.
18. Wong, S. S.; Röllgen, F. W.; Manz, I.; Przybylski, M. *Biomed. Mass Spectrom.* **1985**, *12*, 43.
19. Wooley, E. M.; Tomkins, J.; Hepler, L. *J. Solution Chem.* **1972**, *1*, 341.
20. Sunner, J.; Kulatunga, R.; Kebarle, P. *Anal. Chem.* **1986**, *58*, 2009.
21. Field, F.H. *J. Phys. Chem.* **1982**, *86*, 5151-5123.
22. Todd, P.J.; Groeneveld, G.S. *Anal. Chem.* **1986**, *58*, 895-899.
23. Munson, M. S. B.; Field, F. H. *J. Am. Chem. Soc.* **1966**, *88*, 2621.
24. Schröder, E.; Münster, H.; Budzikiewicz, H. *Org. Mass Spectrom.* **1986**, *21*, 707.
25. Kriger, M.S.; Cook, K. D.; Short, R. T.; Todd, P. J. *Anal. Chem.* **1992**, *64*, 3052-3058.

**CHAPTER THREE. ELUCIDATION OF THE FRAGMENTATION
MECHANISMS OF ORGANIC NEGATIVE IONS FORMED BY FAST ATOM
BOMBARDMENT MASS SPECTROMETRY**

Mass Spectrometric Analysis of Digoxin and Related Cardiac Glycosides

One of the major advantages of mass spectrometry as an analytical technique is that, through the m/z values and the relative abundances of the ions formed in the ionization and fragmentation process, it gives direct information related to the structure of the molecule under study. The information provided by the mass spectrum, however, can only be utilized for structure elucidation if the mechanism of the fragmentation of the molecular ion is known. In the case of electron ionization, the fragmentation mechanisms are well described and the relationship between the structure of the analyte and the m/z values as well as the relative abundances of the ions in the mass spectrum are well understood [1]. The development of new desorption/ionization techniques, such as FAB [2], extended the applicability of mass spectrometry for larger, highly functionalized molecules, but at the same time created a complex situation in terms of mass spectral analysis. Namely, the connection between the mass spectrum and the structure of the analyte is well described by the mechanistic rules for the positive, odd-electron ions formed by EI mass spectrometry. The same relationship is not understood and explained in FAB, where the analytes are usually detected as the protonated molecule in the positive ion mode, and as the deprotonated molecule in the negative ion mode. In the previous chapter models were presented and evaluated for the mechanism of ion formation in Fast Atom

Bombardment. In case of large analytes the exact site of ionization is difficult to determine. As a large, multifunctional molecule can have more than one acidic or basic site, secondary interactions can make the problem even more complex by effecting the proton affinities of the different functional groups. Furthermore, the ions formed in FAB are even electron ions for which the fragmentation mechanisms are not as well described as for odd electron ions. As was shown, positive and negative ions can be formed by fast atom bombardment. The choice between obtaining positive or negative ion spectra depends primarily upon the compound to be analyzed, as in some cases the negative ion spectra provide additional information about the structure of the molecule. The fragmentation of the ions formed in the negative mode is different from that of in the positive mode, and quite fascinating due to the different stabilization factors for positive and negative ions. Although progress in the elucidation of the fragmentation of even-electron organic anions has been reported the mechanistic pathways are not as well described, not even in the case of earlier techniques like electron capture (EC) [3] or negative ion chemical ionization (NCI) [4], as for the positive ions, thus the mechanistic aspects of the fragmentation for larger organic negative ions should be considered. In particular we focus here on the spectra of cardiac glycosides. These classes of compounds were chosen as models for this study because they have several oxygen containing functional groups and form negative ions easily, thereby making it possible to perform MS/MS studies. Finally, the positive ion study of these molecules by Light and Allison [5] did not imply the presence of extensive secondary interactions, thus suggesting a relatively simple model compound for our experiments. In this chapter a comparative study of the molecules digoxin and related cardiac glycosides together with their aglycone components are presented. The tools that are to

be used in this study are available on a conventional double focusing instrument - high resolution mass spectrometry (peak matching) and collisionally-activated dissociation (CAD) methodology - for providing information about the negative ions produced by FAB, and their fragmentation. In order to elucidate the fragmentation mechanisms, besides the above mentioned instrumental analysis (high resolution experiments, linked scanning), deuterium exchange studies and chemical modification were also performed.

Experimental

The cardiac glycosides and the aglycones were obtained from Sigma Chemical Co., St. Louis, MO, and were used without further purification. The digoxin and gitoxin were dissolved in a methanol:chloroform 1:1 mixture to concentrations of $5 \mu\text{g } \mu\text{L}^{-1}$. The aglycones were dissolved in methanol at the same concentrations. Two microliters of these samples were transferred to the FAB probe tip and mixed with the glycerol matrix. In some cases the matrix was methanol:glycerol 1:1 mixture in order to make the amount of matrix used reproducible. All FAB analyses were performed on a JEOL HX-110 double-focusing mass spectrometer (JEOL, Ltd., Tokyo, Japan) of forward geometry with an accelerating voltage 9.9 kV and a FAB gun voltage of 5 kV with xenon FAB gas. All CAD experiments were performed by linked scanning (at constant B/E) controlled with a JEOL JMA-DA5000 software and using He as the collision gas. The experiments were done under single collision conditions, therefore the helium was introduced into the collision cell so that the signal for the parent ion was attenuated by 10%, which produces single collision conditions [6]. Two, different, deuterium exchange

experiments were performed. In the first case, only the labile hydrogens on the OH groups were exchanged according to the procedure described in reference [7]. In the second experiment three additional, non-labile, hydrogens were replaced by deuterium using the method given by Soldin *et al.* [8]. The sample solutions were made in deuterated methanol. Deuterated glycerol was used as the matrix. In order to avoid the back exchange the stainless probe tip of the mass spectrometer was rinsed with D₂O and bombarded with the Xe beam for about five minutes in the ion source of the mass spectrometer immediately before the analysis. The permethylation of the digoxin was done according to the procedure by Ciucanu [9].

Results and discussion

The way to the understanding of the fragmentation pathways begins with the assignments for the fragment ions. This is especially difficult problem in the case of fast atom bombardment mass spectrometry where the background of chemical noise is large due to the 'peak-at-every-mass' phenomenon and peaks resulting from the matrix itself. A detailed study of this is given in reference [10]. Furthermore, in the case of the negative mode the intensity of the peaks formed is generally smaller than in the positive mode. Thus, it is difficult to distinguish some low intensity fragment ions from the background noise. The only possibility to overcome the background from the matrix is the CAD analysis of the analyte ions. However, this kind of investigation requires precursor ion candidates with high abundance, thus extensive studies can be done only on ions characterized by high ion currents.

In the evaluation of the mechanistic possibilities the previously described [11] Light/Kassel/Allison (LKA) nomenclature will be used to identify both the ionic and the neutral species formed and addressed.

I. The mechanism of the ion formation in the Fast Atom Bombardment of digoxin in glycerol.

The structure of digoxin and some of the major proposed fragment ions are shown in Figure 3.1 (Case A). The negative ion FAB spectrum of digoxin is shown in Figure 3.2a and the linked scan mass spectrum of $[M-H]^-$, m/z 779, in Figure 3.2b, (M represents the intact molecule). The FAB mass spectrum contains peaks representative of the deprotonated molecule $[M-H]^-$, m/z 779, and fragment ions derived from the digoxin and the glycerol matrix (G) adduct ions $[G_n-H]^-$ (denoted by *). All of the fragment ions appear at odd m/z values thus they are even electron ions. The results of the collisionally activated dissociation (CAD) studies are summarized in Table 3.1.

The first important question is how the desorption/ionization process occurs in the case of digoxin in a glycerol matrix. As was mentioned earlier there has been a variety of pathways proposed for the ion formation in FAB, and their relative contribution is suggested to depend on the system under study. We will start this discussion by eliminating those ionization channels that are not probable in our system. One possible mechanism is that the ions are formed in the solution preceding the desorption via Brönsted acid/base reactions. However, this mechanism is more likely for the formation of both positive and negative ions in systems where, for instance, the analyte contains groups with dissociable protons and the matrix has a dielectric constant high enough to support the ion formation in solution. In

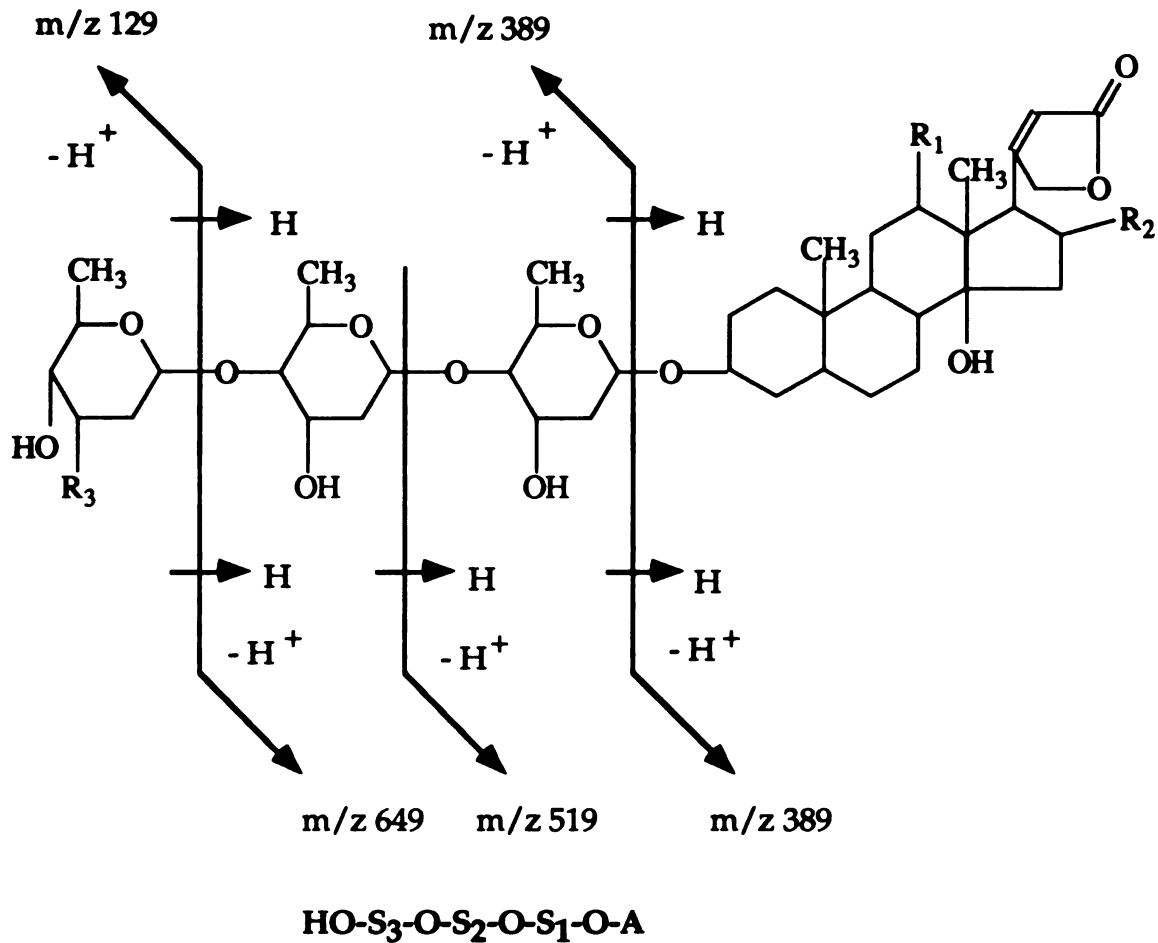


Figure 3.1 Structures of the cardiac glycosides.

The m/z values of the fragment ions are for the anions of digoxin.
(In the shorthand notation S denotes the digitoxose, O is the glycosidic oxygen and A stands for the aglycone.)

A = Digoxin

B = Gitoxin

C = Digitoxin

R₁ = OH

R₁ = H

R₁ = H

R₂ = H

R₂ = OH

R₂ = H

R₃ = OH

R₃ = OH

R₃ = OH

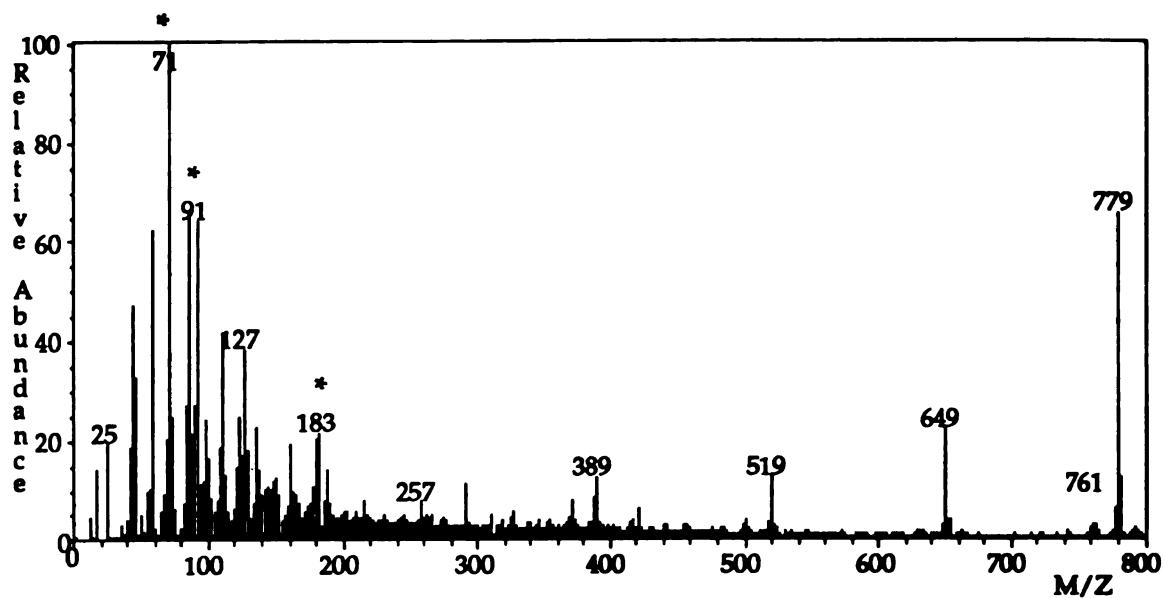


Figure 3.2a The negative ion FAB spectrum of digoxin in glycerol matrix.

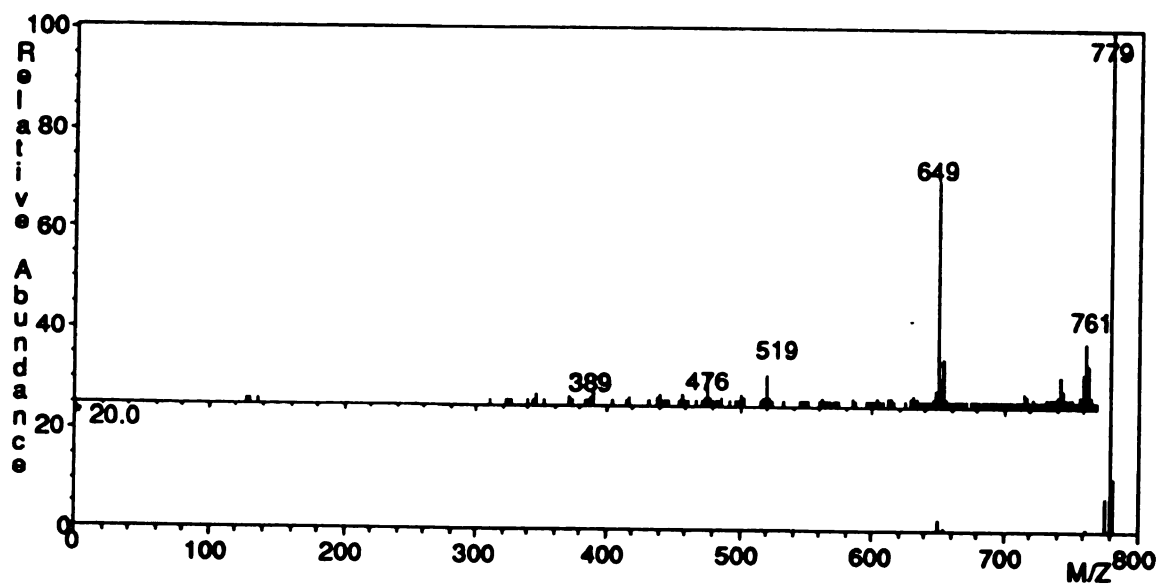
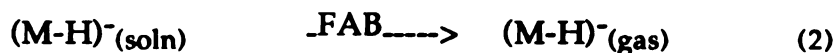
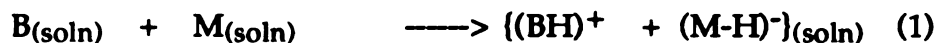


Figure 3.2b The linked-scan CAD spectrum of digoxin parent ion $[M-H]^-$ at m/z 779.

such a case according to the relative acidity of the analyte and the matrix, proton transfer reactions can occur.

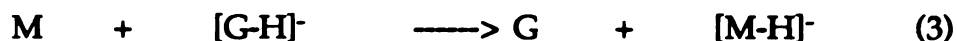


B = base, M = analyte

soln = in solution

Where B can be matrix or an additive. This mechanism probably has some contribution to the ion formation in the case of digoxin, but there is experimental evidence that suggests that this is not the dominant process. Namely, if this process is the major one in the D/I, than applying a matrix that is a stronger base than glycerol, like triethanolamine, should enhance the ion abundance in the spectrum. A similar effect is expected as a result of increasing the pH of the glycerol by adding NaOH. To the contrary, our experiments showed a decrease in the peak intensity in both cases, which rules out the primary role of the solution chemistry in the ion formation. The other possibility is that the analyte and the matrix are desorbed as neutrals, and the ionization occurs in the gas phase as it was reported by Rouse and Allison for a variety of analytes, among these for digoxin [12]. In their KIDS-by-FAB experiments they ejected K^+ ions into the ion source thereby making it possible to analyze the desorbed neutral species through their potassium adducts. They found that in case of digoxin in glycerol only one new analyte-related peak can be observed at m/z 819 (positive ion mode) representing the K^+ adduct of the intact digoxin. Thus their conclusion was

that FAB results in the intact desorption of digoxin from the glycerol matrix and the analyte undergoes proton transfer reactions in the gas phase.



There is one more possibility to be considered here, exclusively for the formation of negative ions. Negative ion formation can take place by electron capture, as a result of a reaction between the gas phase molecules and thermal electrons formed under the fast atom bombardment:



G = glycerol

M = analyte

Green et al [13] reported the negative FAB spectrum of glycerol. According to them the most important ions are the deprotonated molecule at m/z 91, the ion at m/z 89 that is formed by losing H₂ from the deprotonated glycerol. The ion at m/z 71 is formed by eliminating a water molecule from the [G-H]⁻ ion. Finally, the ion at m/z 59 is a result of a methanol loss from the deprotonated glycerol. Also there are some glycerol cluster ions in the spectrum. The study of the negative FAB glycerol spectrum raises the question, that if the ion formed originally was the G⁻: can it lose a hydrogen atom, thus stabilizing the negative charge on the remaining alkoxide anion?



The above electron capture process can be accompanied by a gas-phase acid-base reaction between the analyte and the matrix, like reaction (3).

These are the possibilities to consider for the ion formation in the gas phase. To decide which of these is operational in the case of digoxin in glycerol let us examine the negative FAB spectrum in Figure 3.2.

II. The formation of the $[M-H]^-$ quasi-molecular ion.

1. Thermochemical considerations for proton transfer reactions.

The negative ion FAB mass spectrum of digoxin is very similar to its OH^-/CI mass spectrum reported by Bruins [14] thus confirming the role of gas-phase acid-base chemistry (mainly reactions like (3)) in the mechanism of the ion formation for digoxin in FAB. In Table 3.2 where we summarized the tentative assignments for digoxin fragment ions we also included the results of Bruins marking the ions which are present in the negative ion chemical ionization spectra as well as in the negative ion FAB spectrum. Bruins [14] also studied the OH^-/CI spectrum of gitoxin, which is an isomer of digoxin (Figure 3.1 Case B) and found an odd electron ion at m/z 762. According to him the neutral gitoxin molecule loses a water and the dehydrated neutral product captures a thermal electron, generating an ion at m/z 762. He did not observe any other odd electron ion in the spectra. Thus the fact that all the ions in the FAB spectrum of digoxin are even electron ions suggests that the electron capture is not a likely process for primary ion formation. We believe that the ions are formed in the gas phase via Brönsted acid/base reactions, first the deprotonated analyte molecule is produced, and the fragmentation follows deprotonation. Therefore the discussion of the digoxin spectrum should start with the consideration of the possibilities regarding the

Table 3.2 Digoxin fragment ions, deuterium exchange results.

m/z	rel.int. ^a	composition	designation	max Δm ^b	maxΔm ^c
779*	100	C ₄₁ H ₆₃ O ₁₄	[A- ^H OS ₁ OS ₂ OS ₃ OH] ⁻ [AOS ₁ OS ₂ OS ₃ O] ⁻	+7	+8
777	2	C ₄₁ H ₆₁ O ₁₄	[A- ³ HOS ₁ OS ₂ OS ₃ OH] ⁻ [A- ^H OS ₁ OS ₂ OS ₃ OH-H ₂] ⁻		
763	2.1	C ₄₀ H ₅₇ O ₁₄	[A- ^H -CH ₄ OS ₁ OS ₂ OS ₃ OH] ⁻		
761*	2	C ₄₁ H ₆₁ O ₁₃	[A- ^H -H ₂ OOS ₁ OS ₂ OS ₃ OH] ⁻ [A- ^H OS ₁ OS ₂ OS ₃ OH-H ₂ O] ⁻		
649*	20	C ₃₅ H ₅₃ O ₁₁	[A- ^H OS ₁ OS ₂ OH] ⁻ [AOS ₁ OS ₂ O] ⁻	+5	+7
647	1	C ₃₅ H ₅₁ O ₁₁	[A- ³ HOS ₁ OS ₂ OH] ⁻		
631	1	C ₃₅ H ₅₁ O ₁₀	[A- ^H OS ₁ OS ₂ OH-H ₂ O] ⁻ [A- ^H -H ₂ OOS ₁ OS ₂ OH] ⁻		
519*	8	C ₂₉ H ₄₃ O ₈	[A- ^H OS ₁ OH] ⁻ [AOS ₁ O] ⁻	+4	+6
501	1.5	C ₂₉ H ₄₁ O ₇	[A- ^H OS ₁ OH-H ₂ O] ⁻ [A- ^H -H ₂ OOS ₁ OH] ⁻		
389*	3	C ₂₃ H ₃₃ O ₅	[A- ^H OH] ⁻	+2	+5
387	3	C ₂₃ H ₃₁ O ₅	[A- ^H OH-H ₂] ⁻		
		C ₁₈ H ₂₇ O ₉	[HOS ₃ OS ₂ OS ₁ - ^H -3H] ⁻		
371*	2	C ₂₃ H ₂₉ O ₄	[A- ^H OH-H ₂ O] ⁻	+2	+3
129*	2	C ₆ H ₉ O ₃	[HOS ₃ - ^H -H] ⁻	+0	+0
127*	3	C ₆ H ₇ O ₃	[HOS ₃ - ^H -3H] ⁻	+0	+0
111*	2.8	C ₆ H ₅ O ₂	[HOS ₃ - ^H -3H-H ₂ O] ⁻	+0	+0

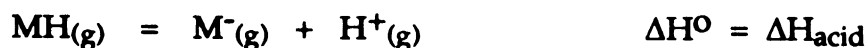
a: relative intensity

b: maximum mass shift after deuterium exchange in the negative mode in the isotopic cluster. First type of experiments: digoxin-d₆ prepared by the method described in reference [7].

c: maximum mass shift after deuterium exchange in the negative mode in the isotope cluster. Second type of experiments: digoxin-d₉ prepared using the procedure in reference [8].

The ions denoted by * are present in the OH⁻/CI spectrum of digoxin reported by Bruins [14].

formation of the quasi-molecular ion, $[M-H]^-$. This is the most abundant analyte ion in the spectrum and characterized by the ion current at m/z 779. In order to determine its structure several questions have to be discussed. Where is the site of the deprotonation? What is the deprotonating agent? In the case of the deprotonated molecule formed by FAB the study of the literature on the negative CI could be beneficiary [15]. Despite the fact that much work emphasizes the inevitable role of gas phase acid-base reactions in the mechanism of the ion formation in FAB [16], little information is available in the FAB literature about this problem. In the evaluation of our data we would like to address this question also. The similarities between the negative FAB spectrum of the digoxin and its OH^-/CI spectra suggest that the deprotonation occurs presumably in the gas phase by a proton transfer from one of the acidic sites of the digoxin to a Brönsted base, probably an ion from the glycerol matrix. There are many possible deprotonation sites in the digoxin molecule. The extended structure of the digoxin, based on crystallographic data [17] indicating the possible sites of the deprotonation, is shown in Figure 3.3. Their gas phase acidities were estimated based on acidities of smaller compounds with similar sites [18]. Where secondary interactions, e.g. hydrogen bonds, could affect the acidity the effect was taken into consideration. The magnitude of these interactions and their effects on the gas phase acidities is described in references under [19]. On the basis of these estimates in Figure 3.4 it can be seen that the possible deprotonation sites of the digoxin molecule have an acidity in the range of 1550-1750 kJmol^{-1} . (It should be noted here as a reminder, that the gas phase acidity is defined as the enthalpy change for the reaction:



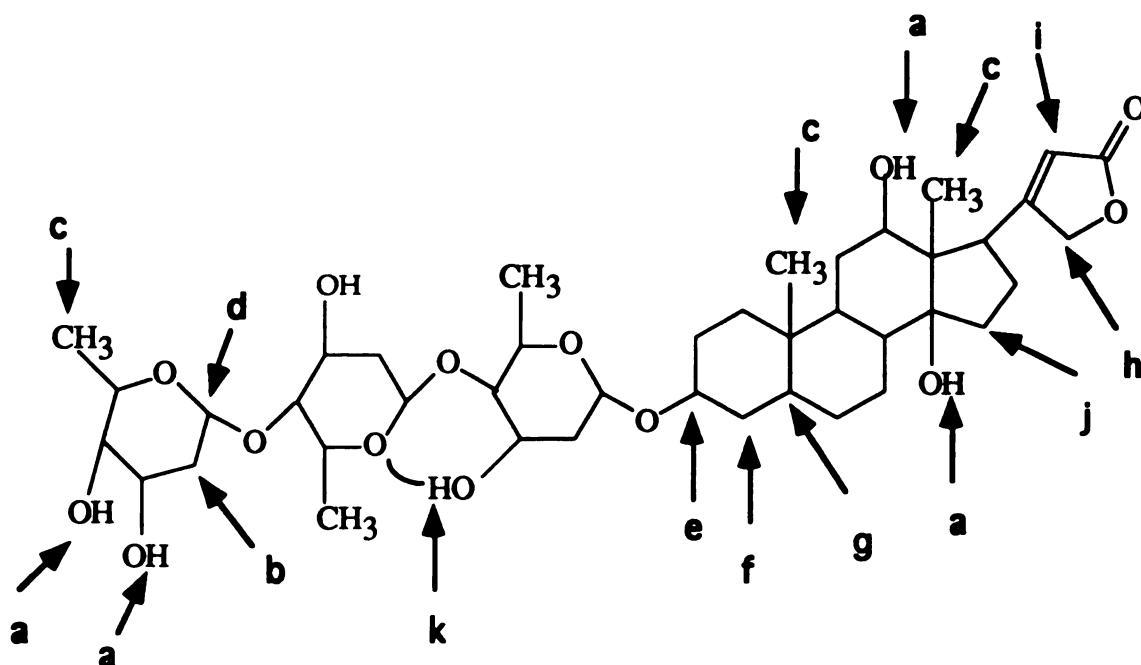


Figure 3.3 The extended structure of digoxin based on crystallographic data, showing the possible deprotonation sites.

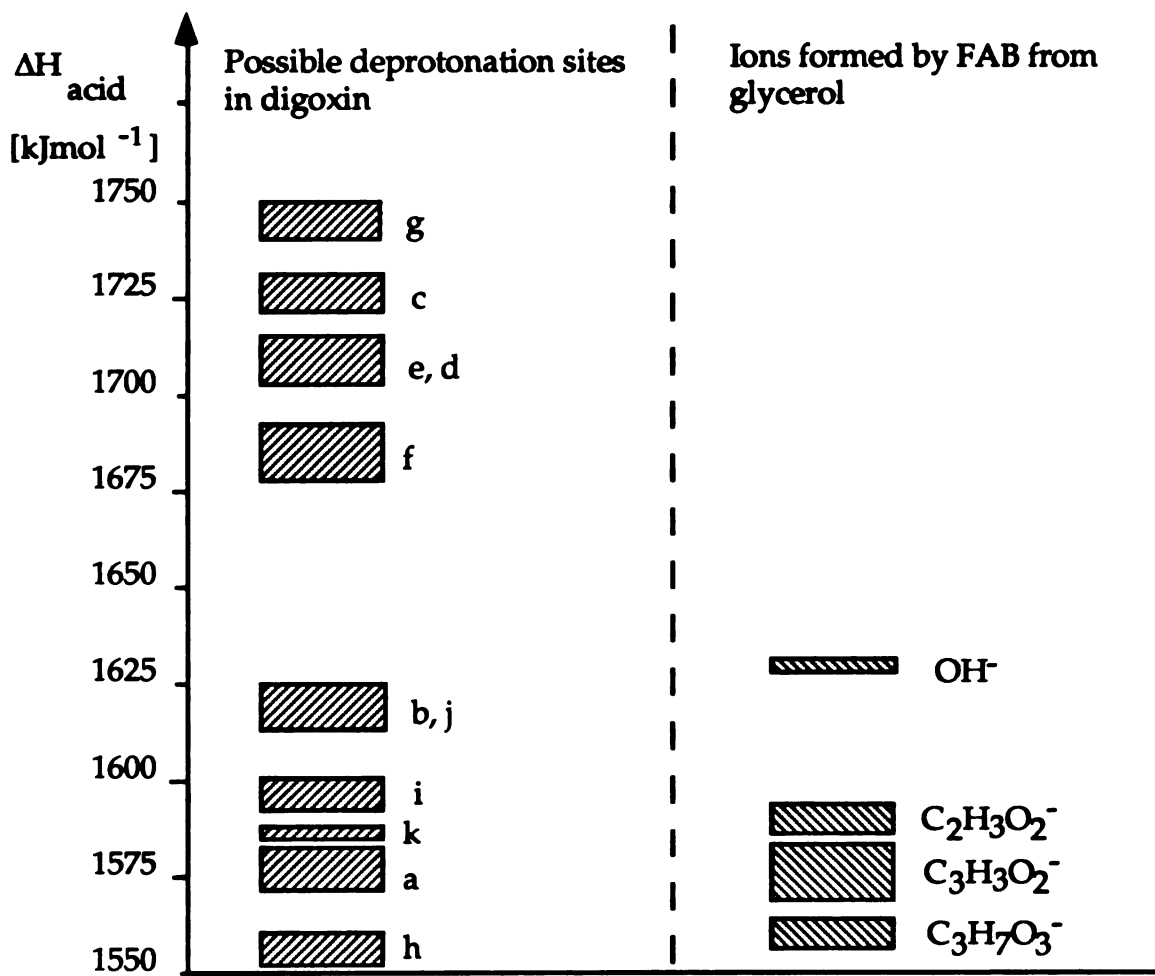


Figure 3.4 Estimates of the gas phase acidities of the acidic sites in the digoxin structure, and the estimates of the acidities of the possible deprotonating agents from the glycerol [20].

According to this definition the ΔH_{acid} values are positive, that is the smaller they are the easier it is to form the deprotonated molecule.) Also shown in Figure 3.4 are the gas phase acidities of the ions present in the negative FAB spectrum of glycerol, that were determined as candidates for deprotonating agents [20]. These values are in the range of 1550-1600 kJmol⁻¹. Note also that the fragment ions of the glycerol are stronger acids than the deprotonated glycerol, [G-H]⁻. If the gas phase acidity values approximated in Figure 3.4 are correct the deprotonation of most of the sites of digoxin by the deprotonated glycerol or glycerol fragment ions would be endothermic. However, proton transfers between the primary and secondary OH groups, and the CH₂ group in the lactone ring of the analyte molecule, and the deprotonated glycerol anions is thermodynamically possible. In Figure 3.4 the gas phase basicity of the OH⁻ ion which is the reagent ion in Bruins negative chemical ionization experiments, as well as a possible reagent ion according to our results [20], is also included. The heat of reaction for the protonation of the hydroxide ions is 1635 kJmol⁻¹ thus the deprotonation of the primary and secondary OH groups in the digoxin molecule by OH⁻ is exothermic reaction suggesting the same structure for the pseudo-molecular ion and thereby accounting for the similarities between the negative ion FAB and the negative CI spectra.

2. Time dependence studies on the mass spectra of digoxin in glycerol

The FAB mass spectra of pure glycerol and digoxin in glycerol were collected and monitored for a period of twenty minutes. In Figure 3.5 the time

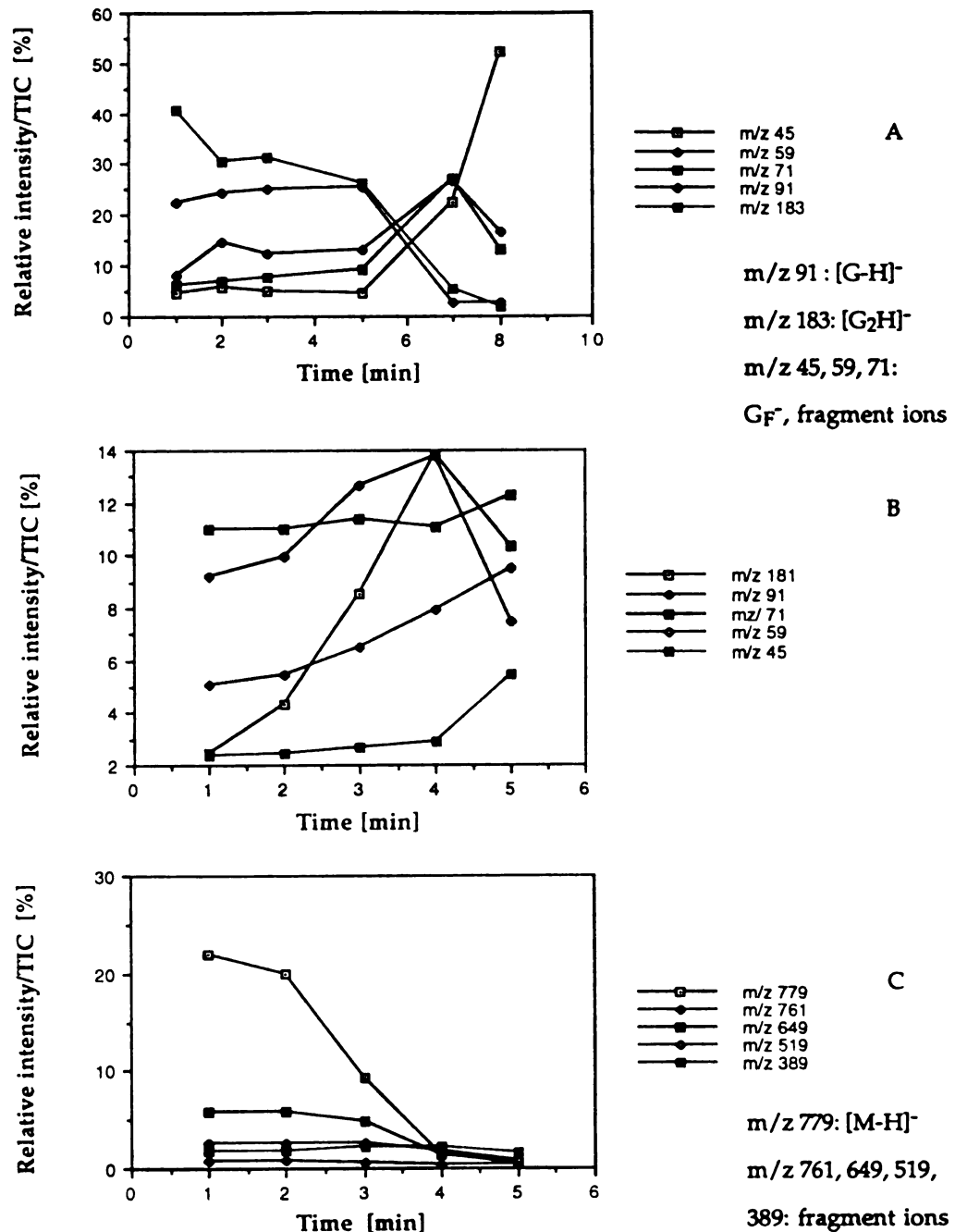


Figure 3.5 Time dependence of the relative intensities of the ions from pure glycerol (A), and the ions from the glycerol matrix (B) containing digoxin (C).

dependence of the relative intensities as the percentage of the total ion intensity for various ions is shown. In the pure glycerol spectrum originally the most abundant ion was $[G_2-H]^-$ at m/z value 183 and the ions at m/z 91, $[G-H]^-$, m/z 59, $[G-H-CH_3OH]^-$, m/z 71, $[G-H-H_2-H_2O]^-$ and m/z 45 carried a smaller portion of the total ion current. However as time elapsed the relative intensity of the ion currents at m/z values 91, 71, 59 and 45 increased (Figure 3.5a). In another experiment we monitored the mass spectrum of digoxin in glycerol for twenty minutes. In this case, in the first scan the most abundant glycerol ion is characterized by an ion current at m/z 71 and the deprotonated digoxin was the most abundant analyte ion. In the later scans the relative abundance of the pseudo-molecular ion of digoxin decreased as the relative abundance of digoxin fragment ions increased as well as the relative intensity of the ion currents at m/z values 91 and 183 and 181. By the time all the digoxin was desorbed the most abundant matrix ions in the spectrum were the ions at m/z 71 and 181. The change in the relative abundances of the matrix and analyte ions with time is shown in Figure 3.5b and c. The fact that the changes in the glycerol spectrum with time are different from the changes observed in the presence of the analyte emphasizes one very important feature of FAB/MS. That is during the mass analysis it is not the actual sample introduced into the mass spectrometer, that is analyzed, but the products of the ion-molecule reactions taking place in the high pressure, high temperature selvedge region. By studying the time dependence of the mass spectra we can gain information about these reactions. The KIDS-by-FAB spectra of glycerol and digoxin in glycerol reported by Rouse and Allison [12] suggest that FAB induces the desorption of neutral glycerol and digoxin molecule which undergo proton transfer reactions in the gas phase producing the protonated and deprotonated species which given the necessary energy

can fragment. They also concluded that the formation of glycerol clusters occurs in the gas phase. Our time dependent studies provide more information about the identity of the reactive species in the selvedge. In the case of digoxin in glycerol at the beginning of the experiment the deprotonated digoxin is the most abundant ion in the spectrum carrying more than 20 % of the total ion current, and suggesting that it has the highest partial pressure in the selvedge region. At the same time there is no significant matrix-cluster formation which has two implications. One is that the probability of a collision between two glycerol molecules is low thereby cluster formation is not possible, and the other is that there is cluster ion formation but these ions are acting as deprotonating agents and neutralized in the process. The increase in the relative abundance of the deprotonated glycerol and the glycerol fragment ions (m/z 91, 71, 59 and 45) as the ion current corresponding to the digoxin ions decreases implies the involvement of these ions in the deprotonation of digoxin. Our conclusion is that the deprotonating agent is probably the deprotonated glycerol, and possibly the fragment ions of glycerol. The above observations are consistent with the "gas phase collision model" and our time dependent studies [20, 21].

3. Deuterium exchange experiments.

To gain more information about the structure of the $[M-H]^-$ anion, deuterium exchange experiments were performed in which deuterated glycerol was used as the deuterating reagent. The exchange was realized on the probe tip of the mass spectrometer by first applying the analyte solution and then after the evaporation of the solvent in the vacuum lock of the instrument quickly adding the deuterio-glycerol. Under these circumstances exchange of the most

labile hydrogens can be expected. The extent of the deuterium exchange may provide information about the relative acidities of the different OH groups in the digoxin, which not only contain the labile hydrogens, but also the possible sites of the deprotonation in the gas phase. Thus information about their relative solution acidities could be useful for our considerations about the formation of the $[M-H]^-$ ion. To be exchanged, the hydrogen of the digoxin must be less acidic than that of the deuterating reagent and the difference in the acidities should not be greater than $40\text{-}80\text{ kJmol}^{-1}$ for effective exchange [22]. The knowledge of the active hydrogen content of the molecule provides an important constraint in the deduction of the overall structure of the analyte as well as its subunits. The comparison of the original spectrum to the spectra taken after the hydrogen-deuterium exchange can provide important information about the mechanism of the fragmentation [23]. The accuracy of the determination of the number of exchangeable hydrogens is very satisfactory in positive FAB/MS [24]. The spectrum of the deuterium-exchanged digoxin is shown in Figure 3.6. The calculation of the active hydrogen content of the molecule and the extent of the exchange is summarized in Table 3.3. After correcting the relative intensities for the natural isotopes the distribution of the deuterium content of the quasi-molecular ion is calculated as well as the extent of the deuteration. The number of labile hydrogens in the digoxin, according to the results of the calculations in Table 3.3, is seven. Also interesting, that the relative abundance of the peaks representing the ions containing six and seven deuteriums (at m/z values 785 and 786) is the same, and each is about ten percent of the total intensity. This suggests that in about ten percent of the total possible exchange a non-labile hydrogen is extracted to form $[M-H]^-$, not

Table 3.3 Digoxin: Hydrogen-deuterium exchange experiments

Negative ion mode				Positive ion mode					
Number of ^2H in the $[\text{M}-\text{H}]^-$	m/z	relative abundance*	^2H % distribution	Extent of deuteration %	Number of ^2H in the $[\text{M}+\text{Na}]^+$	m/z	relative abundance*	^2H % distribution	Extent of deuteration %
0	779	2.00	1.08	0.0	0	803	3.00	1.71	0.0
1	780	1.95	1.06	0.15	1	804	2.78	1.57	0.22
2	781	6.14	3.32	0.96	2	805	6.53	3.71	1.06
3	782	14.51	7.86	3.38	3	806	13.11	7.44	3.19
4	783	32.96	21.26	12.12	4	807	22.70	12.87	7.36
5	784	82.29	44.56	31.64	5	808	44.59	25.28	18.07
6	785	18.28	9.90	8.51	6	809	62.95	35.69	30.62
7	786	18.76	10.16	10.16	7	810	10.89	6.17	6.17
8	787	1.51	0.80		8	811	9.82	5.5	
				Exchange extent: 66.92%					Exchange extent: 66.69%

* The relative abundances are corrected for the natural isotopes.

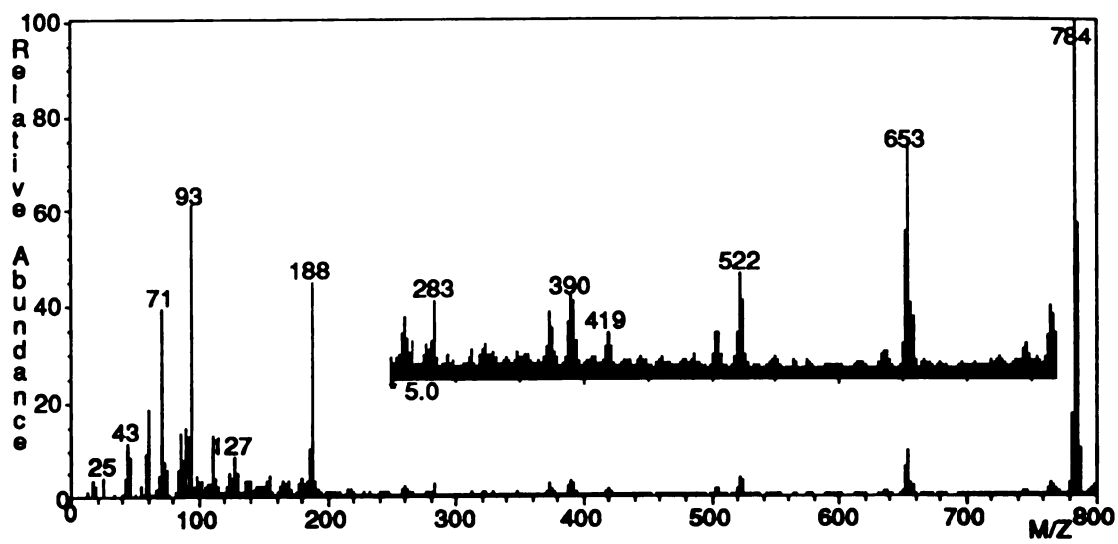


Figure 3.6 The negative ion FAB spectrum of the deuterium-exchanged digoxin-d₆.

$[M-D]^-$. This non-labile site is probably the CH_2 group of the lactone substituent. The fact that the nominal mass peak of the quasi-molecular ion cluster is shifted by five mass units from m/z 779 to m/z 784 has some important implications. On the one hand, it can suggest that the precursor of this ion, at m/z 784, originally contained six deuteriums and lost one deuteron in the ion formation process, $[M_{d6}-D]^-$. On the other hand, the five mass unit shift means that the ion at m/z 784 contains five deuteriums and can be written as $[M_{d5}-H]^-$. This is in accordance with the fact that in 90% of the total exchange extent the alkoxide hydrogens are replaced by deuterium. However, as the deuterium content of the quasi-molecular ion at m/z 784 could not be determined unambiguously additional measurements were carried out in the positive ion mode. Namely, NaCl was added to the solution of the matrix and the analyte in order to get more accurate information about the number of labile hydrogens exchanged in the digoxin, as the quasi-molecular ion in that case is the Na^+ -adduct of the digoxin and not the protonated or deuterated molecule, making it unambiguous to determine the number of deuteriums present, from the mass shift after the deuteration. The result of these experiments is also presented in Table 3.3. In the positive ion mode the quasi-molecular ion appeared at m/z 809 which is in accordance with the incorporation of six deuteriums, and can be designated as $[M_{d6} + Na]^+$. The exchange extent is 66.69% in the positive, and 66.92% of the maximum possible in the negative ion mode. This is lower than expected for a compound with only seven exchangeable hydrogens. The low extent is probably due to back exchange that is probably fast in this case as the basicity of the glycerol is close to that of the functional groups of digoxin containing the labile hydrogens. According to DePuy *et al.* [25] the H-D exchange for carbanions in the gas phase is effective if the gas phase basicity of the anion is

not more than about 20 kcal/mol greater than that of the deuterating reagent gas, but in the case of closer basicities the rate of the back exchange is large making the extent of the deuteration low. Similar effects are expected in the case of exchange in solution. The general appearance of the spectrum of the deuterium exchanged digoxin is the same as before the exchange. This suggests that the fragmentation mechanism was not effected by exchanging the hydrogens with the heavier deuteriums. The mass shifts due to the deuteration for the fragment ions of the digoxin are summarized in Table 3.2. The fact that the CH₂ site in the lactone ring takes part in the deuterium exchange reaction suggests that its relative acidity is greater compared to that of the other C-H type hydrogens. We note here that under high temperature and basic conditions not only the two hydrogens at site h in Figures 3.3 and 3.4, are exchanged in addition to the OH hydrogens but also the hydrogen at site i. The results of these latter exchange experiments will be discussed later in the context of the fragmentation mechanisms. Under mild conditions only site h is participating in the deuterium exchange and as it can be seen it is really one of the most acidic sites of the digoxin. Although the acidity of a proton in an ether, next to the O, is in the range of 1625-1640 kJmol⁻¹, the acidity can increase due to resonance stabilization of the anion. This increase is about 100 kJmol⁻¹ according to reference [26]. In the case of the deprotonation at site h, resonance stabilization occurs through an enolate ion, involving the carbonyl group and the negative charge is delocalized in the lactone ring. Comparing the acidities of the OH groups and site h in the digoxin molecule to the acidity of the ions in the glycerol spectrum it can be concluded that any of these sites in the digoxin can be deprotonated by the deprotonated glycerol. According to this there can be several possible assignments for the structure of the deprotonated molecule [M-H]⁻, at m/z

779. The proton can be lost from the sugar as well as from the aglycone moiety. The designation of this ion in the LKA scheme, considering the intact molecule as $[AOS_1OS_2OS_3OH]$, can be $[AOS_1OS_2OS_3O]^-$, if the proton is from the terminal sugar moiety, and $[A-HOS_1OS_2OS_3OH]^-$, if the deprotonation occurs in the aglycone portion of the molecule.

4. Study of the permethylated digoxin

Since the structure of the quasi-molecular ion still could not be determined unambiguously, it seemed logical to block the deprotonation sites. The permethylated derivative of the digoxin was prepared. In the permethylation reaction all the OH groups were replaced by OCH₃ groups. The permethylated digoxin showed very poor response in the negative ion mode thus suggesting that the replacement of the acidic hydrogens makes the ionization, not desorption, more difficult. At this point it would not be justified to decide in favor of any of the possibilities for the site of deprotonation. The study of the fragmentation pattern should provide some additional information that can serve as proof for the exact site of the deprotonation. Regarding the fragmentation we assume that all the fragmentation follows the deprotonation and there is no fragment ion formation directly in the desorption/ionization process. How should we consider the deprotonated molecule in the context of the fragmentation?

III. The fragmentation pattern in the negative FAB spectrum of digoxin.

1. Structural assignments for the ions at m/z values 777 and 761.

Bowie classified the fragmentation pathways for even-electron organic negative ions [15] as follows:

1. Simple homolytic cleavage reactions where loss of a radical forms a stable anion. (For instance:



2. Reactions that occur by initial formation of an anion/neutral complex which may then undergo a variety of reactions involving the bound anion, including direct displacement of the anion, and deprotonation, elimination processes.

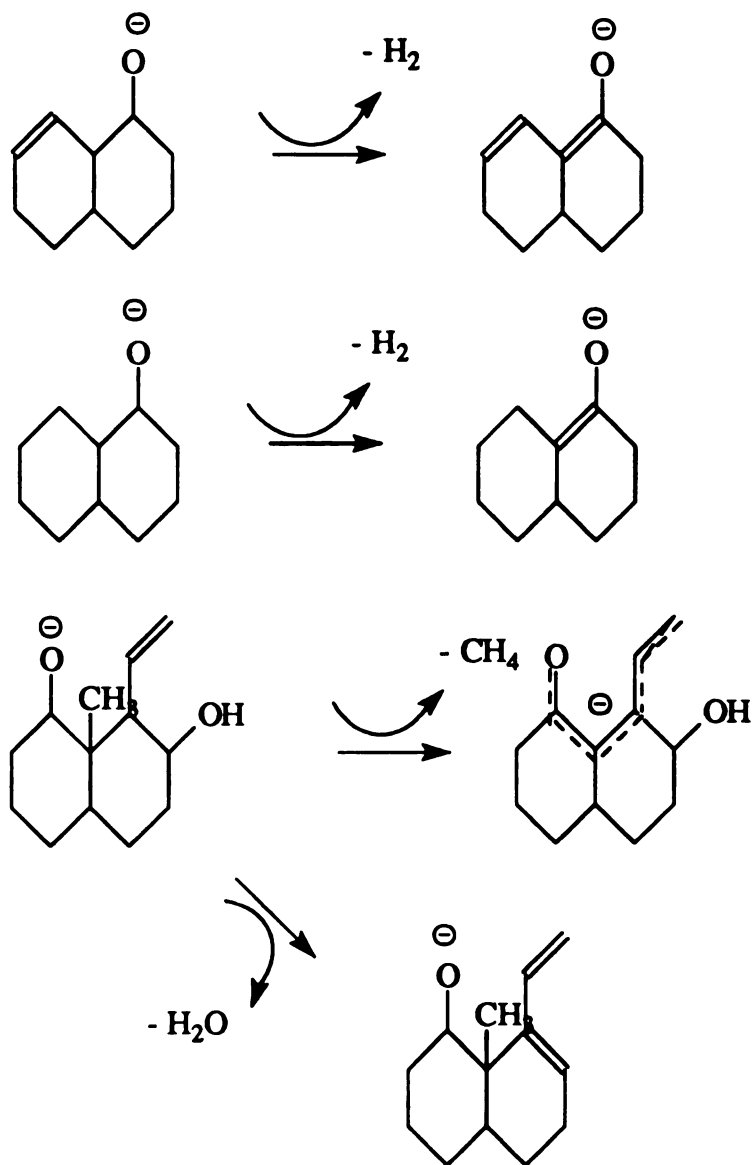
3. Reactions that are not specifically directed by the first formed deprotonated species, but where proton transfer to that species forms a new anion isomer that may fragment as in 2, above.

4. Rearrangement reactions, including internal nucleophilic substitution/displacement and skeletal rearrangement reactions.

Besides these major types of fragmentation a fifth possibility is the remote site fragmentation which occurs remote from the charged center (often in systems where the fragmenting and charged centers are clearly separated because of the rigidity of the molecule) [27]. In our case we will consider the possibility of inductive cleavages (elimination reactions leading to the extension of the conjugation in the ring system thus stabilizing the negative charge), and remote site fragmentations.

In general we can consider a couple of possibilities for elimination reactions in negatively charged ring systems. Elimination, depending on the structure of the molecule, can involve the loss of small molecular weight

compounds such as H₂, H₂O, CH₄ etc. Regarding the sites of the reaction, in general, there are three possibilities: 1,1 or 1,2 eliminations and eliminations via six-membered ring complexes. In the case of negative ions the place of elimination relative to the charge site could be very important because of the possible stabilization of the negative charge via extending the conjugation. This stabilization can be the driving force in the reaction since, in general, during the elimination process two covalent bonds are cleaved forming one double bond, which is energetically not favored. In Scheme 1 we considered some possibilities for eliminations in ring systems. Next we consider which of the above reactions can take place in the case of digoxin. The highest mass fragment ion has an m/z value 777, designated by [M-H-H₂]⁻ as it can be formed by losing molecular hydrogen from the deprotonated molecule. Indication for the loss of 2 amu consecutively with 18 amu, from deprotonated mono- and oligosaccharides has been reported in the literature [28, 29]. These are also well known neutral losses in the case of cyclohexane diols [30] and steroid diols [31] and are explained as a molecular hydrogen loss accompanied by a water molecule loss. Thus, we would like to discuss the possible structural assignment for the ion at m/z 777 together with the next highest mass fragment ion that is also characterized by a small ion current at m/z 761, and is 18 mass units below the mass of the deprotonated molecule. These neutral losses are probably due to elimination of H₂ and H₂O from the deprotonated digoxin, and as the site of the elimination is not known yet, we designate them as [M-H-H₂]⁻ and [M-H-H₂O]⁻. Though the ion currents corresponding to these fragment ions are small in the low resolution FAB spectrum of digoxin, they are enhanced in the CAD spectrum of the parent ion at m/z 779, [M-H]⁻. The significance of the peak due to the elimination of water can be appreciated more comparing the negative FAB spectra of the



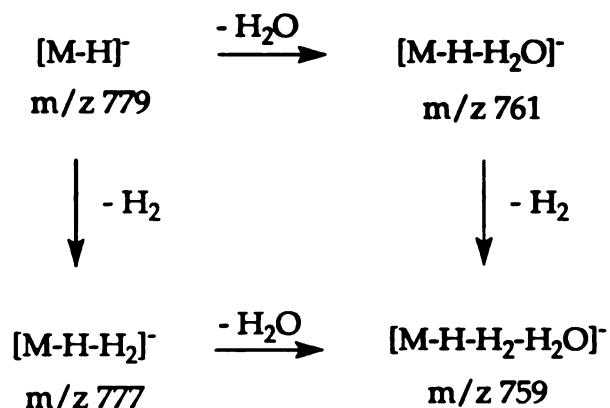
Scheme 1

Eliminations from ring systems

digoxin and one of its isomers, gitoxin (Figure 3.1 Case B), which differs from the digoxin in the position of one OH group in the aglycone portion of the molecule. The negative FAB spectrum of gitoxin is shown in Figure 3.7. The ratio of the relative abundance of the $[M-H]^-$ ion to the $[M-H-H_2O]^-$ is 100:3 in the case of digoxin, and 100:18 for gitoxin. Also another peak appears in the

spectrum of the gitoxin at m/z 743, which can be attributed to the loss of a second water molecule, $[M-H-2H_2O]^-$. The ratio of its relative intensity to that of the deprotonated molecule is $75:100 = [M-H-2H_2O]^-:[M-H]^-$. These peaks due to the water and molecular hydrogen loss(es) are missing from the positive ion spectra reported by Light and Allison [5] that, on the one hand, suggests the operation of different fragmentation mechanisms in the negative ion mode, and on the other hand, offers the possibility of the use of negative FAB mass spectrometric analysis to distinguish between these two isomeric compounds. The determination of the origin of these fragment ions at m/z 777 and 761 is not straightforward as they can be formed by eliminating H_2 and H_2O from the aglycone as well as from the digitoxose residues. According to the LKA scheme, assuming that the deprotonation takes place at the aglycone, the label of the ion with m/z value of 777 is $[A-H-H_2OS_1OS_2OS_3O]^-$ if the molecular hydrogen is from the aglycone and $[A-HOS_1OS_2OS_3OH-H_2]^-$ if the elimination occurs from the sugar residue. Similarly the designation of the ion at m/z 761⁻, if the elimination occurs in the aglycone portion, is $[A-H-H_2^OO S_1OS_2OS_3OH]$, and $[A-HOS_1OS_2OS_3OH-H_2O]^-$, if the water is lost from the sugar unit. Experimental proof for the origin of this water elimination can be provided by the CAD study on the parent ion at m/z 761. The results of the CAD studies on the major fragment ions in the digoxin spectrum are summarized in Table 3.1. As it can be seen in the linked scan spectrum of the parent ion at m/z 761 there are ions at m/z 649, designated as $[A-HOS_1OS_2OH]^-$, corresponding to the loss of a dehydrated terminal sugar, as well as at m/z 633, $[A-H-H_2^OO S_1OS_2OH]^-$, which is formed by losing an intact sugar thereby suggesting water loss from the aglycone portion of the molecule. These two ions are characterized by similar relative intensities thus suggesting that the water could be lost from the aglycone as well as from

the sugar portion with equal probability. The possibility of the dehydration in the intermediate sugar unit could not be excluded either. We shall return to discuss this later. The water loss also occurs from the ion at m/z 777, $[M-H-H_2]^-$, resulting in the formation of the ion represented by the ion current at m/z 759, designated as $[M-H-H_2-H_2O]^-$. These elimination processes are outlined in Scheme 2.



Scheme 2

Eliminations from the deprotonated digoxin.

In order to decrease the number of these possible assignments and evaluate the mechanism of the eliminations, the spectrum of digoxigenin (the aglycone portion of the digoxin) was taken. As can be seen in Figure 3.8 the major fragment ions in the negative FAB spectrum of the digoxigenin are the deprotonated molecule at m/z 389, and the ion formed by an H_2 loss from the deprotonated molecule at m/z 387. There is a large ion current at m/z 371,

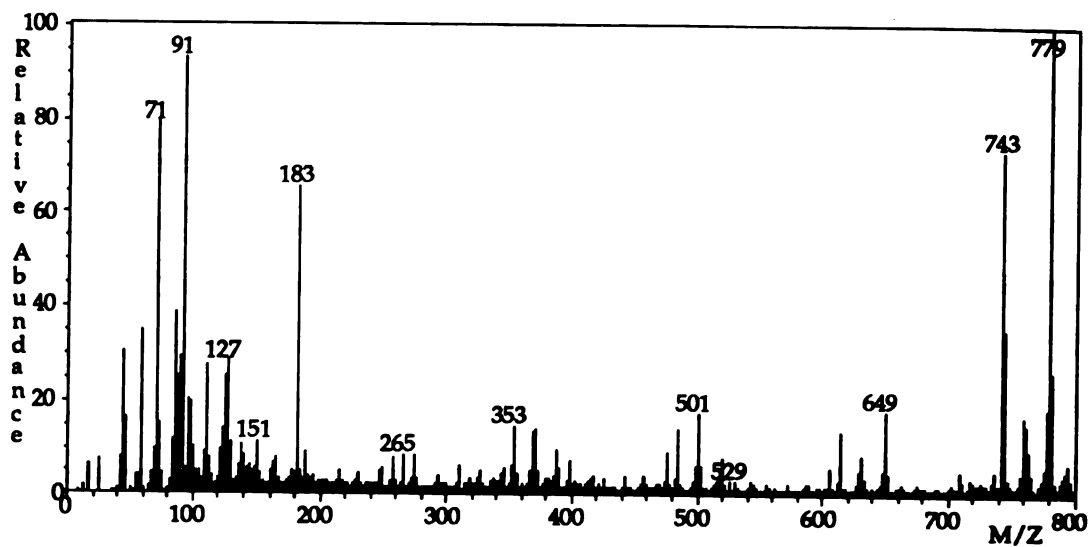


Figure 3.7 The negative ion FAB spectrum of gitoxin.

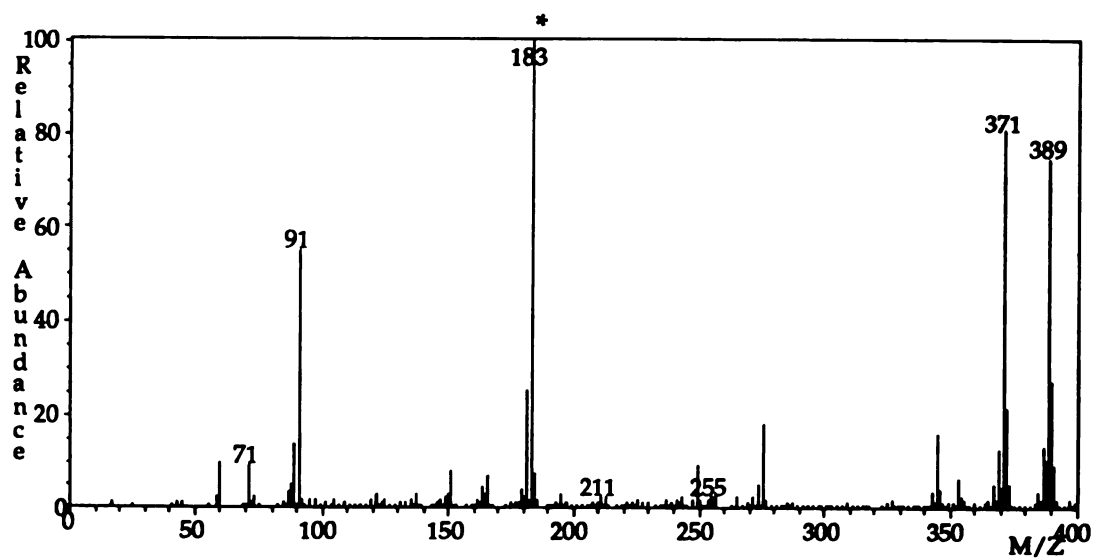
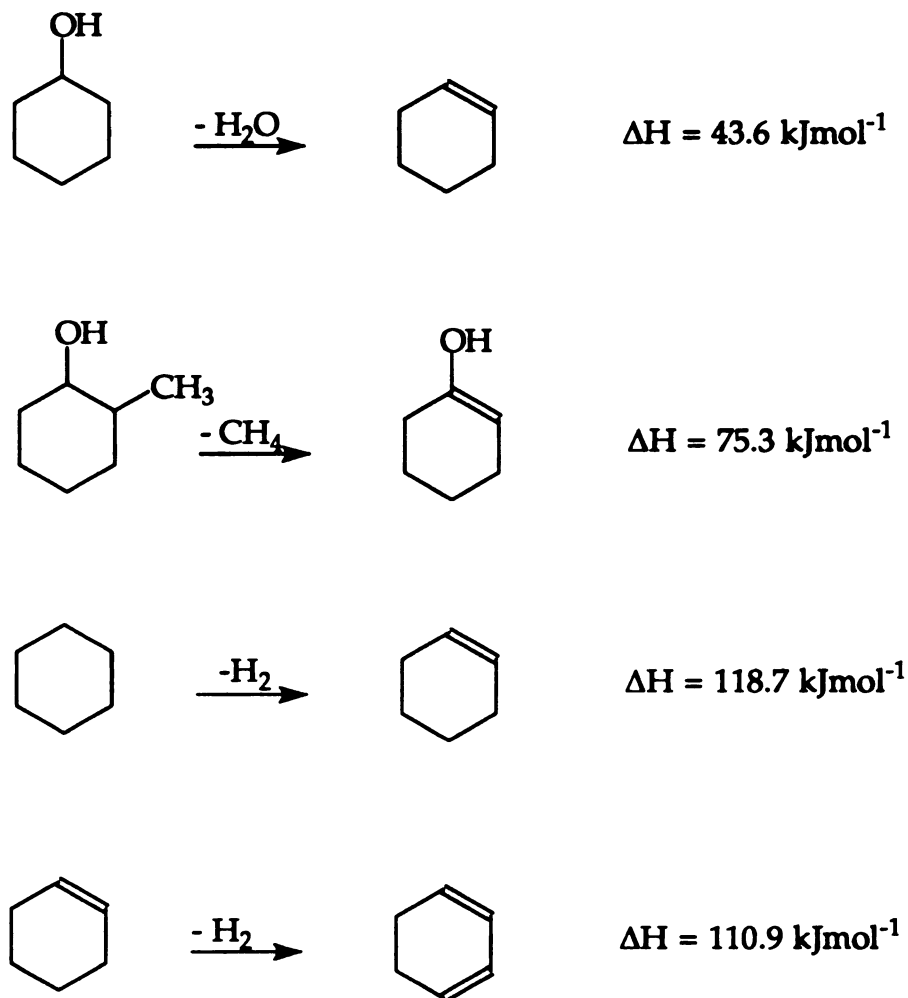


Figure 3.8 The negative ion FAB spectrum of digoxigenin.

which is $[M-H-18]^-$ that can be formed by a water loss from the deprotonated molecule or by losing a methane from the $[M-H-H_2]^-$ ion. However, the relative intensity of the peak at m/z 371, $[M-H-18]^-$, is about six times greater than the relative intensity of the peak at m/z 387, $[M-H-H_2]^-$ suggesting that the water loss is the dominant process, not the molecular hydrogen loss. It should be pointed out also that a consecutive CH_4 elimination from $[M-H-H_2]^-$ should have been represented by a smaller ion current as it would originate from the ion formed by the molecular hydrogen loss (as there is no ion current at m/z 375 which would correspond to $[M-H-CH_4]^-$). Moreover, the peak at m/z 371 is also accompanied by a peak at m/z 369, $[M-3H-H_2O]^-$, confirming that the peak at m/z 371 is not a result of a subsequent H_2 and CH_4 loss. The probability of the H_2O loss versus the consecutive $[H_2 + CH_4]$ elimination can be further justified by thermochemical data. Substituted cyclohexanes were used as model compounds in calculating heats of reactions for the elimination processes mentioned above. According to these the dehydration of cyclohexanol requires 43.6 kJmole^{-1} energy [18]. In contrast 75.3 kJmole^{-1} energy is required to eliminate methane from methylcyclohexanol, and $118.7 \text{ kJmole}^{-1}$ is the heat of reaction for the elimination of H_2 from cyclohexane. Elimination of H_2 from *cyclohexene* forming the conjugated compound is less endothermic, $110.9 \text{ kJmole}^{-1}$. This suggests that water losses are expected before losses of H_2 and CH_4 from a cyclic system such as the aglycone of digoxin and that elimination of H_2 after loss of H_2O is possible.



Scheme 3

Thermochemistry of eliminations from cyclohexanol and cyclohexenol

The appearance of these peaks due to H_2O and H_2 losses, in the spectrum of the digoxigenin, suggests that the peaks at m/z values 777 and 649 in the spectrum of the digoxin can be attributed to similar neutral losses from the aglycone portion of the molecule. However, the possibility of eliminating the water and the hydrogen molecules from the sugar portion of the molecule still cannot be excluded. In order to identify the sites of the elimination, additional deuterium exchange experiments were performed according to the procedure described by Soldin *et al.* [8]. They reported that, after keeping the

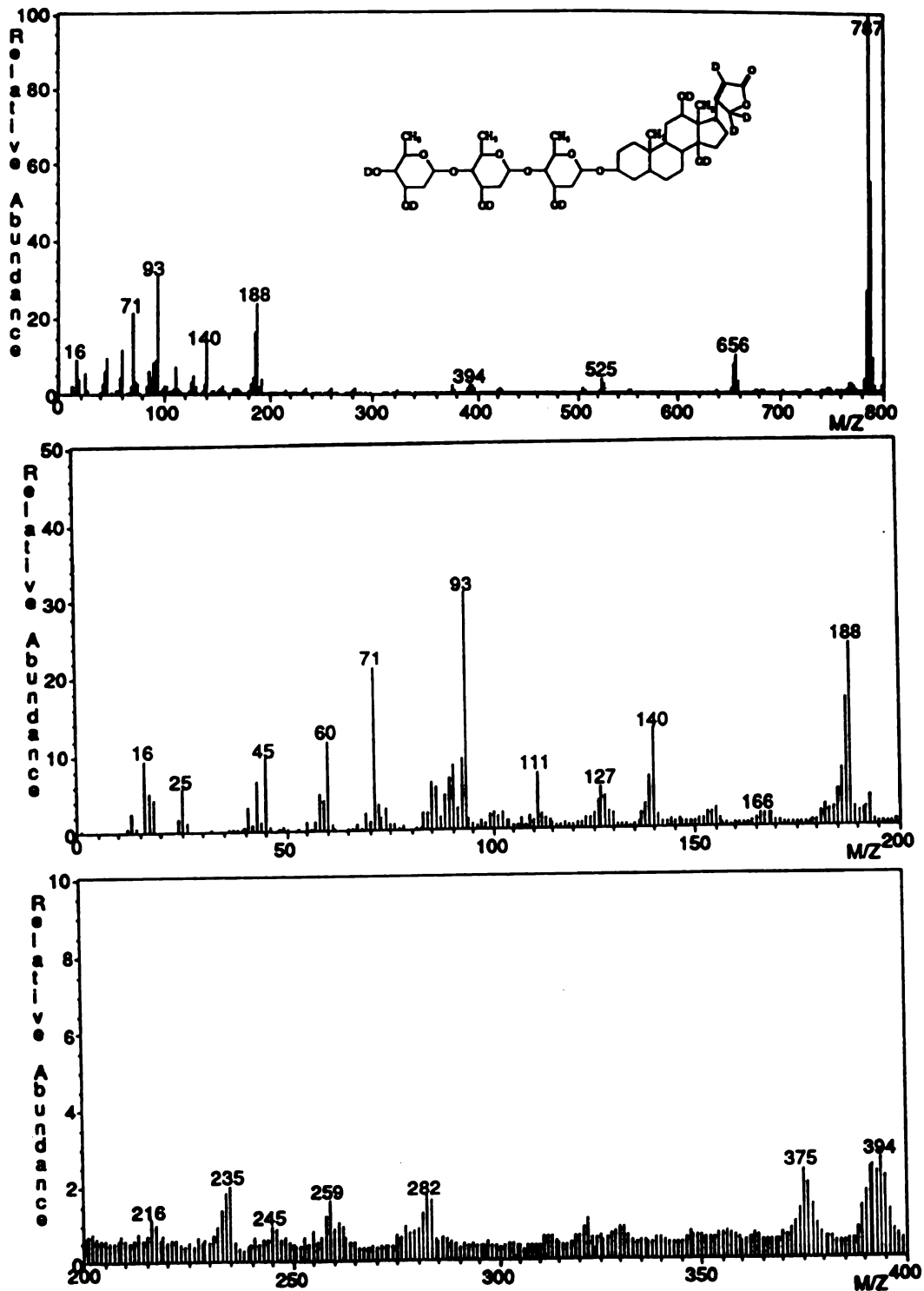


Figure 3.9 The negative ion FAB spectrum of digoxin-d₉.
(The bottom two charts are partially magnified.)

digoxin in D₂O at 363 K in a vacuum sealed vial for 17 hours under basic conditions, not only the OH protons are exchanged but also the protons at sites h and i in the butenolid ring. This means the incorporation of nine deuterons shifting the signal of the deprotonated (dedeuterated) molecule by eight mass units to m/z 787. The mass spectrum of this fully deuterated digoxin is shown in Figure 3.9, the mass shifts of the various ions in the spectrum are shown in Table 3.3. In the linked-scan spectrum of this ion, losses of 17 and 19 were observed suggesting the elimination of CH₃D and HOD. This provides evidence for 1,2 elimination of water. The mechanism of the methane loss is not straightforward. In order to eliminate CH₃D the deuterium from one of the OD groups has to be shifted. There are three possibilities for this shift. In two of these the deuterium is shifted from either one of the OD groups in the 12 or 14 position to the methyl group (position 18) via a five membered ring or in the third case the deuterium is shifted from site h (position 21 in the butenolid ring) to the methyl group through a six membered ring. To prove the involvement of site h in the methane elimination we back-exchanged the OH sites leaving only the three sites in the butenolid ring deuterated. In order to determine the deuterium content of the digoxin after this back-exchange the positive ion FAB mass spectrum was taken in the presence of Na⁺ ions. In this spectrum the quasi molecular ion, of the analyte, [M+Na]⁺, appeared at m/z 806 which means that the molecular weight of digoxin is shifted to 783 after the back-exchange meaning the presence of three deuteriums. Furthermore, the linked-scan studies showed losses of non-deuterated sugar thereby proving that the deuterium is incorporated in the aglycone unit. In the negative ion spectra (Figure 3.10), the quasi-molecular ion is characterized by an ion current at m/z 781. Thus, a deuteron is removed from the digoxin-d₃ upon the formation of this ion.

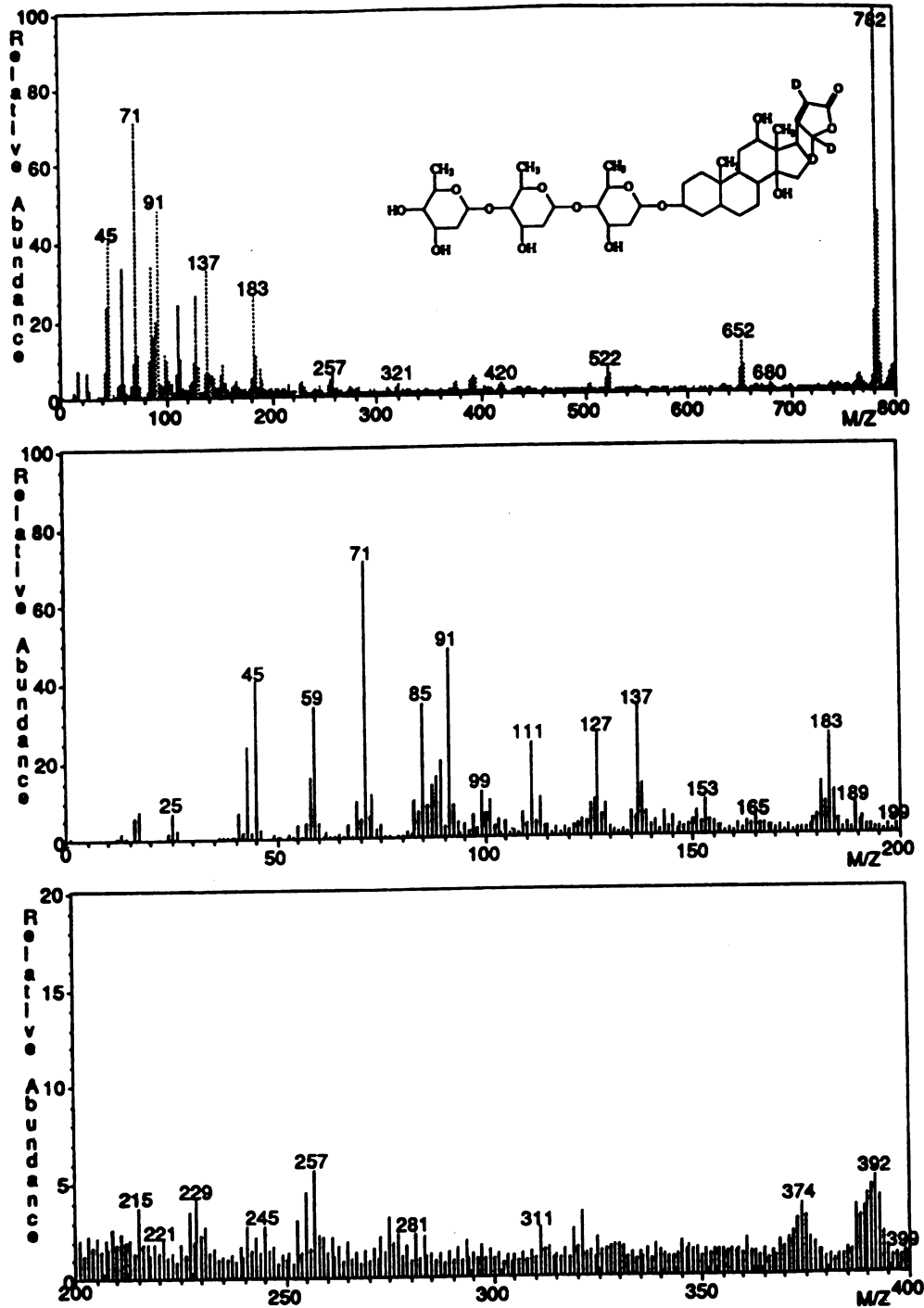
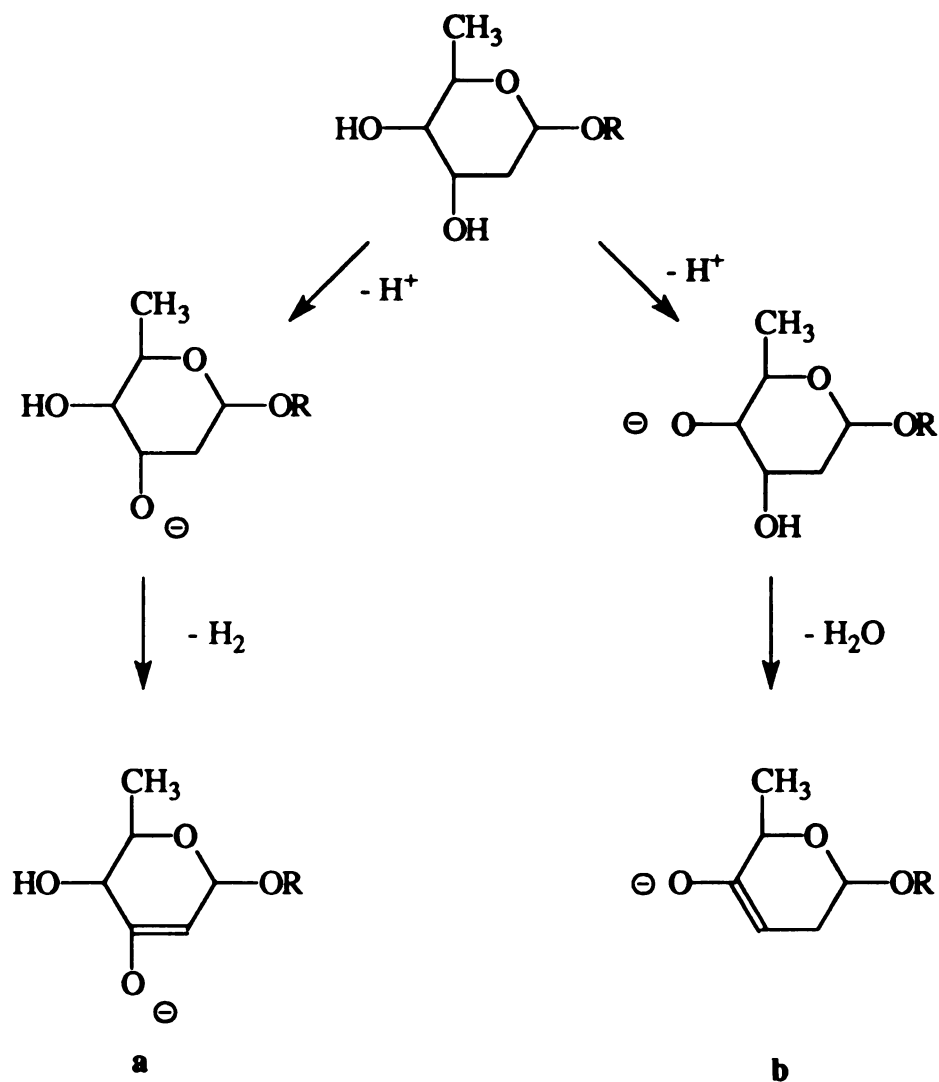


Figure 3.10 The negative ion FAB spectrum of digoxin-d₃.
(The bottom two charts are partially magnified.)

This is evidence for the deprotonation at site h in the butenolid ring. The loss of 17 was observed again thereby proving the shift of the deuterium from site h to the methyl group. The site of the water loss can be identified using the linked-scan spectrum of the parent ion 761 from the undeuterated digoxin. The loss of a dehydrated sugar produces an ion with m/z 649, and the loss of an intact terminal sugar results in an ion at m/z 631. Both of these ions are present in the CAD spectrum with similar relative intensities thereby providing evidence that the water loss can occur from the terminal sugar as well as from the intermediate sugars or from the aglycone. Examine the linked spectrum of the ion at m/z 631 (unfortunately it also contains fragment ions from the ion at m/z 633). In this spectrum there is an ion at m/z 501 which shows that the parent ion contained an intact sugar unit. This means that the ion at m/z 631 could be dehydrated in the first sugar or in the aglycone moiety. To decide which of these two sites is more probable let us look at the linked-scan spectrum of the parent ion 501. There is an indication for the loss of a dehydrated sugar (fragment at m/z 389) and also there is another ion at m/z 371 which indicates a dehydrated aglycone. From these results we can conclude that the elimination of water can take place from the terminal sugar units as well as from the aglycone moiety. Regarding the latter case consider again the spectrum of the gitoxin which has the same trisaccharide unit as the digoxin and differs only in the positions of the OH groups in the aglycone portion of the molecule (C-12 in digoxin, C-16 in gitoxin). In the case of gitoxin the loss of H_2O is enhanced, which can be due to the proximity of the OH group on C-16 to the possible charge site. According to Montaudo [28] the water elimination in oligosaccharides is a charge initiated process, which suggests that if the water was eliminated from the sugar portion of the digoxin, the spectra of digoxin and gitoxin would be

similar, since their sugar residues are identical. This also confirms that the deprotonation takes place in the aglycone portion of the molecule and the neutral losses under discussion are the results of inductive cleavage reactions in the aglycone. Based on the above observations the structural assignments for the fragment ions discussed so far can be made. These are the following. The ion at m/z 779 is designated as $[A-HOS_1OS_2OS_3OH]^-$, the assignment of the ion at m/z 777 is $[A-^3HOS_1OS_2OS_3OH]^-$, and finally the ions formed by the elimination of water from the above two ions at m/z values 761 and 759 can be designated as $[A-H-H_2OOS_1OS_2OS_3OH]^-$ and $[A-^3H-H_2OOS_1OS_2OS_3OH]^-$ respectively. These can be further justified by literature data. Loss of H_2 and H_2O from the $[M-H]^-$ alkoxide anions in the case of diols is a well-known phenomenon [30]. Similar results were reported in the OH^- negative chemical ionization spectra of $17\xi-R-5\alpha, 14 \beta$ -androstane- $14,17\xi$ -diols [31]. In our case the digoxin has three possible deprotonation sites in the aglycone portion. These are the two OH groups and the CH_2 group in the lactone ring. However, if the deprotonation occurs at one of the OH groups the resulting alkoxide anion can be stabilized by an intramolecular hydrogen bond involving the other OH group. According to references [30] and [31], if such a stabilization can take place, further fragmentation is inhibited, so we assume that the digoxin is deprotonated in the CH_2 group of the lactone ring. This deprotonation site is labeled as **h** in Figures 3.3. and 3.4, and is expected to be one of the most acidic sites in the molecule. Thus the H_2 and H_2O elimination reactions are inductive cleavages. They seem to further extend the conjugation to the D ring of the steroid structure. Possible structures of the products are presented in Figure 3.11. As a result of the subsequent water and molecular hydrogen losses the ring conjugation is extended, which provides a basis for the

stabilization of the negative charge remaining in this portion of the molecule. The elimination from the sugar portion is also possible. Possible mechanism for this is presented in Scheme 4.



Scheme 4

Elimination of water and hydrogen from the deprotonated terminal digitoxose

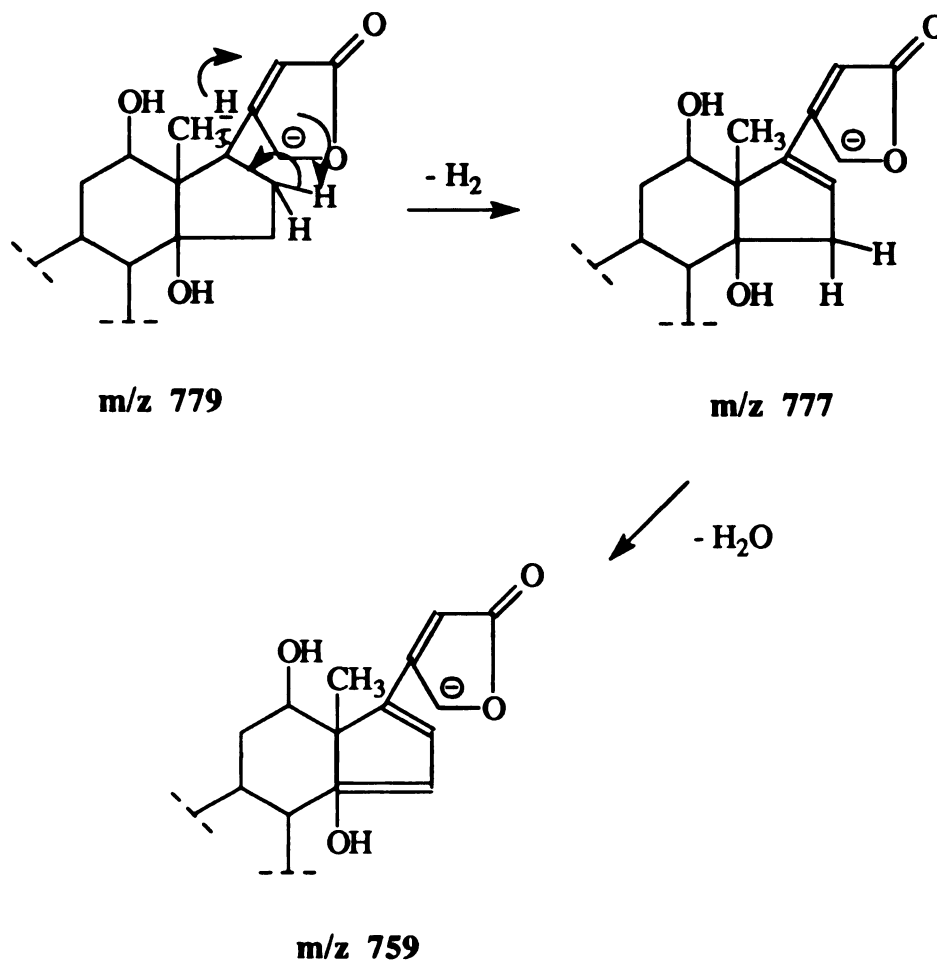


Figure 3.11 Possible structures for the digoxin fragment ions at m/z values 779, 777 and 759.

2. Discussion of the structure of the fragment ions characteristic of the cleavage of the glycosidic bonds (m/z 649, 519, 389 and 387, 129, 127, 111).

The following ions are characteristic of the cleavage of the glycosidic bonds. The first of them is represented by the ion current at m/z 649. The terminal glycosidic bond is cleaved such that the glycosidic oxygen remains on the fragment containing the aglycone. This cleavage, if our assumption about the site of the deprotonation being in the aglycone part is correct, should be accompanied by a hydrogen shift from the leaving sugar unit thus resulting in an ion at m/z 649 and a neutral loss of 130. This ion can be designated as $[A-HOS_1OS_2OH]^-$. Similar to the terminal glycosidic bond cleavage, fragmentation occurs also about the other two glycosidic bonds of digoxin followed by H shifts leading to ions at m/z 521, designated as $[A-HOS_1OH]^-$ and at m/z 389, labeled as $[A-HOH]^-$. The other possibility would be deprotonation in the sugar moiety followed by inductive cleavage of the glycosidic bonds. Thus, the ions produced are $[AOS_1OS_2O]^-$, $[AOS_1O]^-$ and $[AO]^-$. The corresponding ions from the lost sugar moieties appear at m/z values 129, 127 and 111. Since the neutral sugar portion lost in the cleavage of the terminal glycosidic bond has a mass of 131 Da if there is no H-shift from it to the aglycone containing moiety, and 130 Da after a H-shift, the ion corresponding to this has an m/z value of 129, $[HOS_3-H-H]^-$ and the ion at m/z 127 can be obtained via a molecular hydrogen loss from it. The ion at m/z 111 is formed by the elimination of a water molecule from the ion at m/z 129. Another ion at m/z 387 could have two different origins. This ion could be formed by a hydrogen molecule loss from the aglycone ion (m/z 389) and be designated as $[A-H-H_2OH]^-$ or could come from the sugar moiety after an H₂ loss, $[HOS_3OS_2OS_1-H -3H]^-$. The confirmation of these assignments

could be done by peak matching, however the intensity of these ions is very small and accurate mass measurement is hard to achieve. So the following experiment was done to confirm the origin of the ions at m/z 387 and at m/z 389. The spectrum of the digitoxin (case C in Figure 1) was taken. The spectrum is shown in Figure 3.12. Digitoxin has one less OH group on the aglycone, its sugar portion is the same, so its $[A-HOH]^-$ ion should appear sixteen mass units below the mass of the corresponding ion from the digoxin, that is at m/z 373. In the negative FAB mass spectrum of the digitoxin there is an ion at m/z 373, $[A-HOH]^-$, and also another ion at m/z 371, whose assignment is $[A-HOH-H_2]^-$, and is the result of a molecular hydrogen loss from the aglycone, consistent with our assignment for the structure of the ion at m/z 387 in the case of digoxin. But an ion at m/z 387 is also present in the digoxigenin spectrum, which must come from the sugar moiety. These experiments confirmed again that the ion current at m/z 387 in the spectrum of digoxin has two origins. It has contributions from both the sugar and also from the aglycone portion of the molecule and can have a double assignment. The extent of these contributions could be determined by separate studies of the CAD spectra of the sugar and the aglycone moiety. However, the small intensity of these ions makes these experiments hard to realize accurately. It is interesting to note the pattern in the fragment ions characterizing the sugar moieties. They are all appearing three mass units below the mass of the corresponding neutral. For example the ions at m/z 129 and 127 are corresponding to the neutral species with a mass of 131. This can be explained assuming that during the cleavage of the glycosidic bond an anion dipole complex is formed. When this complex dissociates one possibility is that the aglycone containing part carries the negative charge and the sugar is the neutral. However, there is another possibility for a proton exchange between

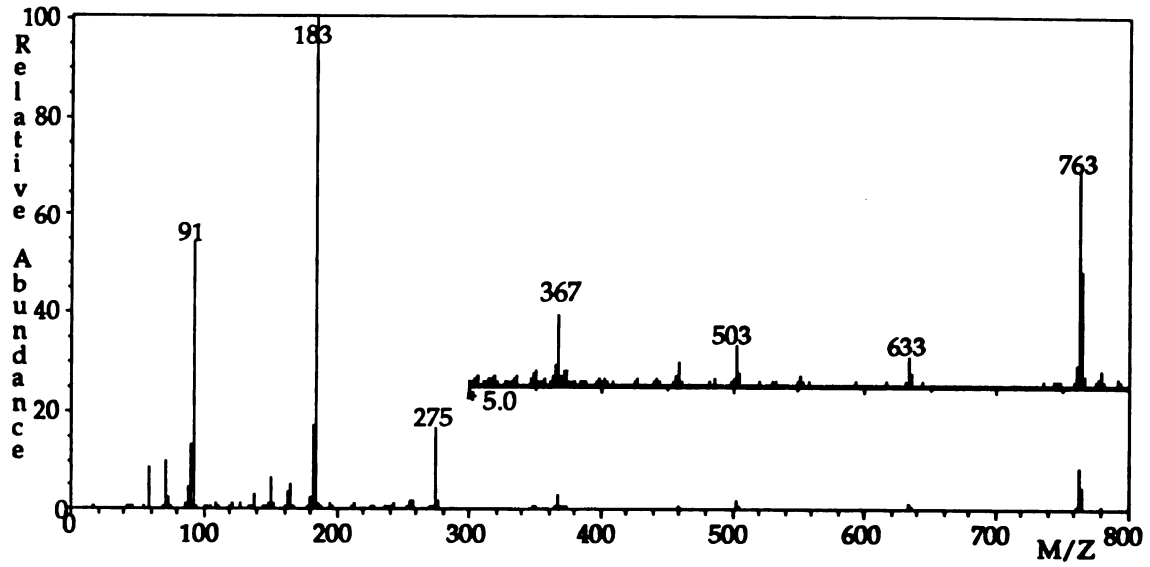
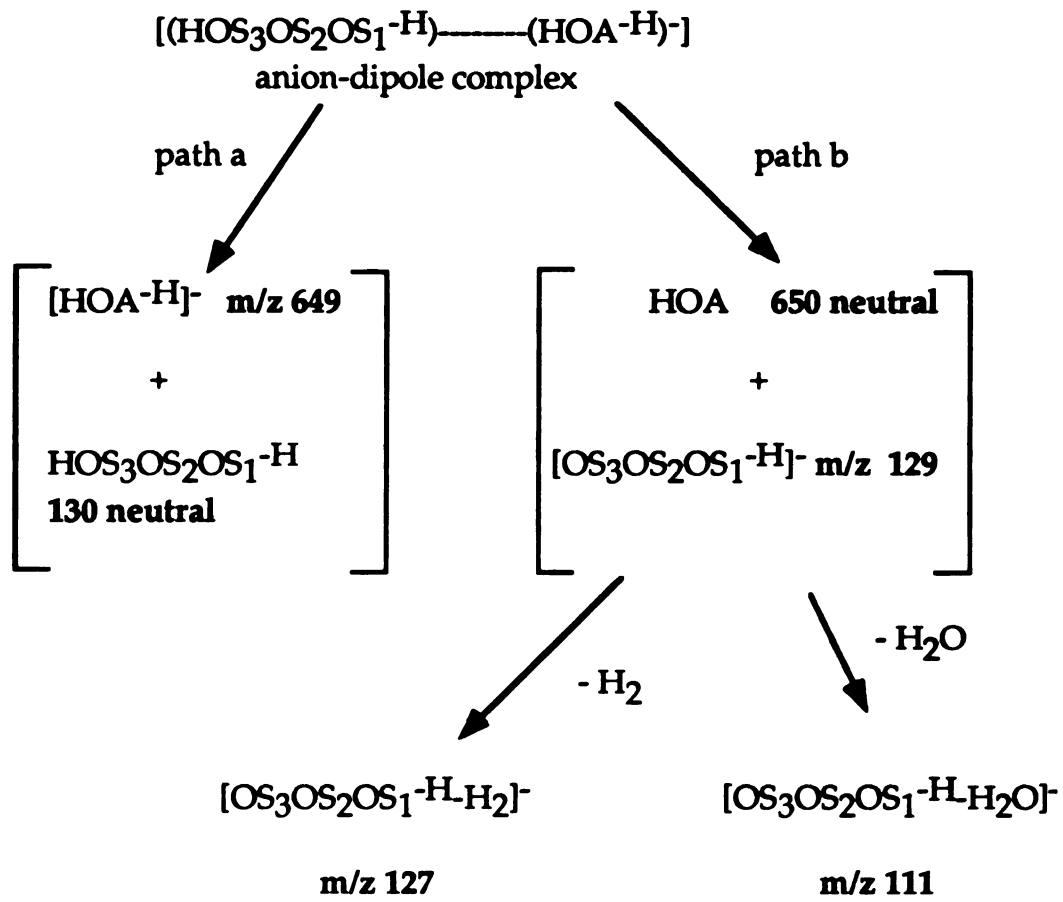


Figure 3.12 The negative ion FAB spectrum of digitoxin.

the aglycone containing anion and the sugar forming the ions at m/z 389 and 129 which can be designated as $[\text{HOS}_3\text{OS}_2\text{OS}_1\text{-H-H}]^-$ and $[\text{HOS}_3\text{-H-H}]^-$ respectively. These ions can fragment further by eliminating H_2 or H_2O . These processes are outlined in Scheme 5 for the cleavage of the terminal glycosidic bond. Another possibility is that the molecular hydrogen loss forming the ion at m/z 777 occurs from the terminal sugar. This is supported by the fact that in the CAD spectrum of the parent ion at m/z 777 the most intense daughter ion is the one at m/z 649, which contains an intact aglycone and two intact digitoxoses.

Besides the ions formed by the water losses from the deprotonated molecule and the cleavages of the glycosidic bonds another type of ion is also formed resulting in the ions represented by the ion currents at m/z 631 and 501. They can be due to a water molecule loss from the digitoxose (sugar) moiety of the ions at m/z 649 and 519, or can be formed by losing the terminal and internal sugars from the $[\text{M-H-H}_2\text{O}]^-$ ion. A CAD study on the parent ions at m/z 631 and 501 will provide experimental evidence for the favor of one of these possibilities. If, in the linked scan spectrum, the loss of the intact sugar can be detected, the ion at m/z 631 should be from the $[\text{M-H-H}_2\text{O}]^-$ ion (m/z 761) by losing its terminal sugar and the formation of the ion at m/z 501 is a similar process from the ion at m/z 631. These processes are consistent with the assumption that the charge is located in the aglycone portion and the glycosidic cleavage occurs remote from the charge site accompanied by H-shift from the sugar residue. This would imply the operation of a mechanism similar to that of proposed by Allison and Light [5] for the glycosidic cleavage in positive mode FAB.



Scheme 5

Cleavage of the terminal glycosidic bond through an anion-dipole complex.

As it can be seen in Table 3.1 loss of an intact sugar can be detected in the CAD spectrum of the parent ion at m/z 501. In the case of the ion at m/z 631 the CAD spectra could not be interpreted unambiguously as the spectrum also contains the daughter ions of the ion at m/z 633. In order to get further proof for the site of the deprotonation and for the occurrence of the hydrogen shift we examined the spectra of the deuterated digoxin- d_9 . In this spectrum (Figure 3.9) the ion formed by cleaving the first glycosidic bond appears at m/z 656 which means that, it is shifted by seven mass units relative to the normal mass spectrum (m/z 649) meaning that there are seven deuteria present in this fragment. This is only possible if the original site of the deprotonation (dedeuteration) was in the terminal sugar, not in the aglycone. Had it been the aglycone, then upon the cleavage of the glycosidic bond two deuteriums would have left with the terminal sugar leaving six behind and after a H-shift the ion would have had an m/z value of 655. In order for this fragment to appear at m/z value of 656 one deuterium has to shift from one of the OH groups of the terminal digitoxose. However, both of these hydroxyl groups are probably too far away from the glycosidic oxygen for such a shift to occur. However, there is an ion at m/z 655 that could have two origins. On the one hand, it can be formed from the ion at m/z 786 through the inductive cleavage of the first glycosidic bond, or it is also possible that it is a product of the remote site cleavage of the first glycosidic bond and formed via a hydrogen shift. The ratio of the relative intensities of the ion currents at m/z 787 to 656 is $100:10.52 = 9.5$ and that of ion currents at m/z 786 to 656 is $65.36:8.17 = 8$. This supports that the ion at m/z 655, indeed, has a double origin and that both the inductive cleavage and the remote site mechanism accompanied by a H-shift are operational. These experiments also yielded important information about the ions from the digitoxose residue. Namely,

the ions at m/z 127 and 111 are not shifted in the negative FAB spectrum of the digoxin-d₉. This is only possible if during their formation they lost the incorporated deuteria. At this point we can conclude that the cleavage of the glycosidic bond can occur via remote site reaction as well as through charge initiated fragmentation. The proposed mechanism has to account for the structure of the sugar ions.

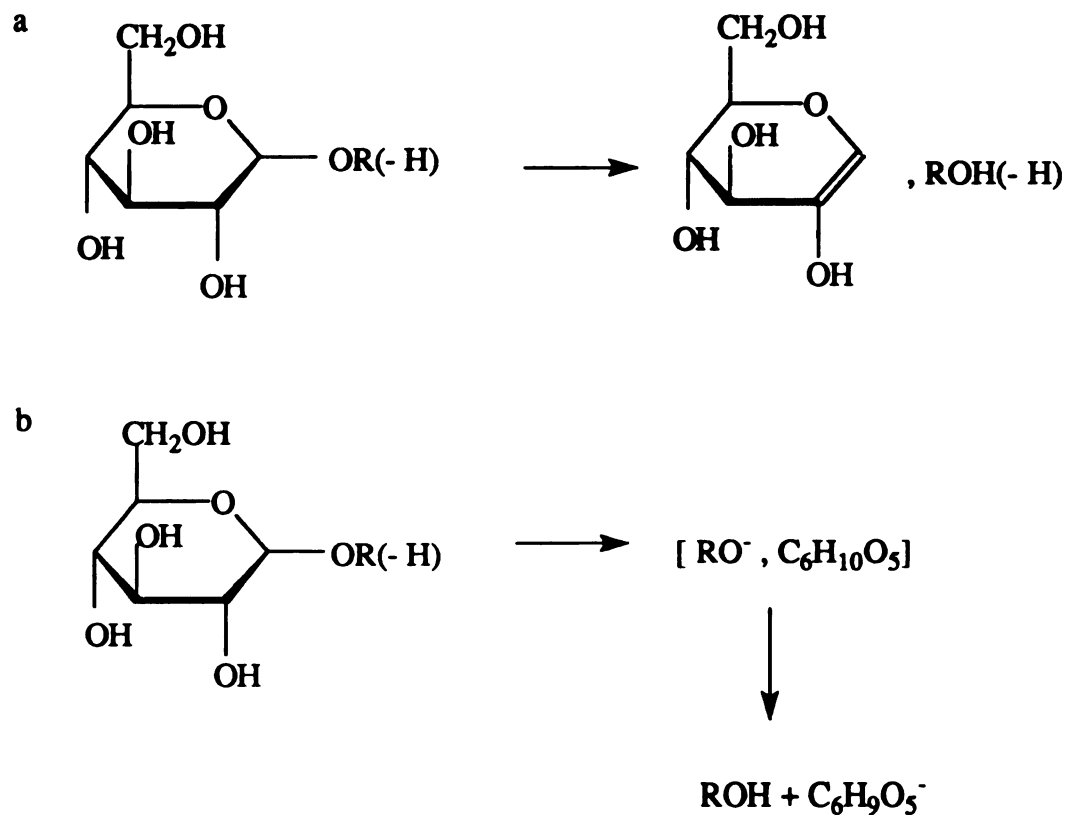
IV. Summary of the tentative assignments for the digoxin fragment ions. The mechanism of the glycosidic cleavage.

Tentative assignments for the fragment ions were based on low resolution mass spectral data and where the intensities of the ions allowed accurate measurements were confirmed by linked scanning and peak matching results. The fragment ions of the digoxin, their compositions and designations can be seen in Table 4.3 together with the mass shifts in the deuterium exchange spectra of digoxin-d₆ and digoxin-d₉.

These assignments can be altered where mechanistic information suggests different possibilities, or rules out one of the double assignments. At this point let us summarize the discussion so far. The data from the mass spectrum of the related cardiac glycosides, gitoxin and digitoxin, and the aglycone digoxigenin confirms that the deprotonation takes place in the aglycone and the fact that the majority of the fragment ions contain the aglycone also supports this, however there are indications that the deprotonation can also occur in the sugar residue. The loss of the water and the molecular hydrogen are probably results of inductive cleavages from the digitoxose moiety and also from the aglycone which, in addition can also eliminate methane. Now we will focus on the mechanism of the glycosidic

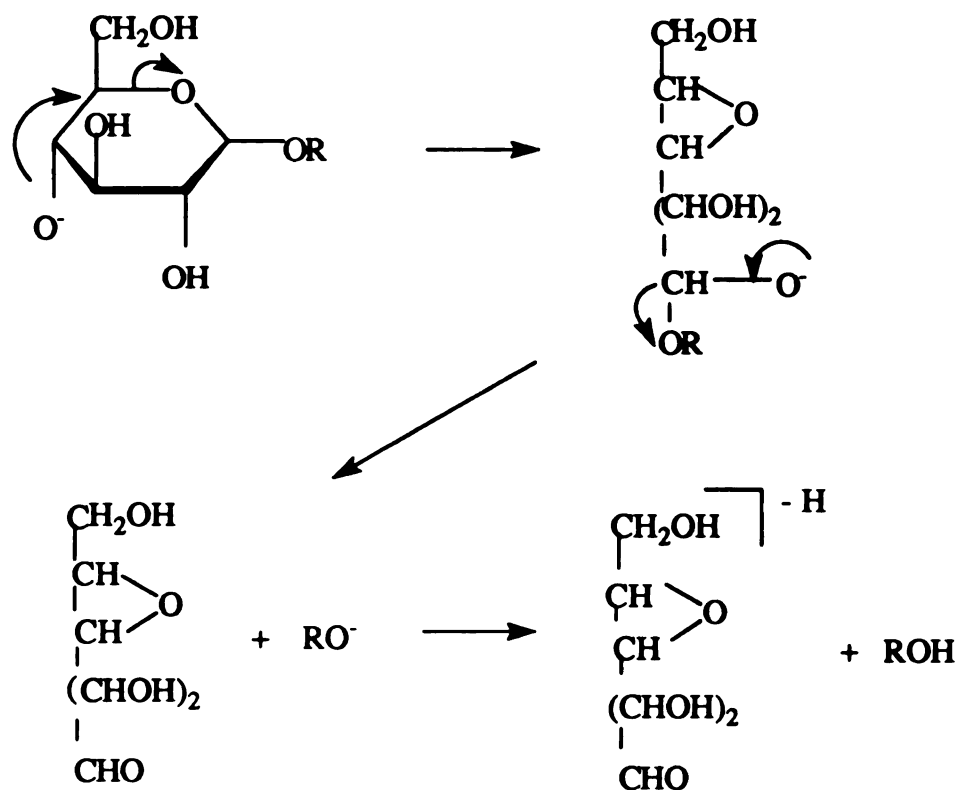
cleavage and see if it can be understood in terms of the above assignments or if they require reconsideration. The cleavage of the glycosidic bonds of oxyanions generated by FAB has been studied by several authors [28, 29, 34-38]. It has been shown that in the negative spectrum of methyl glycosides the main decomposition pathway is the loss of methanol [35] which means that the glycosidic cleavage is accompanied by a hydrogen shift. According to the proposed mechanisms for the glycosidic cleavage in oligosaccharides in their negative ion spectra [34, 35] one possibility is a hydrogen atom transfer to the interglycosidic oxygen atom from the C-2-H bond of the sugar ring (Scheme 6 a) followed by the cleavage of the glycosidic bond. An alternative pathway could be a proton exchange between the anion which is formed in the first decomposition step, and the remaining part of the sugar. In this case the hydrogen atom in the hydroxylic group of the methanol molecule comes from the most acidic sites of the sugar molecule, i.e. from the hydroxyl groups (Scheme 6 b). In these cases the cleavage takes place remote from the charged site. These processes both are consistent with our proposed mechanism in Scheme 5. However in solution chemistry it was shown that arylglycosides were cleaved by strong bases, such as OH^- , or CH_3O^- , through a vicinal attack by the C-2 oxyanion on the anomeric carbon atom [38]. According to Savagnac *et al.* [36] in the gas phase the chemistry is different. They proved that the hydroxyl group at C-2 does not participate since the glycosidic cleavage was not affected by a 2-O methylation. It was also observed experimentally that the configuration of the anomeric carbon has no effect on the cleavage which rules out the possibility of an intramolecular nucleophilic attack on C-1, that would be expected to be highly stereospecific. They suggest that the glycosidic cleavage occurs after opening the sugar ring by a vicinal attack at the C-5 carbon atom. Then the formed hemi-acetals

fragment into methanolate anion and 4,5 anhydro sugar which exchange another proton before their separation into charged and neutral species (Scheme 7).



Scheme 6

Possible reactions for the glycosidic cleavage of deprotonated oligosaccharides



Scheme 7

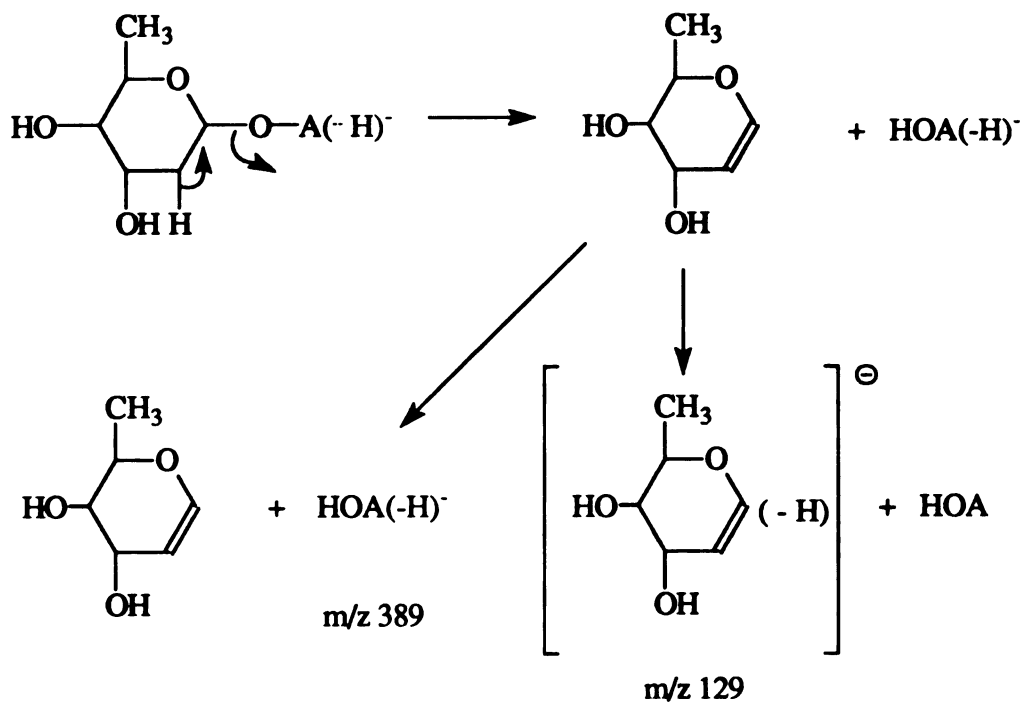
Charge induced cleavage of the glycosidic bond through hemiacetals.

In these cases the fragmentation is induced by the charged site. Studying the spectrum of digoxin it seems that in our case the charge remote fragmentation is the more probable, as it is consistent with the previously proposed H-shifts and the higher relative intensity of the ion containing the aglycone after the glycosidic cleavage. However as we concluded from the study of the digoxin-d₉, charge induced cleavage is also operational in which case the anion-dipole complex, formed in the first step, dissociates by transferring a proton from the sugar to the aglycone containing anion forming the ion at m/z 129 in the case of the terminal digitoxose. It is

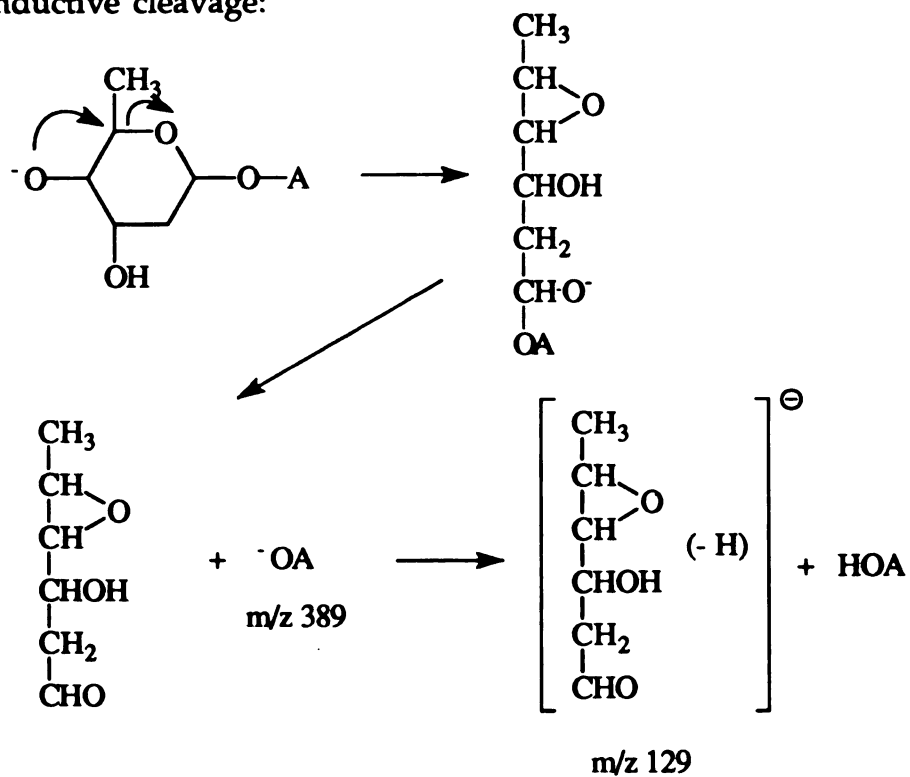
interesting to mention that although there are some ions present from the terminal sugar unit in the low resolution FAB spectrum of digoxin they are missing from the CAD spectrum of the parent ion at m/z 779. The implication is that there is a different mechanism operational in the CAD experiment. Such a behavior has been reported by Gross [39] who found that the collisional activation of the $[M-H]^-$ anions of sulfate steroid conjugates predominantly yields fragment ion arising from reactions occurring remote from the charge site. However, in the case of glucuronide conjugates, ions primarily from charge driven fragmentations are present in the linked scan spectrum of the quasi-molecular ion. As in the normal FAB spectrum of digoxin the formation of the ions at m/z 129 and 127 can be explained by both charge-initiated process and charge-remote processes as well. It is possible that in CAD, the remote site fragmentation is the major process. This can be understood since in the charge-remote mechanism the driving force is the internal energy content of the molecule which can be increased by collisions with the inert gas [40]. Furthermore, if an anion-dipole complex is formed as an intermediate during the glycosidic cleavage only the primary decomposition products of this complex would be expected to appear in the CAD spectra. Thus, those species that are formed via proton transfer within this complex could disappear from the CAD spectrum implying that under MS/MS conditions the anion-dipole complex decomposes before the transfer reaction can occur between the dipole and the anion. This is accordance with the results of Longevialle and Botter [41] who calculated that the reorientation for a proton transfer in difunctional steroids would take about 10 psec. Thus, complex-mediated proton transfers are reactions of low energy ions. The above mentioned fragmentation pathways, both the remote-site and the charge-induced glycosidic cleavage, are outlined in Scheme 8. The proposed

charge induced mechanism for the glycosidic cleavage not only is in accordance with the structures of the sugar fragment implied by the results of the deuterium exchange experiments but also explains the different appearance of the MS/MS and the normal MS spectra.

Remote site cleavage:



Inductive cleavage:



Scheme 8

Conclusions

The mass spectrometric analysis of the digoxin and related cardiac glycosides were performed by negative ion mode FAB mass spectrometry. Our studies suggest that in the case of digoxin in glycerol, in the desorption/ionization process, the ionization occurs after desorption, in the gas phase via Brönsted acid/base reactions. This is confirmed by the similarities between the negative FAB spectrum and the negative OH/CI spectrum reported by Bruins [14]. The deuterium exchange experiments and the study of the gitoxin FAB spectra suggest that there is no single, specific deprotonation site for the digoxin. In case of such a large molecule with many possible deprotonation sites one has to take into account a distribution of deprotonated species at different sites. It is highly likely that not the most stable quasi-molecular ion produces the majority of fragment ions in the spectrum. In our case, the digoxin is deprotonated in both the aglycone and also in the sugar residue.

The data presented from the digoxin mass spectrum show that the majority of the fragment ions contains the aglycone portion, suggesting that after the fragmentation the negative charge most likely resides in this residue. There are three major types of fragment ions. First, there are ions that are formed by the elimination of water, methane and molecular hydrogen. Second and third, ions resulted from the cleavage of the glycosidic bond and either contain the aglycone moiety or formed from the carbohydrate residue. The loss of H₂ and water from the aglycone is a facile process, which can be rationalized by the extension of the conjugated double bond system. The elimination processes are taking place by charge retention in the aglycone containing fragment. However, it was shown that similar small neutral

losses can occur from the sugar residues also. The relative intensities of these ions are significantly different and characteristic in the case of isomeric molecules. The cleavage of the glycosidic bonds was explained as a result of a remote charge fragmentation and also as an inductive cleavage involving an anion-dipole complex intermediate. In the latter case the sugar ions observed in the spectrum can be formed by transferring a proton from the digitoxose containing dipole to the aglycone containing anion. This is consistent with the fact, that these ions corresponding to the digitoxose fragments are missing from the CAD spectrum of the $[M-H]^-$ parent ion. The mechanistic study suggests that, although to a different extent, remote site cleavages accompanied by H-shift, as well as charge initiated processes can occur in the case of large organic anions. In the latter case it is proposed that a long range hydrogen transfer occurs within the anion dipole complex. Under high energy conditions (CAD) this complex simply dissociates before the proton transfer can take place.

From the comparative study of the spectra of digoxin and related cardiac glycosides, together with their aglycone portions it can be concluded that the negative FAB/MS is a valuable tool to distinguish between the isomers of these compounds.

REFERENCES

1. McLafferty, F.W. *Interpretation of Mass Spectra*, 3rd ed.; University Science: Mill Valley, CA, 1980.
2. Barber, M.; Bordoli, R.S.; Sedgewick, R. D.; Tyler, A. N. *J. Chem. Soc. Chem. Commun.* 1981, 325.
3. Hunt, D. F.; Crow, F. W. *Anal. Chem.* 1978, 50, 1781-1784.
4. Smith, A.L.C.; Field, F.H. *J. Am.Chem. Soc.* 1977, 99, 6471.
5. Light, K.J.; Allison, J. *J. Am. Soc. Mass Spectrom.* 1990, 1, 455.
6. Holmes, J. L. *Org. Mass. Spectrom.* 1985, 20, 169.
7. McCloskey, J. A. In *Methods in Enzymology*, Ed. McCloskey, J.A. 1990, 193, pp. 329. Academic Press, San Diego.
8. Deber, C.M.; Stone, J.; Soldin, S.J. *Anal. Letters* 1989, 22(13&14), 2783.
9. Ciucanu, I.; Kerek, F. *Carbohydr. Res.* 1984, 131, 209.
10. Caldwell, K.A.; Gross, M. L. *J. Am. Soc. Mass Spectrom.* 1994, 5, 72.
11. Light, K.J.; Kassel, D.B.; Allison, J. *Biomed. Environ. Mass Spectrom.* 1989, 18, 177.
12. Rouse, J. C.; Allison, J. *J. Am. Soc. Mass Spectrom.* 1993, 4, 259.
13. Gaskell, S.J.; Brownsey, B.G.; Brooks, P.W.; Green, B.N. *Biomed. Mass Spectrom.* 1983, 10, 216.
14. Bruins, A.P. *Int. J. Mass Spectrom. and Ion Phys.* 1983, 48, 185.

15. **Bowie, J.H. *Mass Spectrometry Reviews* 1990, 9, 349.**
16. **a: Schroder, E.; Munster, H.; Budzikiewicz, H. *Org. Mass Spectrom.*, 1986, 21, 707.**
b: Sunner, J.; Morales, A.; Kebarle, P. *Anal. Chem.* 1987, 59, 1378.
c: Sunner, J.A.; Kulatunga, R.; Kebarle, P. *Anal. Chem.*, 1986, 58, 1312.
17. **Go, K.; Kartha, G.; Chen, J.P. *Acta Cryst.* 1980, B36, 1811.**
18. **Lias, S.G.; Bartmess, J.E.; Liebman, J.F.; Holmes, J.L.; Levin, R.D.; Mallard, W.G. *J. Phys. Chem. Ref. Data* 1988, 17, Suppl.1.**
19. **a: Aue, D.H.; Webb, H.M.; Bowers, M.T. *J. Am. Chem. Soc.*, 1973, 95, 2699.**
b: Longevialle, P.; Milne, G. W. A.; H.M. Fales *J. Am. Chem. Soc.*, 1973, 95, 6666.
20. **Szekely, G.; Allison, J. *J. Am. Soc. Mass Spectrom.* 1997, 8, 337.**
21. **Sunner, J.A.; Kulatunga, R.; Kebarle, P. *Anal. Chem.*, 1986, 58, 2009.**
22. **Noest, A. J.; Nibbering, N.M.M. *J. Am. Chem. Soc.* 1980, 102, 6427.**
23. **Debrauwer, L.; Paris, A.; Rao, D.; Fournier, F.; Tabet, J.C. *Org. Mass Spectrom.*, 1992, 27, 709.**
24. **Sethi, S. K.; Smith, D.L.; McCloskey, J.A. *Biochem. and Biophys. Res. Comm.* 1983, 112, 126.**
25. **Squires, R.R.; DePuy, C.H.; Bierbaum, V.M. *J. Am. Chem. Soc.*, 1981, 103, 4256.**
26. **Bowers, M.T. *Gas Phase Ion Chemistry*, Academic Press, New York 1979 p.117-118.**
27. **Adams, J. *Mass Spectrom. Rev.* 1990, 9, 141.**

28. Garozzo, D.; Giuffrida, M.; Impallomeni, G.; Ballistreri, A.; Montaudo, G. *Anal. Chem.* **1990**, *62*, 279.
29. Ballistreri, A.; Montando, G.; Garozzo, D.; Giuffrida, M.; Impallomeni, G. *Rapid Comm. Mass Spectrom.* **1989**, *3*, 302.
30. Gaumann, T.; Stahl, D.; Tabet, J.C. *Org. Mass Spectrom.* **1983**, *18*, 263.
31. Beloeil, J.C.; Bertranne, M.; Stahl, D.; Tabet, J.C. *J. Am. Chem. Soc.* **1983**, *105*, 1355.
32. Roy, T. A.; Field, F. H.; Lin, Y. Y.; Smith, L. L. *Anal. Chem.* **1979**, *51*, 272.
33. Bush, K. L.; Glish, G. L.; McLucky, S. A. *Mass Spectrometry/Mass Spectrometry: Techniques and Applications of Tandem Mass Spectrometry*; VCH: New York, **1988**.
34. Dell, A.; Ballou, C. *Carbohydr. Res.* **1983**, *120*, 95.
35. Dell, A.; York, W.S.; McNeil, M.; Darvill, A.D.; Albersheim, P. *Carbohydr. Res.* **1983**, *117*, 185.
36. Prome, J.; Aurelle, H.; Prome, D.; Savagnac, A. *Org. Mass Spectrom.* **1987**, *26*, 6.
37. Garozzo, D.; Impallomeni, G.; Montando, G.; Spina, E. *Rapid Comm. Mass Spectrom.* **1992**, *6*, 550.
38. Gasman, R.C.; Johnson, D.C. *J. Org. Chem.* **1966**, *31*, 1830.
39. Tomer, K.B.; Gross, M.L. *Biomed. Environ. Mass Spectrom.*, **1988**, *15*, 89.
40. Wysocki, V. H.; Bier, M.E.; Cooks, R.G. *Org. Mass Spectrom.* **1988**, *23*, 627.

41. a: Longevialle, P.; Botter, R. J. *J. Chem. Soc. Chem. Commun.* **1980**, 823.
b: Longevialle, P.; Botter, R. J. *Int. J. Mass Spectrom. Ion Phys.* **1983**, 47, 179.
c: Longevialle, P.; Botter, R. J. *Org. Mass Spectrom.* **1983**, 18, 1.

CHAPTER FOUR. MATRIX-ASSISTED LASER DESORPTION IONIZATION MASS SPECTROMETRY

Introduction to Matrix Assisted Laser Desorption Ionization - Time of Flight Mass Spectrometry (MALDI-TOF MS)

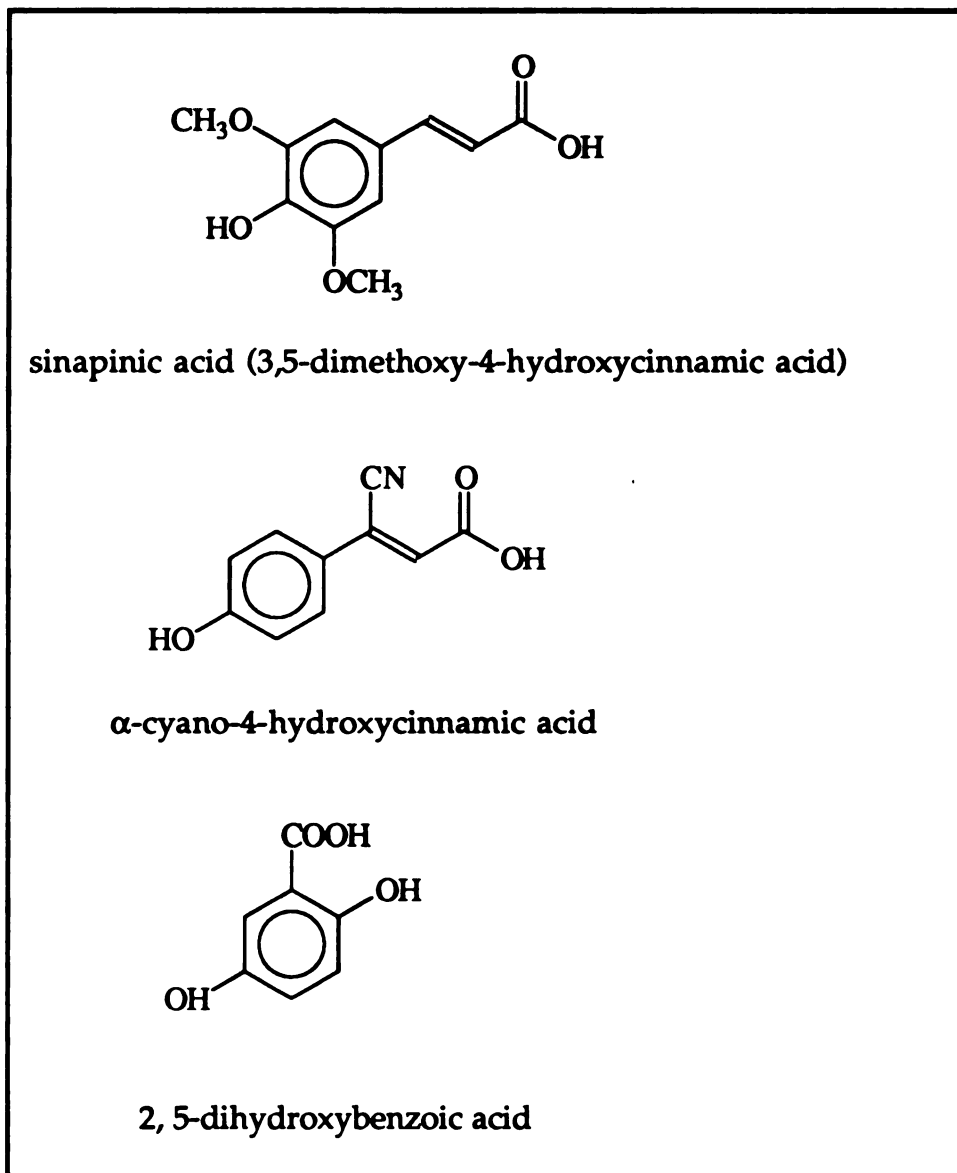
Among the numerous desorption/ionization techniques developed in the past two decades for the analysis of large, non-volatile and thermally labile compounds, matrix-assisted laser desorption/ionization and electrospray (ES) show the greatest promise for the mass spectrometric analysis of biopolymers with molecular weights ranging from a few thousands to a few hundred thousand Daltons [1].

The first attempts to generate ions of organic molecules by direct laser desorption/ionization date back to the early 1970s [2, 3]. However, the size of the molecules that can be desorbed and ionized was limited to ~ 1,000 Da for biopolymers and up to 9,000 Da for synthetic polymers. In these early laser desorption experiments the desorption is the result of resonant absorption at the laser wavelength, thus the molecular weight limitation is believed to be due to the photodissociation of the sample. The main breakthrough toward higher molecular masses came when Hillenkamp and Karas' research group realized that the use of a matrix could circumvent this problem [4].

As the technique now stands, a small amount of analyte molecules, which usually exhibit only moderate absorption at the laser wavelength, is embedded in a solid matrix consisting of small, highly absorbing species. The most often used matrices are sinapinic acid (3,5-dimethoxy-4-hydroxycinnamic acid), 2,5-dihydroxybenzoic acid, and α -cyano-4-

hydroxycinnamic acid. The structures of these compounds are shown in Table 4.1.

Table 4.1 The structures of the most commonly used MALDI matrices.



The production of ions in matrix-assisted laser desorption/ionization depends on the production of a suitable composite material, consisting of the matrix and the analyte biopolymer.

Practical methods for MALDI sample preparation

A number of different methods have been described in the literature for growing analyte-doped matrix crystals. The original method described by Karas and Hillenkamp has been named as the "dried-droplet" method. It involves drying a droplet of a solution containing the matrix (1-10 millimolar) and the analyte (1-10 micromolar). A variant of this method was proposed by Vorm, *et al.* [5]. They first placed a thin layer of the matrix compound onto a metal surface and then put a droplet of analyte-containing solution on top of the layer of the matrix compound. As the droplet dries it dissolves some of the matrix which crystallizes onto the substrate matrix layer when the droplet dries completely. The crystallized matrix layer is very thin, allowing for more reproducible mass measurements.

It is possible to grow large, protein-doped crystals under near-equilibrium conditions, rather than in a rapidly drying droplet [6]. Supersaturated matrix solutions containing the protein will form crystals that can be used directly in an ion source. Supersaturation can be achieved by heating and cooling or by slow evaporation. The slow crystallization method produces higher doping levels than the dried droplet method, especially if there is gentle agitation of the crystallization chamber during the crystal growth.

A recently developed technique of producing crystals for use in MALDI ion sources involves growing thick films of matrix crystals [7]. The substrate for the crystals, usually a flat piece of metal, is first covered with the matrix material, by rapidly drying a solution of the matrix dissolved in an organic

solvent, such as 2-propanol. The small matrix crystals that cover the surface are then crushed and smeared over the substrate surface, resulting in a well-adhered layer of crystalline matrix. A saturated solution containing the matrix and the analyte is then deposited onto the surface and allowed to dry slightly. The crystalline material on the substrate acts to seed crystal formation at many sites on the surface, resulting in the rapid growth of a rather uniform polycrystalline film of analyte-doped matrix crystals over the surface. The liquid drop can be removed by blotting. The resulting film is very strongly adhered to the substrate and can be washed thoroughly to remove any contaminants that were present in the sample solution.

The prepared samples are introduced into the mass spectrometer where the deposit is desorbed/ionized by a pulsed laser. The laser pulse widths are typically in the 1-100 ns range. The lasers used most often emit in the UV-range of the spectrum and the radiation wavelength depends on the laser type, most often 266 nm (frequency-quadrupled Nd-YAG laser) or 337 nm (N₂-laser). The spectra presented in this work were obtained on an instrument equipped with a pulsed N₂ laser emitting at 337 nm, with a laser pulse width of 3 ns. The irradiance is controlled by an attenuator and is increased gradually until the desorption/ionization threshold is reached. The irradiance of the laser has proven to be one of the most critical parameters in the MALDI experiment. The threshold irradiance is typically $\sim 1 \text{ MW/cm}^2$ [8], and is necessary to produce ions from the sample. Below this threshold the ion production falls off to the fifth power of the laser irradiance [8]. Laser irradiances higher than the threshold dramatically decrease the mass resolution in the spectra obtained. The size of the laser spot and the angle of incidence of the laser beam on the sample surface do not seem to be critical. Laser spot sizes of 10-300 μm in diameter and angles of incidence of 30°-75°

are used typically. Because of the pulsed nature of the ion ejection, the ions are usually analyzed by time-of-flight (TOF) mass spectrometers.

Time-of-flight mass spectrometry

The most straightforward TOF spectrometer consists of an ion source and a collector situated at the opposite end of an evacuated tube. The ions are formed in the ionization region of the source, in the case of MALDI, by irradiating the sample with a laser. They are then accelerated out of the source toward the collector by a constant or a series of constant electric fields. Assuming that all ions ejected from the target have zero initial velocity, they all acquire the same kinetic energy ($KE = 1/2 mv^2 = zeV_{acc}$). Thus, the velocity of the ions in the field free region is a function of the ratio of their mass, m , to their charge, z . Therefore, when the ions reach the collector they have separated into bunches corresponding to m/z . If only singly charged ions are present, the lightest group reaches the detector first and is followed by groups of successively heavier mass. The flight time of the ions can be calculated by the following equation:

$$t = t(\text{in ion source}) + t(\text{in flight tube}) = \sqrt{\frac{m}{z}} \left[\sqrt{\frac{2d}{eV_{acc}}} + L \sqrt{\frac{1}{2eV_{acc}}} \right] \quad (4.1)$$

where V_{acc} = accelerating voltage, V_{acc}/d = electric field in ion source, z = number of charges, $e = 1.609 \times 10^{-19}$ C, m = mass of the ion, and L = the length of the flight tube. Time of flight instruments are well suited to be combined with an ion source producing ions at a point source in space and time and also have a theoretically unlimited mass range which is essential for the

analysis of large molecules. A unique advantage of the TOF mass spectrometers is the speed with which a spectrum can be obtained. A second advantage is that the entire mass spectrum can be recorded for each ionization pulse. The third major advantage is that, the accuracy of a TOF mass spectrometer depends on electronic circuits rather than on extremely accurate mechanical alignment and on the production of highly uniform magnetic fields. The main disadvantage of the TOF mass spectrometers has been their limited resolution. If all ions were formed in a plane parallel to the source electrodes and with zero initial velocity the flight time would be the same for all ions which had the same m/z , and the resolution would be limited only by the detecting equipment. In practice, the resolving power of a TOF mass spectrometer depends on its ability to reduce the time spread caused by the ever-present initial space and initial kinetic energy distributions. In the case of MALDI-TOF mass spectrometry, since the sample is in solid form deposited on a sample plate, the low resolution is primarily due to the relatively large initial kinetic energy spread of the ions rather than the initial spatial distribution of the ions. This energy spread is a result of the explosive expansion of the matrix from the surface which accelerates the ions by supersonic jet formation [9]. Efforts have been made to improve the resolution by decreasing the initial kinetic energy spread of the ions by preparing more homogeneous samples, using reflectrons or applying time-lag focusing [10] to correct for the energy distribution.

In a reflectron instrument, an ion mirror (reflector) as first proposed by Mamyrin and coworkers [11] is placed in the flight path of the ion packets. The reflectron voltage is higher than the source voltage thereby ensuring that all the ions (those above normal energy as well) get reflected. Ions with higher energy penetrate the mirror further before reversing direction, while

low energy ions reverse early. By properly selecting the mirror voltage and the mirror and drift tube lengths, all the ions in a packet will arrive at the detector at the same time even though they left the source with different energies.

Time-lag focusing as introduced by Wiley and McLaren [10], uses a time delay between the formation of the ions and the application of the accelerating potential. During this delay time, the ions, because of their initial velocities, move to new positions which sacrifices the space resolution. However choosing the proper delay time corrects for the initial energy (velocity) distribution, thereby improving the resolution in overall. The concept of time-lag focusing can be understood with the help of Figure 4.1.

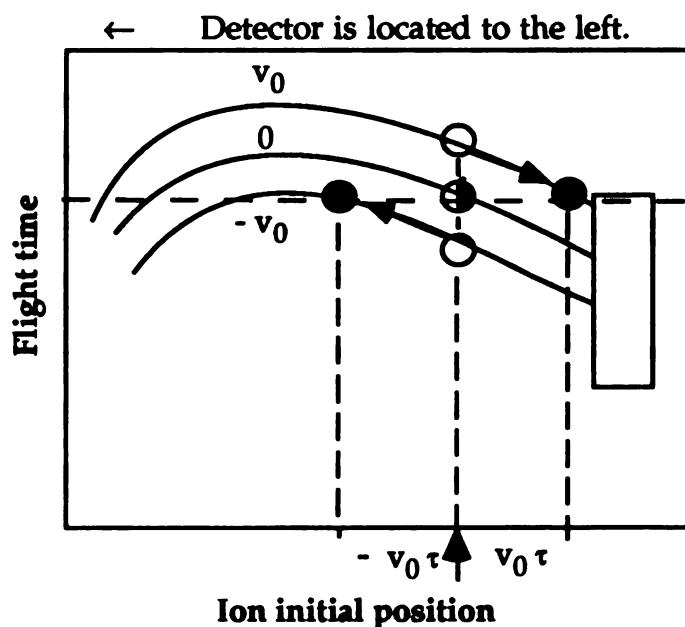


Figure 4.1 Curves of flight time *vs.* initial position used in discussion of time lag focusing. Adapted from reference [10].

Consider three ions produced at the same initial position but with different initial velocities 0 , and $\pm v_0$. Without time lag their flight time would be

different, as indicated by the open circles in Figure 4.1. The ion with $-v_0$ having the shortest flight time, and the one with $+v_0$ the longest, since this latter ion at first moves away from the detector against the accelerating field until it stops and starts to be accelerated out of the source. Thus, the difference in the flight times of the ions having initial velocities $+v_0$ and $-v_0$ is the so called turn around time. Since the velocities do not change, during the lag period each ion moves on its own curve to a new position (indicated by black circles) which changes its flight time. By appropriate choice of the lag τ a situation can be achieved where the flight time is the same for all three ions. The same concept is applied in MALDI-TOF mass spectrometry in the recently introduced method of delayed-ion extraction (DE) [12, 13]. In this case, besides the above described energy focusing effect, it is also believed that, in the DE experiment, ions are allowed to disperse in the ion source due to their initial velocity while the neutrals are pumped away [12]. The reduction in ion-molecule collisions minimizes the associated spread in translational energies.

Recent advances in coupling MALDI with Fourier-transform mass spectrometry (FT-MS) also show great potential in accurate analysis of high mass (i.e., $> 10,000$ Da) ions [14-16].

The experiments described in this dissertation were done on a Voyager Elite MALDI-TOF mass spectrometer (Perceptive Biosystems, Vestec BioSpectrometry Products, Cambridge, MA). The schematic diagram of this reflectron-time-of-flight mass spectrometer is shown in Figure 4.2.

In the Voyager Elite MALDI-TOF mass spectrometer, the ions generated by irradiating the sample with the laser are accelerated by a two stage electric field of maximum 23.5 kV toward the flight tube (field free

region). The flight times of the accelerated ions can be calculated using equation 4.1. However, in practice, the mass of an ionic species is not

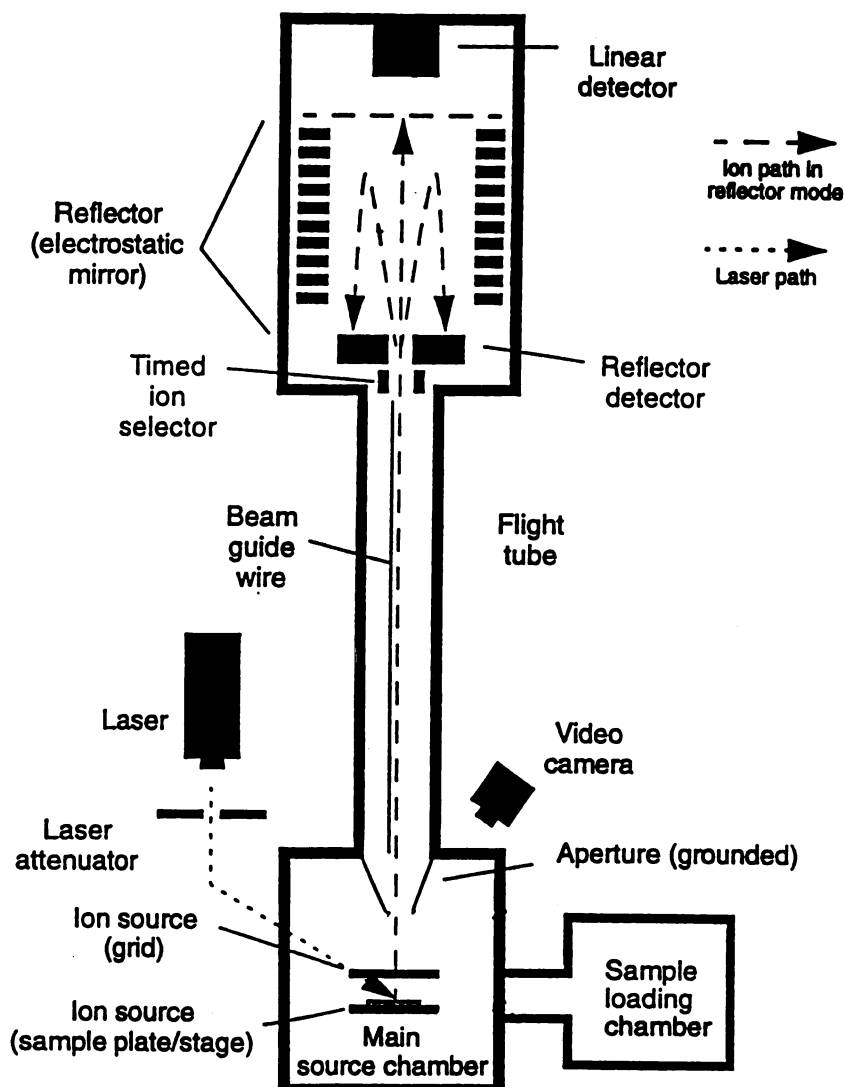


Figure 4.2 Schematic diagram of the Voyager Elite Single-Stage Reflectron Time-of-Flight Mass Spectrometer.

calculated by that equation. Instead, the mass-to-charge ratio values are assigned by calibration. The square root of the mass-to-charge ratio value, m/z , is proportional to the flight time for a given mass spectrometer with fixed values of d , V_{acc} , and L . That is,

$$\sqrt{\frac{m}{z}} \sim t$$

$$\text{or, } \sqrt{\frac{m}{z}} = c_1 \times t \quad 4.2$$

The flight time, t , is the duration between the time when the ions were generated and when they reach the detector. However, the actual starting time is difficult to measure, so a reference point in time is registered by a photodiode which receives a part of the pulsed laser beam. The time relative to this reference point, t' , and the actual flight time, t , differ by a constant value, c_2 . Therefore,

$$\sqrt{\frac{m}{z}} = c_1 \times t' + c_2 \quad 4.3$$

At least two known points of $(m/z, t')$ values, obtained by the use of standard samples, are necessary to calculate the values of c_1 and c_2 .

The most common type of detector is composed of a conversion dynode and an electron multiplier. The former generates electrons or small ions from the impinging ions. The latter multiplies the number of electrons to generate a larger electrical current. The detector used on the Voyager Elite, is a microchannel plate. Microchannel plates are photo-electric devices consisting of a parallel array of independent channel electron multipliers capable of ion, electron, UV-photon, and soft-X-ray detection and signal amplification. Thus, they function as a conversion dynode and as an electron

multiplier at the same time. Typical channel diameters are in the range of 10-100 μm and have length-to-diameter ratios between 40 and 100. The channel matrix is usually fabricated from lead-glass and the channel walls are coated with a semiconductor, for instance silicon-dioxide. High output technology (HOT) microchannel plates (MCP) are capable of a signal amplification of 10^7 [17].

The main problem in ion detection is that the high mass ions generated by MALDI move too slow to generate electrons efficiently on the conversion electrode. The yield of secondary electrons from the conversion electrode is a function of the momentum of the impinging ions [1]. A high acceleration voltage in the ion source or post-acceleration before the detector may be used to increase the momentum of ions and thus increase the detection efficiency. Post-acceleration is often used in the reflectron-time-of-flight instruments, with typical acceleration voltages of 3~5 kV.

MALDI spectra are dominated by peaks representing the intact protonated molecules in the positive ion mode. Peaks corresponding to fragmentation are rarely observed in the spectra. The lack of fragmentation makes this technique ideal for mixture analysis [18-20]. Although, peptides and proteins are the main biocompounds investigated by MALDI, the technique can be applied to oligonucleotides [21-25], oligosaccharides [26-28], glycoconjugates [29, 30] and synthetic polymers [31-33].

Later studies using reflectron-TOF mass spectrometers revealed that MALDI ions undergo post-source fragmentations [34, 35], but the fragments are not separated from the protonated molecules by a linear TOF mass spectrometer. However, in a reflectron-TOF instrument they could be separately detected. As was mentioned earlier in this Chapter, in the reflectron-TOF instruments an ion mirror is placed at the end the flight tube.

Without potential applied to the reflector, all fragment ions from post-source decay (PSD) are detected at the end of the first field free (FFR) region as an increase in the peak width of the intact $[M+H]^+$ because they have approximately the same velocities as this precursor ion. However, these PSD fragment ions have kinetic energies (KE) that are different from each other and less than the precursor ion's, and it is this characteristic that enables them to be separated by their mass in the reflector. By lowering the potential applied to the reflector, a particular mass range of lower KE fragment ions will fully penetrate the reflector comparable to that of the intact $[M+H]^+$ ions at full reflector potential. As a result, these specific PSD fragment ions will become focused onto the second detector at the end of the second FFR. The entire mass range of PSD fragment ions for a particular precursor ion can be detected by lowering the reflector potential in several intervals. Typically, the ratio of the mirror voltage to the acceleration voltage is lowered in steps, in a way that each ratio is about 75% of the preceding ratio. The observable fragment ion mass is proportional to the mirror ratio times the parent ion mass. Basically, the reflectron is tuned to sequentially focus the lower energy fragments, and a series of related spectra are obtained. A special program then combines the spectra into a single spectrum showing the parent ion and its fragments.

Once the formation of PSD fragment ions had been discovered, the question of how the precursor ions are activated for subsequent decomposition has been raised. In the next chapter the results of the work done with regards to the mechanism of activation in MALDI-PSD are described. Glykoalkaloids were used as model compounds. Comparisons are made with high and low energy collisional activation used in FAB-MS.

REFERENCES

1. Hillenkamp, F.; Karas, M.; Beavis, R. C.; Chait, B. T. *Anal. Chem.* **1991**, *63*, 1193A-1202A.
2. Posthumus, M. A.; Kistemaker, P. G.; Meuzelaar, H. L. C.; Brauw, M. C., *Anal. Chem.* **1978**, *50*, 985-991.
3. Kupka, K. D.; Hillenkamp, F.; Schiller, C., *Advances in Mass Spectrometry*, Heyden & Sons, London, Vol. 8A, pp. 935-941 (1980).
4. Karas, M.; Bachmann, D.; Bahr, U.; Hillenkamp, F. *Int. J. Mass Spectrom. Ion Proc.* **1987**, *78*, 53-68.
5. Vorm, O.; Roepstorff, P.; Mann, M. *Anal. Chem.* **1994**, *66*, 3281-3287.
6. Xiang, F.; Beavis, R.C. *Org. Mass Spectrom.* **1993**, *28*, 1424-1429.
7. Xiang, F.; Beavis, R.C. *Rapid Commun. Mass Spectrom.*, **1994**, *8*, 199-204.
8. Ens, W.; Mao, Y.; Mayer, F.; Standing, K. G. *Rapid. Commun. Mass Spectrom.* **1991**, *5*, 117-123.
9. Zhang, J-Y., Nagra, D. S.; Li, L. *Anal. Chem.* **1993**, *65*, 2812-2818.
10. Wiley, W. C.; McLaren, I. H. *Rev. Sci. Instrum.* **1955**, *26*, 1150-1157.
11. Mamyrin, B. A.; Karataev, V. I.; Scmikk, D. V.; Zagulin, V. A. *Sov. Phys. JETP* **1973**, *37*, 45.
12. Brown, R. S.; Lennon, J. J. *Anal. Chem.* **1995**, *67*, 1998.
13. Vestal, M. L.; Juhasz, P.; Martin, S. A. *Rapid Commun. Mass Spectrom.* **1995**, *9*, 1044.
14. Castro, J. A.; Koster, C.; Wilkins, C. L. *Rapid Commun. Mass Spectrom.* **1992**, *6*, 239-241.
15. Castro, J. A.; Koster, C.; Wilkins, C. L. *Anal. Chem.* **1993**, *65*, 784-788.
16. Wood, T. D.; Schweikhard, L.; Marshall, A. G. *Anal. Chem.* **1992**, *64*, 1461-1469.
17. Galileo Electro-Optics Corporation (Sturbridge, MA) Sales Catalog

18. Karas, M.; Bahr, U.; Giebmann, U. *Mass Spectrom. Rev.* **1991**, *10*, 335-357.
19. Karas, M.; Bahr, U.; Ingendoh, A.; Nordhoff, E.; Stahl, B.; Strupat, K.; Hillenkamp, F. *Analytica Chimica Acta* **1990**, *241*, 175-185.
20. Beavis, R. C.; Chait, B. T. *Proc. Natl. Acad. Sci. USA* **1990**, *87*, 6873-6877.
21. Spengler, B.; Ying, P.; Cotter, R. J.; Kan, L. S. *Rapid Commun. Mass Spectrom.* **1990**, *4*, 99-102.
22. Huth-Fehre, T.; Gosine, J. N.; Wu, K. J.; Becker, C. H. *Rapid Commun. Mass Spectrom.* **1992**, *6*, 209-213.
23. Nordhoff, E.; Kirpekar, F.; Karas, M.; Cramer, R.; Hahner, S.; Hillenkamp, F.; Kristiansen, K.; Roepstoff, P.; Leizus, A. *Nucleic Acids Res.* **1994**, *22*, 2460-2465.
24. Tang, K.; Allman, S. L.; Chen, C. H.; Chang, L. Y.; Schell, M. *Rapid Commun. Mass Spectrom.* **1994**, *8*, 183-186.
25. Schneider, K.; Chait, B. T. *Org. Mass Spectrom.* **1993**, *28*, 1353-1361.
26. Harvey, D. J. *Rapid Commun. Mass Spectrom.* **1993**, *7*, 614-619.
27. Stahl, B.; Thurl, S.; Zeng, J.; Karas, M.; Hillenkamp, F.; Steup, M.; Sawatzki, G. *Anal. Biochem.* **1994**, *223*, 218-226.
28. Stahl, B.; Steup, M.; Karas, M.; Hillenkamp, F.; *Anal. Chem.* **1991**, *63*, 1463-1466.
29. Huberty, M. C.; Vath, J. E.; Yu, W.; Martin, S. A. *Anal. Chem.* **1993**, *65*, 2791-2800.
30. Sutton, C. W.; O'Neill, J. A.; Cottrell, J. S. *Anal. Biochem.* **1994**, *218*, 34-46.
31. Bahr, U.; Deppe, A.; Karas, M.; Hillenkamp, F. *Anal. Chem.* **1992**, *64*, 2866-2869.
32. Danis, P. O.; Karr, D. E. *Org. Mass Spectrom.* **1993**, *28*, 923-925.
33. Buerger, H. M.; Mueller, H. M. Seebach, D.; Boernsen, K. O.; Schaer, M.; Widmer, H. M. *Macromolecules* **1993**, *26*, 4783-4790.

34. Kauffman, R.; Kirsch, D.; Kaufmann, R. *J. Phys. Chem* **1992**, *96*, 9678-9684.
35. Kaufmann, R.; Kirsch, D.; Spengler, B. *Int. J. Mass Spectrom. Ion Proc.* **1994**, *131*, 355-385.

CHAPTER FIVE. MALDI/POST-SOURCE DECAY

Do MALDI/PSD Spectra Suggest High- or Low-Energy Collisional Activation?

The MALDI Spectra of Glycoalkaloids and their Use as Probes of the PSD Process

When introduced, matrix-assisted laser desorption/ionization time-of-flight mass spectrometry (MALDI-TOF MS) [1] provided only molecular weight information by yielding a single mass spectral peak for analytes such as peptides. As the use of reflectrons for the analysis of fragment ions developed it was found that peptides did fragment post-source, thus the possibilities of structure elucidation for high molecular weight compounds has been extended by using Post-Source Decay (PSD) analysis [2, 3].

How are ions activated in MALDI-PSD for subsequent fragmentation? One possibility is that the energy is deposited during the D/I process in the form of photoexcitation [4]. Ehring *et al.* [4] proposed a photochemical model for ion formation in UV-MALDI. This model assumes the photoionization of the absorbing matrix molecules, followed by ion/molecule reactions to form the observed ions (protonated molecules in the positive ion mode). The total energy absorbed by the analyte molecules is usually very low, thus their photoionization is negligible. In the above mentioned model, it is proposed that the protonated analyte ions are formed in proton transfer processes between the different matrix-related species and the analyte molecules. The processes leading to protonated and deprotonated analyte molecules are shown in Figure 5.1. The key idea of this ionization model is that ionization of highly absorbing compounds by UV lasers is initiated by a photoionization step yielding radical molecular photoions.

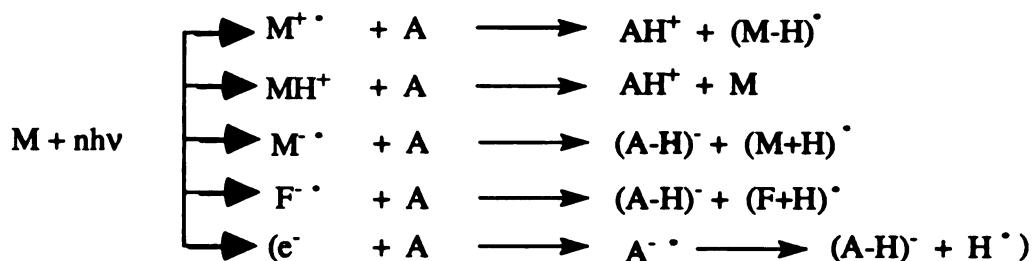


Figure 5.1 Photochemical ionization processes for analyte ions in MALDI. M = Matrix; F = Fragment; A = Analyte

For typical polar organic molecules which all have ionization energies in the range 7.5-9 eV in the gas phase, the required energy may be provided by a resonant two-step absorption (the photon energy: 266 nm, 4.6 eV; 337 nm, 3.7 eV) of two single photons or by sharing the energy of two singly excited molecules. The radical molecular ions may undergo chemical reactions with neutral molecules. As a result of this reaction, protonated matrix or protonated analyte molecules can be formed as shown in Figure 5.1. The absorbing matrix molecules undergo extensive fragmentation. Their fragment ions can also participate in proton transfer reactions with the analyte molecules. The electrons, resulting from the photoionization of the matrix molecules may be captured by an analyte molecule forming a radical anion, which can subsequently be stabilized by losing a hydrogen radical, as also shown in Figure 5.1. In the case of the matrix molecules, their fragmentation can be due to photochemical activation. However, for analytes the energy deposited by the laser radiation is too small to induce considerable fragmentation.

The second possibility is that the activation is due to collisions. If so, collisions could take place during acceleration in the desorbed "plume", or they could take place throughout the flight tube with the residual gas

molecules [3, 5]. In these cases, comparisons with collisionally activated dissociation (CAD) spectra obtained by means of other mass spectrometric methods could be useful to answer the question whether the PSD spectra of peptides, the most highly studied analytes in MALDI, resemble high or low energy CAD spectra. The answer to this might help to understand the contributions of in-plume activation, which would be relatively low energy, and activation in the flight tube, in which case the ions have their highest kinetic energies. Unfortunately peptides may not be the best compounds to probe these questions. Rouse *et. al.* [6] has suggested that the MALDI-PSD spectra are remarkably similar to those obtained by low energy CAD in tandem mass spectrometry in case of peptides. While in case of "in-flight" collisional activation the spectra are similar to those obtained in the high energy CAD [7], since side chain losses are usually observed in case of high energy collisional activation. Others have discussed the fact that the cleavages observed in MALDI-PSD are a combination (or mixture) of both types of CA - high and low energy [8].

High and low energy CAD spectra of glycoalkaloids by means of LSIMS have been recently reported [9]. The spectra are strikingly different, suggesting that such compounds may be good probes of the PSD process. Glycoalkaloids produce strong response in MALDI spectra, and PSD spectra can be obtained which are rich, since glycosidic bonds cleave and the aglycone fragments as well. These results will be presented, and their similarities to high and low energy CAD spectra discussed.

Fundamental Aspects of Collision-Activated Dissociation of Ions

In the second chapter it was discussed how to obtain collisionally activated dissociation spectra on a double focusing mass spectrometer. Next, the basic mechanisms of CAD will be briefly summarized.

Collision-activated dissociation (CAD) [also called collision-induced dissociation (CID)] of ions in a mass spectrometer plays an increasingly significant role in ion structure determination. CAD has attained even greater importance with the advent of fast atom bombardment, laser desorption, matrix assisted laser desorption and electrospray techniques for generating ions from large, nonvolatile molecules. These techniques usually produce (quasi)-molecular ions with very little fragmentation. Collisional activation of these "molecular" ions and subsequent dissociation to various fragment ions provides structural information required for identification and characterization. The CAD studies of polyatomic ions as presently practiced had their origins in the study of metastable ion dissociation in the field-free regions of double focusing mass spectrometers, first introduced as a technique by Barber and Elliott [10]. Collisional activation in time of flight instruments by increasing the flight tube pressure was demonstrated by Jennings [11] and Haddon and McLafferty [12]. These studies showed that CAD spectra were qualitatively similar to those obtained by electron impact ionization, and they provided definitive information on fragmentation pathways. Low-energy CAD experiments were performed by combining two or more quadrupole mass filters in tandem [13].

Basic mechanisms of CAD were investigated in early experimental and theoretical studies of simple di- and triatomic ions [14]. Molecular beam-scattering studies of small molecular ion O_2^+ , N_2^+ , NO^+ and H_2^+ have defined

the basic mechanisms often invoked in discussing the CAD of polyatomic ions at low collision energies [15]. In these small ion systems, particularly at low energy, the dominant dynamics feature is a pronounced peak of product ion intensity that forward scattered with essentially the velocity of the primary ion beam. This follows the predictions of the spectator-stripping model, where one atom (or molecular fragment) is essentially stripped away and the remainder of the ion or molecule proceeds in flight with little or no change in momentum.

For the di- and triatomic ions cited, it is postulated that lengthening the bond connecting the struck atom to the rest of the ion or an electronic state change to a weakly repulsive or nonbonding state causes the bond energy to decrease during the collision to a negligible value so that momentum exchange with the non interacting ion or fragment is minimal [16].

The fundamental studies of small ions have provided invaluable insights into the basic CAD mechanisms. However, it can hardly be expected that these principles can be applied directly to polyatomic ions. For this reason, the pioneering studies of Herman *et al.* [17] on the CAD of CH_4^+ provides a starting point for interpreting the CAD of polyatomic systems. For CH_4^+ , the reaction



was investigated and a number of important characteristics of polyatomic CAD were established.

It is useful to consider CAD as proceeding via two steps that are separable in time. The first is collisional activation where a fraction of an ion's kinetic energy is transferred into internal energy of the ion, followed by unimolecular dissociation of the internally excited ion.





The formal requirement for applying the above two step mechanism is that the neutral M_2 not be present in the force field of the excited ion M_1^{+*} during the dissociation step. This interpretation is rationalized in terms of typical collision times for CAD. For example, if the interaction distance (molecular diameter) is 2 Å, the collision time for an 8-keV energy ion of m/z 44 with a low velocity neutral is 10^{-15} sec, too short for nuclear motion to occur (the time scale for such a process is 10^{-14} - 10^{-13} s). At 5 eV the collision time increases to 4×10^{-14} sec, still much shorter than the time scale typical for an ion dissociation (10^{-12} - 10^{-5} sec) in mass spectrometry. This mismatch in the characteristic excitation and dissociation times allows one to consider the two processes as sequential. Another assumption often made in interpreting CAD experiments is that the relative kinetic energy of the ion and neutral after fragmentation is small. That is the two fragments move collinearly with nearly the same velocity. [For those cases where kinetic energy release cannot be neglected, the maximum in the velocity distribution remains interpretable as the average velocity of the excited precursor ion, while the distribution is broadened by energy release.]

The activation step has been the most elusive goal in understanding CAD. Knowledge of the internal energy distribution of activated ions is the essential first step in applying unimolecular decay theories to describe the fragmentation step. Using the center of mass (CM) reference frame to describe the collision pair, the precursor ion and the neutral collide collinearly at 180° , and the excited ion and the recoiling neutral retreat from the CM after the collision. The kinetic energy and momentum of the CM of the collision pair is unchanged in the collision. In this frame the kinetic energy of the system is

$$KE = 1/2 \mu v_r^2 \quad \text{where, } \mu = M_1 \times M_2 / (M_1 + M_2)$$

M_1 and M_2 are the masses of the colliding particles, and v_r is the relative velocity. Since the kinetic energy of the CM is conserved in a collision process, only the relative kinetic energy of the collision partners is available for conversion into internal energy.

Variations in fragment ion distributions occur because of differences in the amount of acquired internal energy, which depends on the chosen method of activation. Variations in ion distributions can also be attributed to such factors as dissimilar reaction times, the form of energy deposited, the amounts of ion scattering upon excitation, and the different angles over which the ions are collected. Two major methods of ion activation are: collision of accelerated ions with a "stationary" gas phase target in the (1) high-energy (keV) and (2) low-energy (eV) ranges of laboratory kinetic energy.

Mechanism of High-Energy Collisional Activation

In reference [14] Durup discussed four basic mechanisms of CAD:

- (1) vertical electronic excitation to a dissociative state,
- (2) adiabatic dissociation following momentum transfer,
- (3) complete inelastic collision with an orbiting complex formation,
- (4) collision induced pre-dissociation.

Efficient conversion of ion translational energy into internal energy occurs when the collision interaction time (t_c) and the period of the internal mode that is being excited (τ) are comparable [18]. For an ion of m/z 1000 and with a translational energy of 8 keV, the value of t_c for an interaction path with target molecule of several Å is about 10^{-14} sec. The Bohr period of a valence electron is of similar duration. Thus, collisions at kiloelectronvolt energies are expected to result in excitation of electronic modes.

Redistribution of the excitation energy to vibrational modes results in bond cleavage. Excitation of rotational/vibrational modes is also possible but would be less efficient since the interaction time is 10 times shorter than the period of a molecular vibration. From the center-of-mass considerations shown above we have seen that the maximum amount of kinetic energy available for conversion into internal energy of the ion depends on the relative kinetic energies of the ion and the target gas and their masses. Increasing the kinetic energy of the ion or increasing the molecular weight of the collision gas will increase the available energy, whereas increasing the mass of the ion will decrease the available energy. In studies of internal energy deposition it was demonstrated that an average energy of about 1-3 eV (1 eV = 23.06 kcal/mol) is deposited into an ion in a high-energy collision, but that the distribution of deposited energies exhibits a high-energy tail extending beyond 15 eV for internal energy [19, 20]. The probability of a collision depends on the target gas pressure and the collision cross section of the collision between the ion and the target gas species.

Low-Energy Collisions

Low-energy CA is most often carried out in quadrupole and hybrid sector-quadrupole mass spectrometers. Collisions at low energies are no longer expected to result in excitation of electronic modes. The typical interaction time of a projectile ion of mass 200 and a translational energy of 30 eV with a target molecule over a few angstroms is on the order of 10^{-13} sec. This length of time is longer than the time of an electronic transition thus, the probability of the excitation of such a transition is reduced. This interaction time however, is comparable to the reciprocal of most vibrational

frequencies. Under such conditions, the collisions are nonadiabatic, and the interaction is said to have an impulsive character that can effectively induce energy transfer [21]. The subsequent transfer of translational to vibrational energy is believed to occur by internuclear momentum transfer. The most important observation in a comparison of low- and high energy-CA is the superiority of CAD at high energy over low energy for large organic ions. The differences in the extent of fragmentation obtained by using low- and high-energy activation methods can be explained in terms of the amount of internal energy deposited by a collision. High-energy CA deposits an average of 1-3 eV internal energy with a high energy tail up to 15 eV. Conversely, low-energy CA deposits low average energies with an energy distribution exhibiting no significant high-energy tail. It is generally observed, that in high-energy CAD additional fragmentation pathways are opened up and the spectra contain more fragment ions relative to the low energy CAD.

The Use of Glycoalkaloids as Test Compounds for the Mechanism of Activation in MALDI-PSD

In the case of glycoalkaloids, which are nitrogen containing steroidal glycosides found in potato tubers and green tomatoes, the high and low energy CAD spectra are considerably different [9]. We have decided to obtain MALDI-PSD spectra for these compounds to determine which activation mechanism(s) is operational in case of MALDI-PSD. The analysis of these compounds in minute amounts in mixtures (typically well suited for MALDI analysis) is also of importance, since they are natural toxins, occurring in all parts of plants of the Solanum species [22]. These toxins are considered to

form a natural resistance of the plant against parasites and diseases. In the potato plant, high concentrations of glycoalkaloids occur in the peel of the tuber (concentration about 300–600 mg/kg), in the sprouts (about 2000–4000 mg/kg) and in the flowers (3000–5000 mg/kg) [23]. The glycoalkaloid level averaged over the whole potato tuber is about 100 mg/kg. This relatively high level may even increase when the potato tuber experiences a kind of stress situation, e. g. resulting from tuber injury or storing under non-ideal conditions [22, 23]. Glycoalkaloids consist of a C₂₇-steroidal alkaloid skeleton (aglycone) to which one or more sugar groups are attached. (The structures of the glycoalkaloids in this study are going to be shown later together with their mass spectra.) In cultivated potatoes, α -solanine and α -chaconine, with solanidine as the aglycone, form about 95 % of the total alkaloid content [23]. Glycoalkaloids are toxic to humans. The lethal dose is considered to be about 3–6 mg/kg body mass [24].

Experimental

Chemicals. The glycoalkaloids, α -solanine, tomatine, solanidine, tomatidine and solasodine were purchased from Sigma Chemical Co. (St. Louis, MO). The α -cyano-4-hydroxycinnamic acid matrix was obtained from Aldrich Chemical Co. (Milwaukee, WI). Acetonitrile and trifluoroacetic acid (TFA) were purchased from EM Science (Gibbstown, NJ).

Mass Spectrometry. All MALDI spectra were obtained on a Voyager Elite (PerSeptive Biosystems, Vestec BioSpectrometry Products, Cambridge, MA) reflectron TOF mass spectrometer equipped with a nitrogen laser (337nm, 3 ns pulse). The accelerating voltage in the ion source was 20 kV.

Data were acquired with a transient recorder with 5 ns resolution. The matrix selected for this study was α -cyano-4-hydroxycinnamic acid, because it was found to give the best sensitivity. The matrix and the glycoalkaloids were dissolved in acetonitrile:TFA (0.1%) 1: 1 mixture at room temperature. The matrix solution was saturated at room temperature (~ 20 mM). The concentration of the glycoalkaloids was between $1-4 \times 10^{-5}$ M. To prepare the sample 1 μ l of the matrix solution was deposited on the stainless steel sample holder then 1 μ l of the sample solution was applied. The mixture was allowed to dry prior introduction into the ion source of the mass spectrometer. Each spectrum was produced by accumulating 128 laser shots. The accelerating voltage was 20 kV. This voltage was decreased to zero in two stages. In the first stage 74 % of the full acceleration voltage was applied to a grid located at 3 mm from the sample plate. In the second stage the electrode located 3 cm from the sample plate was grounded. The spectra were obtained in continuous extraction mode, unless otherwise stated. In some cases, delayed extraction with 100 ns delay time was used. For each PSD spectrum the mirror ratio was decreased in 8 steps. The laser irradiance was increased by about 5 % in each step. Time-of-flight to mass conversion was achieved by internal calibration.

The high energy CAD spectra were obtained on a JEOL-HX-110 (JEOL, ltd., Tokyo, Japan) of forward geometry with an accelerating voltage of 10 kV and a FAB gun voltage of 6 kV with 5 mA emission current, using xenon as the FAB gas and He as the collision gas. Glycerol was selected as the matrix. Product ion spectra were obtained with 1-2 nmole sample quantities. Precursor ions were selected at a mass resolution of 1000. The total collision probability for an ion with a nominal collision cross section of 5×10^{-16} cm², traversing through a 1-cm collision region, depends on the pressure of the

collision gas as follows. If the main ion beam is attenuated by 30 %, 95 % of the encounters are single, 5% are double and 0% are triple collisions. If the attenuation is 50%, the corresponding values are 70, 20 and 10 % respectively. In general, attenuation higher than 70% corresponds to multiple collisions [25]. In our experiments, the pressure of the collision gas was set to attenuate the precursor ion beam by approximately 50%. Precursor ion beam attenuation of 10% was also tried to test whether the unique features of the high energy spectra exist under single collision conditions as well.

Results and Discussion

The low- and high energy CAD spectra of selected glycoalkaloids were reported by Claeys *et al.* [9]. They also pointed out important differences between the spectra obtained on a VG70SEQ hybrid instrument using Ar as the collision gas at an energy of 50eV (laboratory frame) or lower. Their high energy spectra were recorded on a four-sector instrument with He target gas with an energy of 4 keV under multiple-collision conditions (70% attenuation of the precursor ion beam). According to their evaluation of the spectra low-energy CAD favors charge driven fragmentation of the aglycone rings, while high-energy CAD spectra are more complex and contain additional fragment ions from charge-remote fragmentations, multiple cleavages, or charge-driven rearrangements.

In Figure 5.2 the low- and high-energy CAD spectra reported by Claeys *et al.* [9], the high-energy CAD FAB spectrum and the MALDI-PSD spectrum obtained in our laboratory of tomatidine (M.W. 415) are shown. The MALDI-

PSD spectrum resembles the low-energy CAD spectrum reported, except for the fact that the relative intensities of the ion currents corresponding to fragment ions at m/z 124 and 126 are higher in the MALDI-PSD spectrum. The fragmentation pattern is shown in Figure 5.3. As can be seen in this figure the ions at m/z values 124 and 126 are formed by multiple cleavages of the E ring. It is hard to compare the relative intensities of the ion currents represented in the MALDI-PSD spectra since the spectra are stitched together. Since the high energy spectrum reported was obtained under multiple collision conditions we decided to record the high energy FAB spectrum at lower collision gas pressures to ensure that the unique features of the high-energy spectra persist and were not only present at high collision frequencies. The product ion intensities were very low under our experimental conditions. We found that changing the primary beam attenuation from 10% to 50% and to 75% did not change the composition of the high-energy CAD spectrum, but the relative intensities of the product ions were higher at higher collision frequencies. In Figure 5.2 the FAB-CAD spectrum obtained at 50% primary ion beam attenuation of tomatidine is also shown. It is not

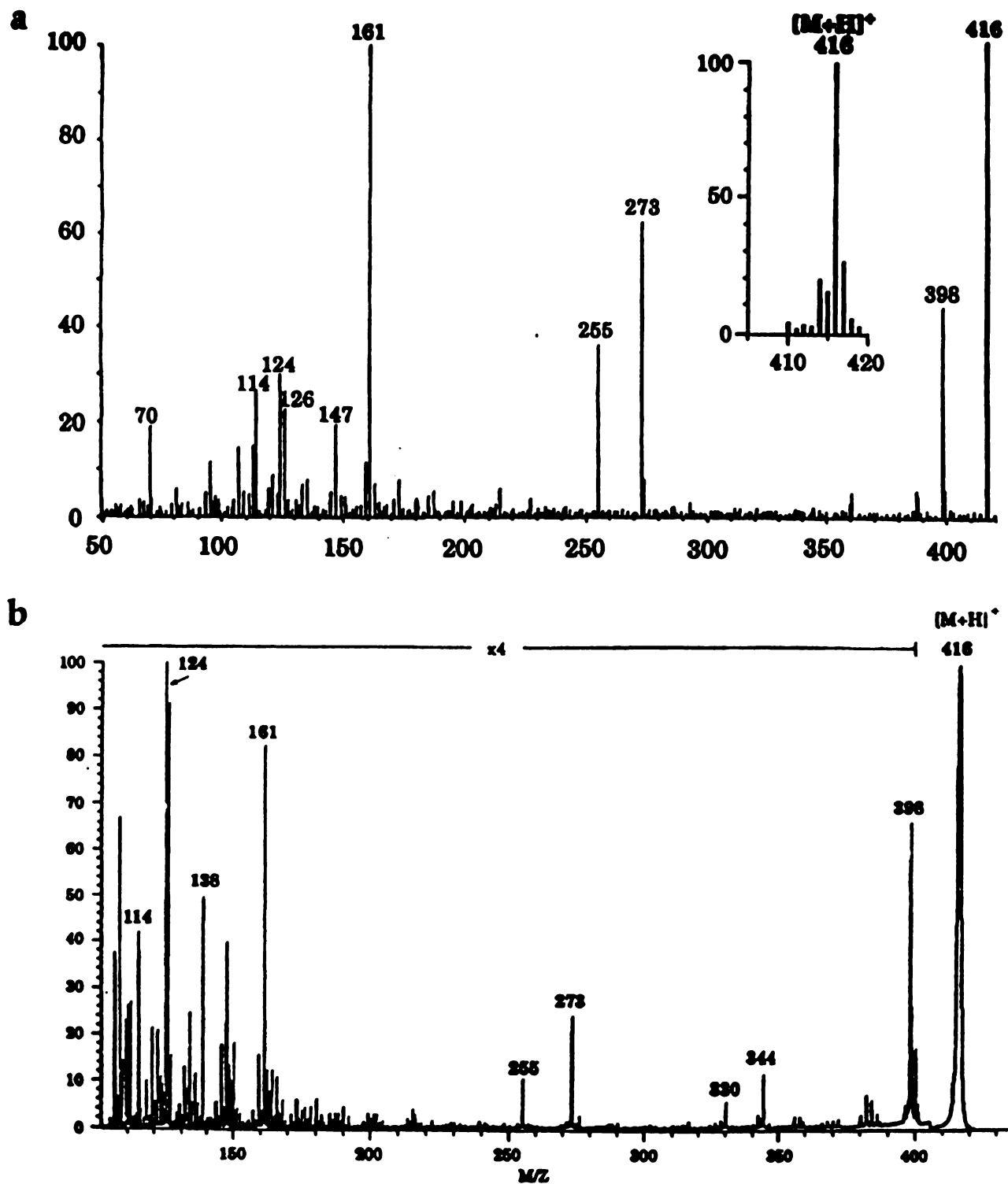


Figure 5.2a (a) Low-energy and (b) high-energy CAD spectra of tomatidine adapted from reference [9].

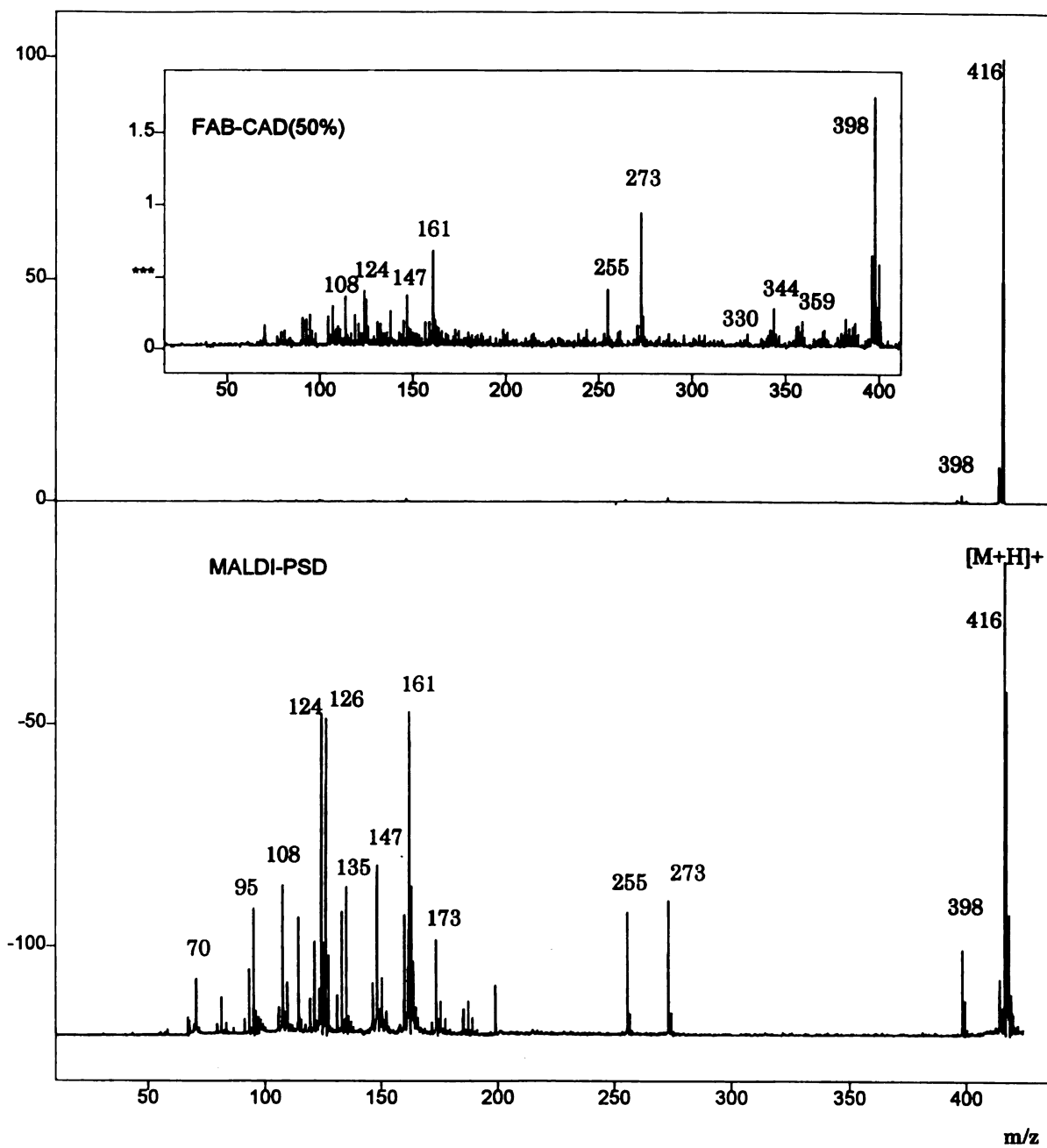


Figure 5.2b The FAB-CAD (top) and MALDI-PSD (bottom) spectra of tomatidine.

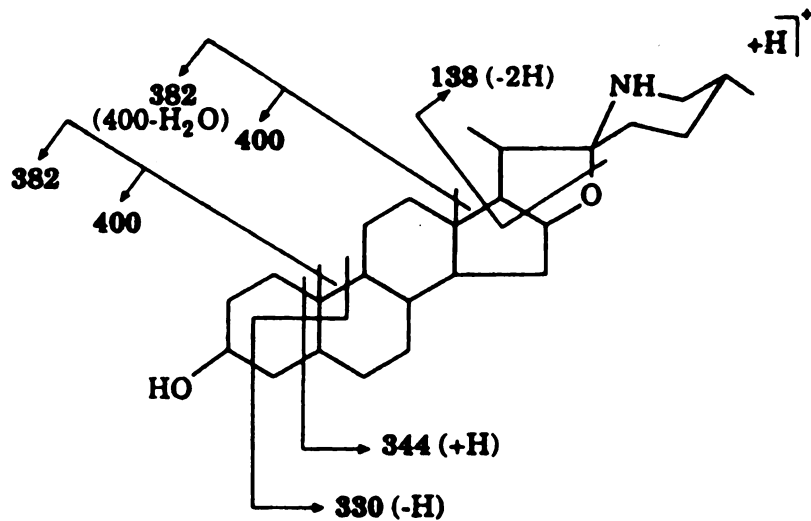
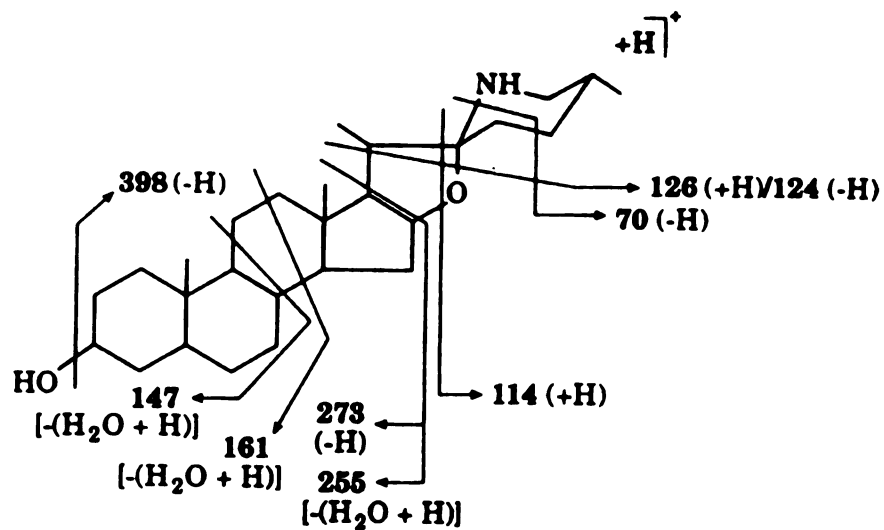


Figure 5.3 Low- and high-energy CAD fragmentations of the various aglycones (tomatidine, solasodine and solanidine) studied. Adapted from reference [9].

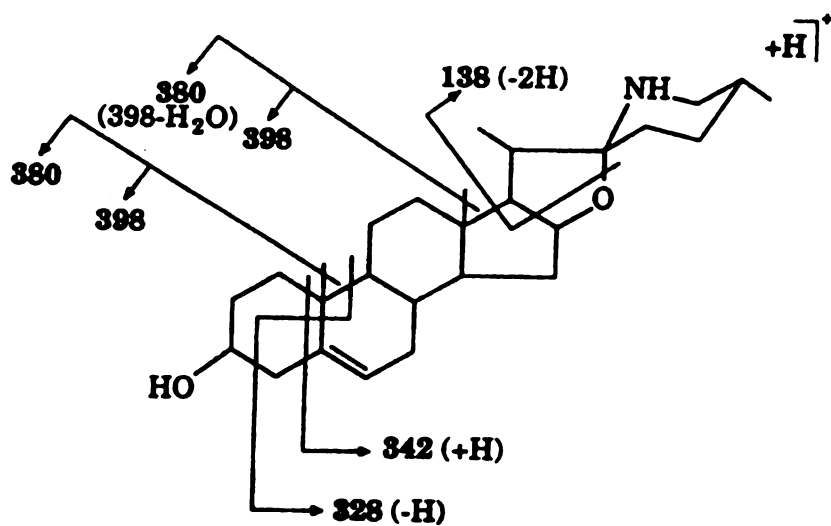
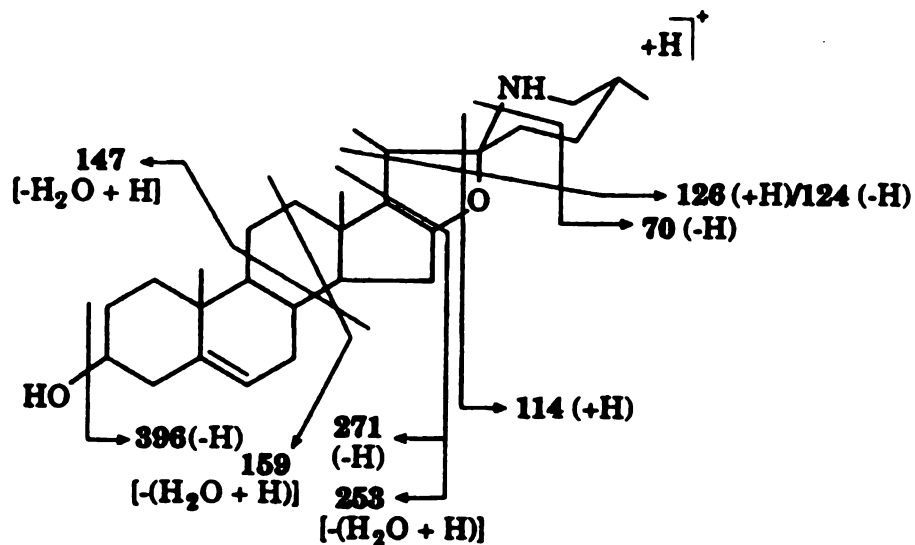


Figure 5.3 Low- and high-energy CAD fragmentations of the various aglycones (tomatidine, solasodine and solanidine) studied. Adapted from reference [9] (cont'd).

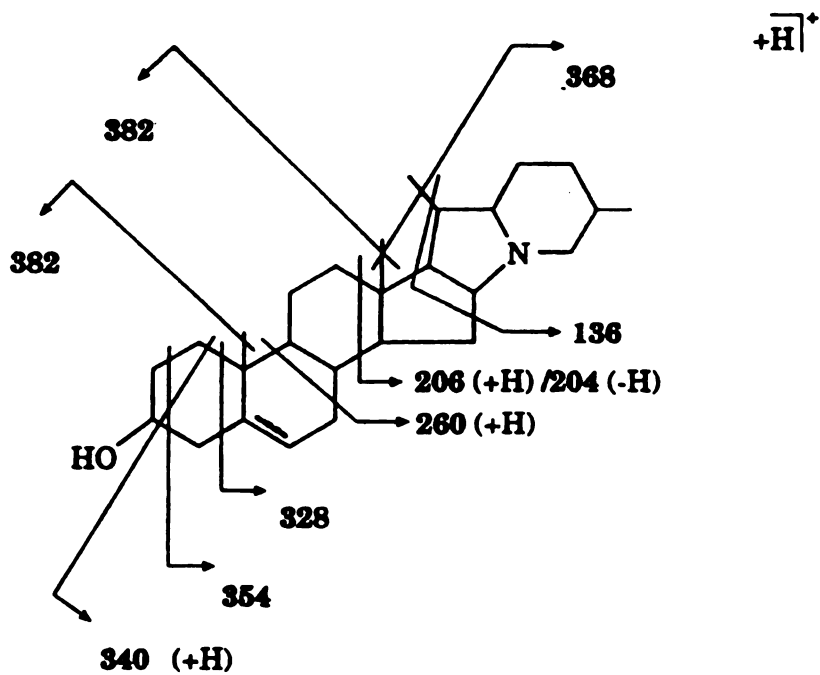
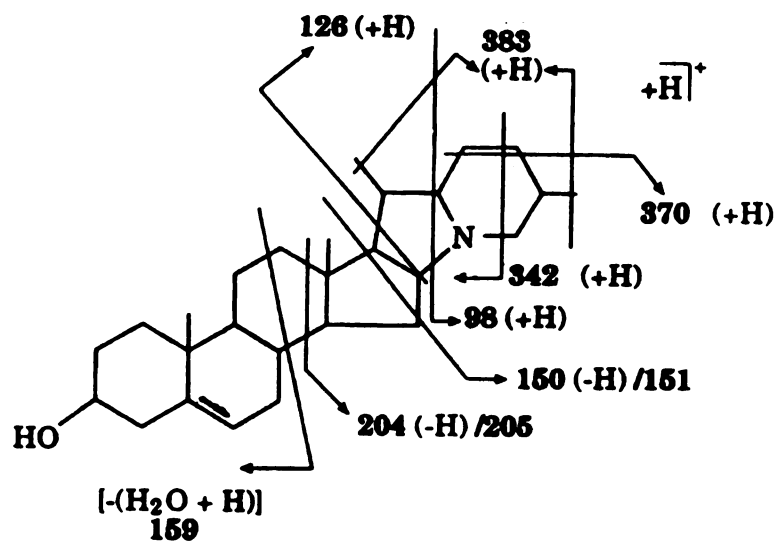
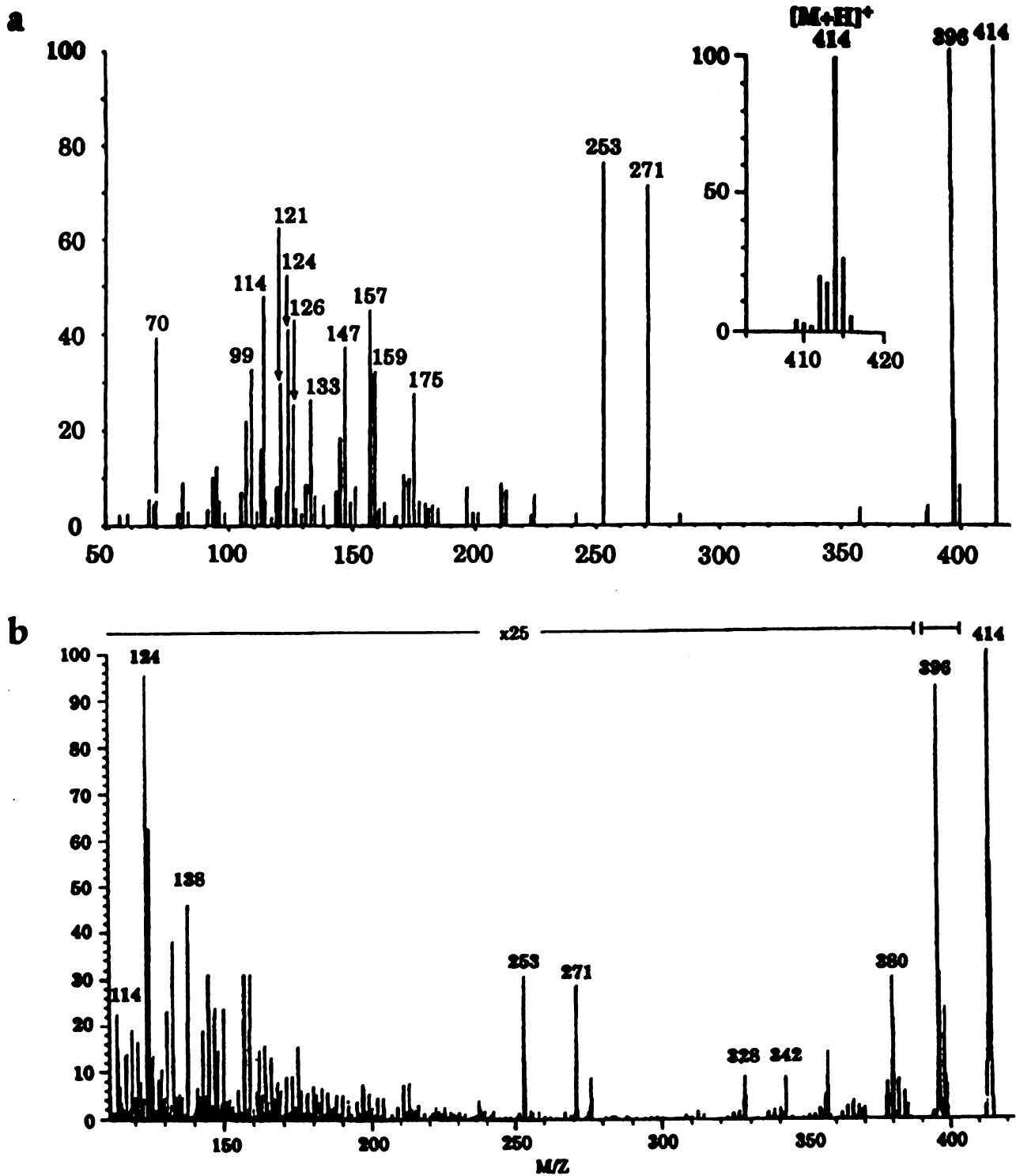


Figure 5.3 Low- and high-energy CAD fragmentations of the various aglycones (tomatidine, solasodine and solanidine) studied. Adapted from reference [9] (cont'd).

identical to the spectrum reported in reference 9, and is not expected to be, since the experimental conditions (acceleration voltages, collision gas pressures, instrument geometries) are different. However, the spectra are very similar and clearly different from the MALDI-PSD spectrum. The ions at mass to charge ratio values, m/z 344, 330 and 138 which appear to be characteristic of high-energy CAD [9] are clearly missing from the MALDI-PSD spectrum. Claeys *et al.* [9] explained the formation of the ion at m/z 344 as the result of a charge remote fragmentation of the A ring (see Figure 5.3). The formation of the other two ions at m/z 330 and 138 is harder to explain. As shown in Figure 5.3, they may be the result of multiple cleavages in the neighboring rings.

The low- and high-energy CAD, the FAB-CAD and the MALDI-PSD spectra of solasodine (M.W. 413) are shown in Figure 5.4. The fragmentation pattern is outlined in Figure 5.3. Again the characteristic high-energy product ions at mass to charge ratio values, m/z , 398, 380, 342 and 328 are clearly missing from the MALDI-PSD spectrum. Also there is an ion current at m/z 357 which is present in our high-energy CAD spectrum as well as in the spectrum in reference 9. The structure of this ion has not been assigned. It is possible that it is formed via multiple cleavages of the A and B rings, since it is 29 mass units above the ion with m/z value 328.

The spectra of solanidine (M.W. 397) are shown in Figure 5.5. The MALDI-PSD spectrum is clearly richer in low mass ions than the low energy CAD spectrum reported by Claeys *et al.* [9], but again is very different from the high-energy CAD spectrum shown also in Figure 5.5. The ions at m/z values 368, 354, 342, 328 are characteristic of high-energy CAD and can be interpreted



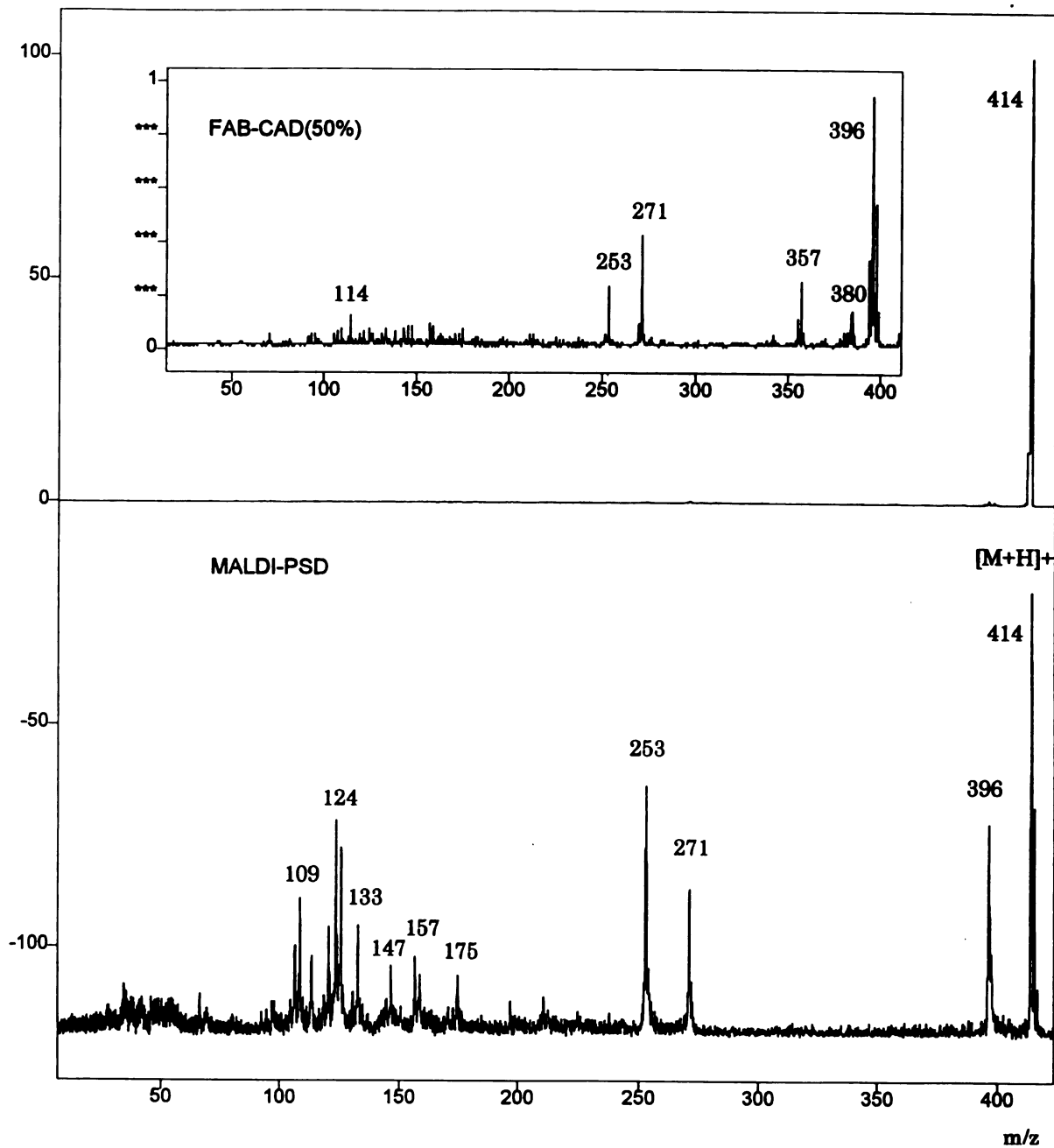


Figure 5.4b The FAB-CAD (top) and MALDI-PSD (bottom) spectra of solasodine.

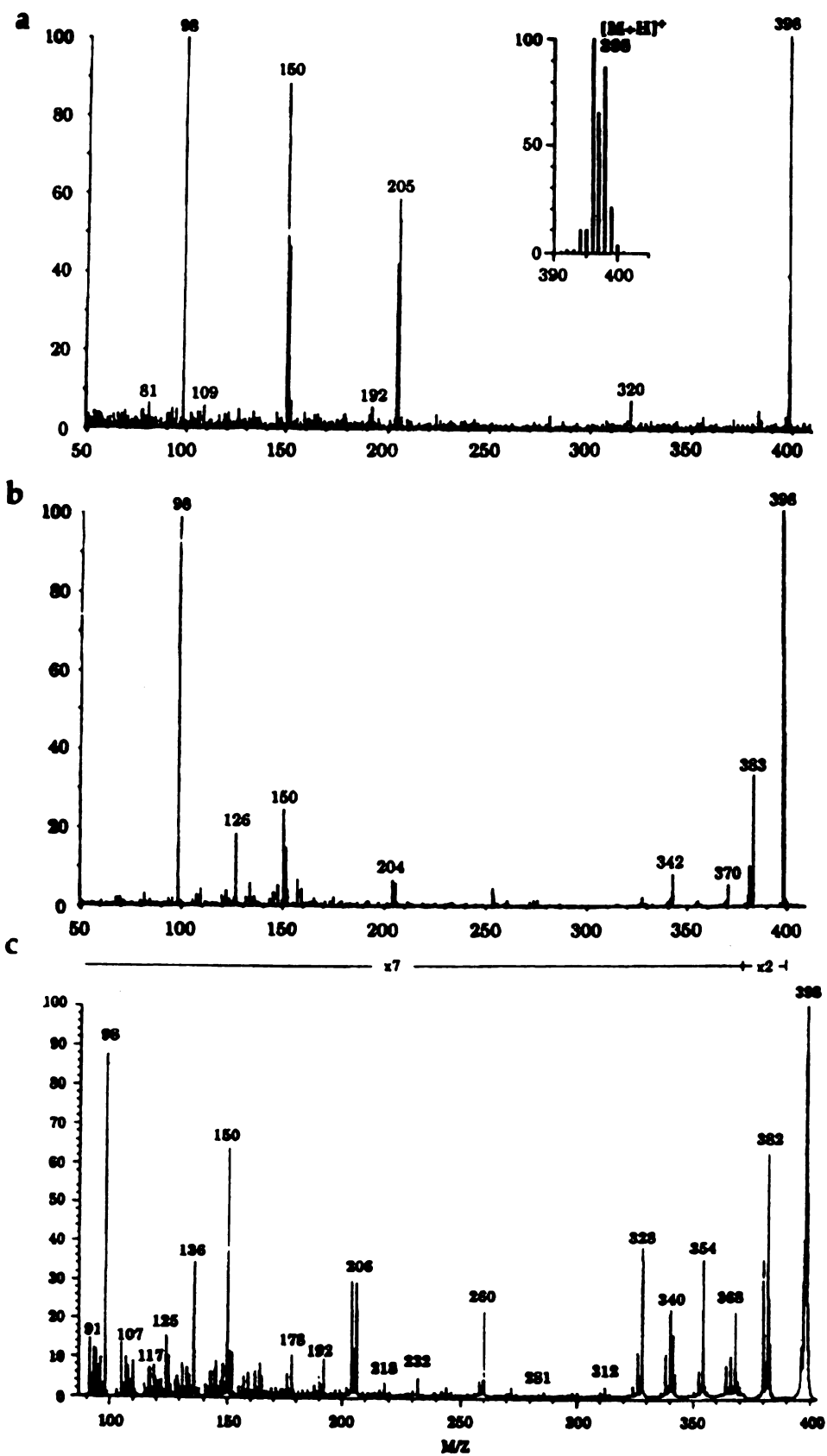


Figure 5.5a (a) 10 eV and (b) 50 eV low- and (c) high-energy CAD spectra of solanidine adapted from reference [9].

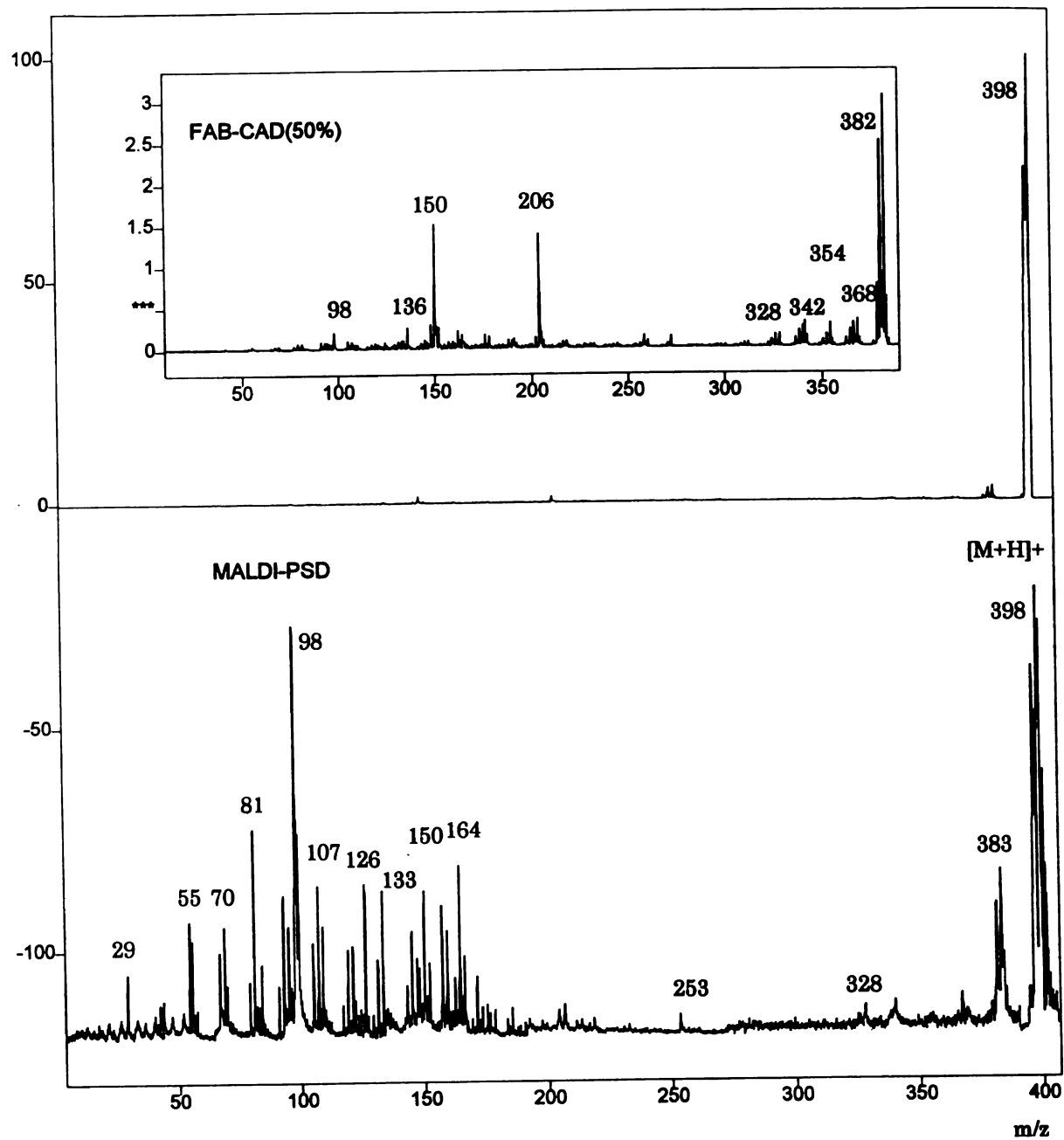


Figure 5.5b The FAB-CAD (top) and MALDI-PSD (bottom) spectra of solanidine.

as a result of multiple cleavages, remote from the charge in the A, B or C rings. The ion represented by an ion current at m/z 136 is also a characteristic high energy fragment resulting from multiple cleavages in the D ring.

Figure 5.6 shows the MALDI-PSD spectrum of tomatine (M.W. 1033). It is clearly different again from the high-energy CAD spectra also shown in Figure 5.6, and is also very different from the low-energy CAD reported in reference 9. The series of Y_n^+ ions at m/z values 902, 872, 578, 416 characteristic of the carbohydrate sequence reported in reference 9 are not present in the MALDI-PSD spectrum. The high-energy CAD spectrum shows ring fragmentations. These fragmentations are shown in Figure 5.7.

Figure 5.8 shows the MALDI-PSD and FAB high-energy CAD spectrum of α -solanine together with the spectra from reference [9]. The PSD spectrum of the $[M+H]^+$ ions shows the formation of Y_1^+ ions at m/z 722 and 706 which correspond to the loss of terminal rhamnose and galactose residues. Other sequence related ions at m/z 398 (Y_0^+) and 380 (Z_0^+) can also be found in the spectrum. These are all present in the low-energy CAD spectrum [9]. However, from the aglycone fragments only m/z 98 is present in the PSD spectrum and the other two ions at m/z 150 and 204 present in the low-energy CAD are missing from the PSD spectrum. Instead, a new ion appears at m/z 126 which could also be a product of a multiple cleavage in the E ring. Two other new ions, not present in the LSIMS and FAB spectra, are the ion at m/z 561 and 366. The former may be rationalized by the simultaneous loss of the terminal rhamnose and galactose residues accompanied by H shifts to the

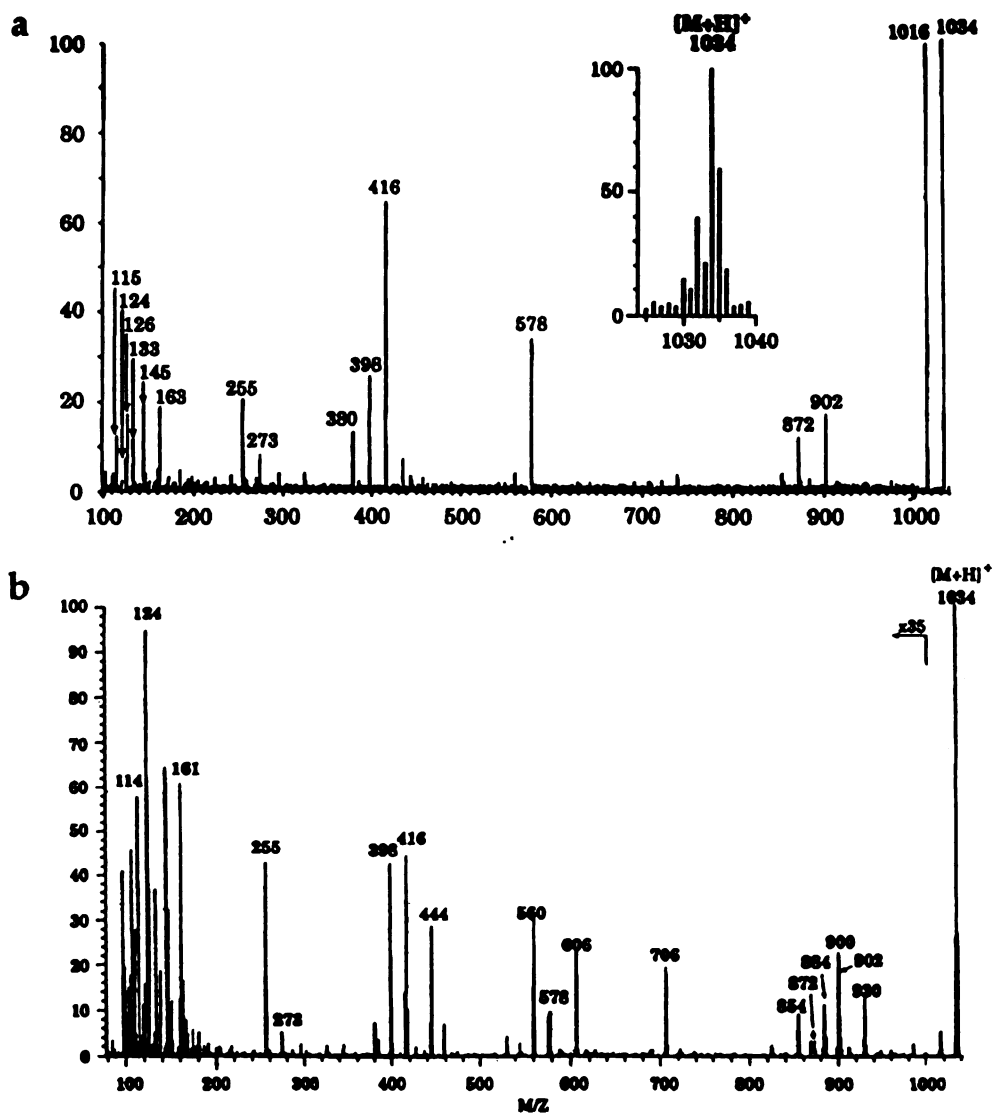


Figure 5.6a (a) Low-energy and (b) high-energy CAD spectra of tomatine adapted from reference [9].

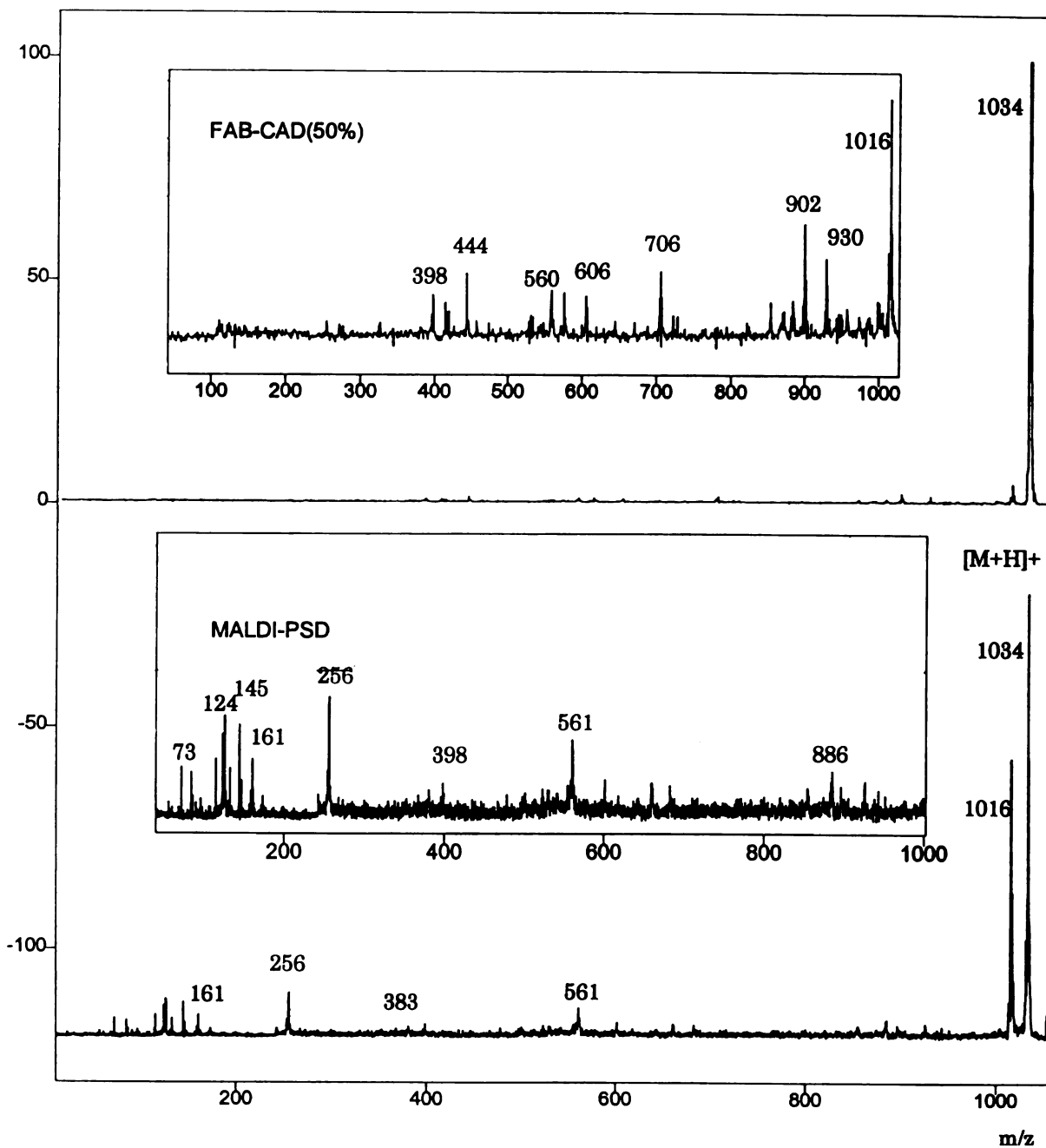
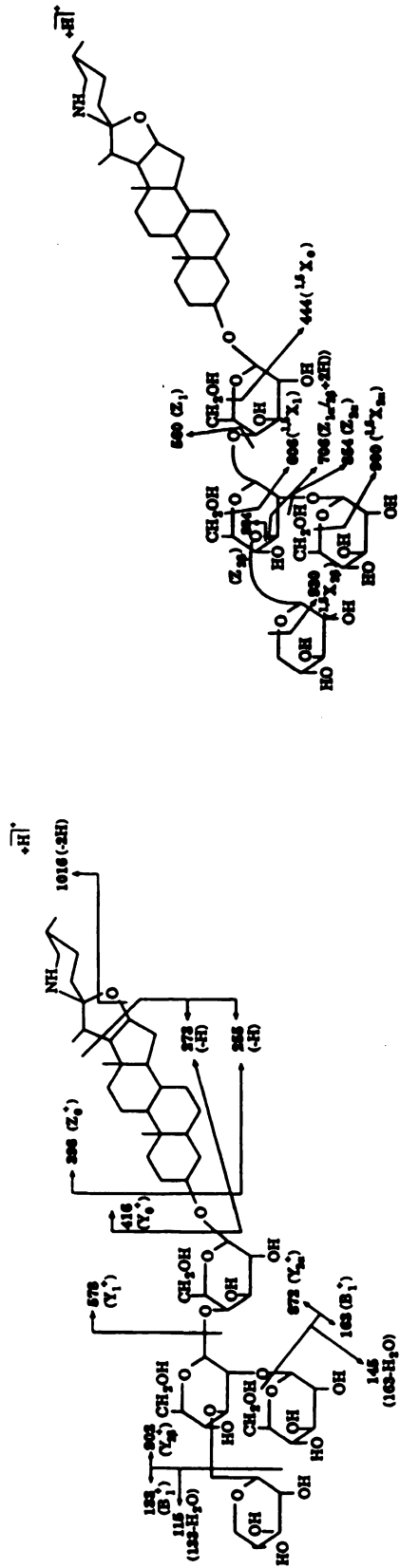
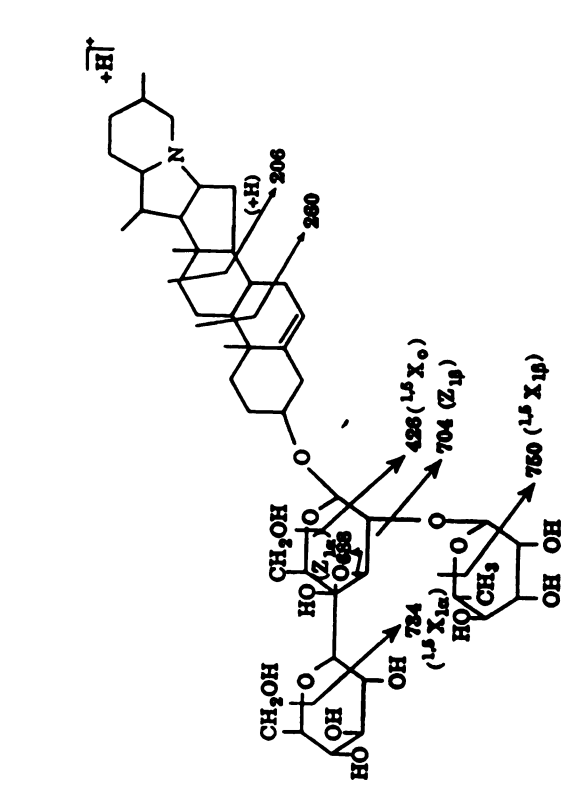


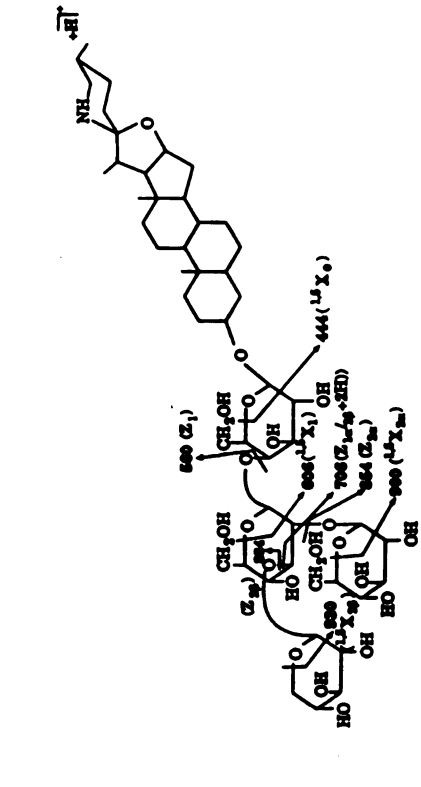
Figure 5.6b The FAB-CAD (top) and MALDI-PSD (bottom) spectra of tomatine.



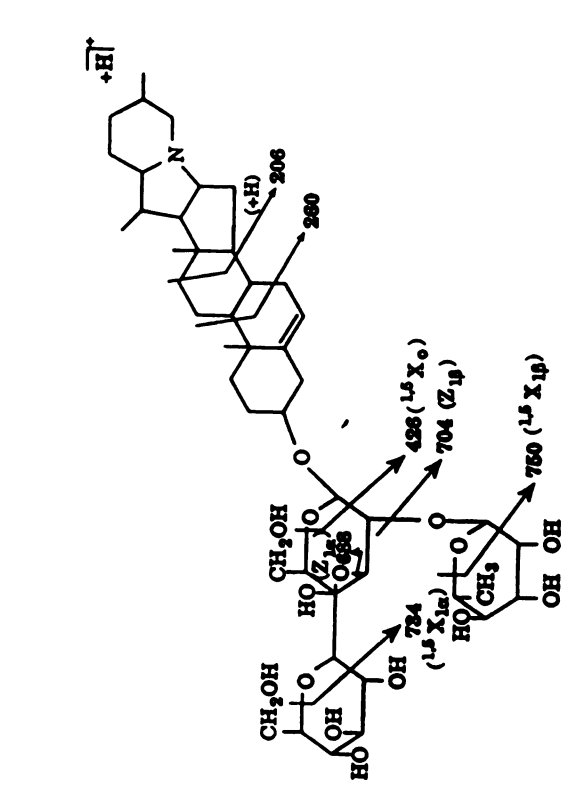
Low-energy CID fragmentations of α -tomatine.



Low-energy CID fragmentations of α -solanine.



High-energy CID fragmentations of α -tomatine.



High-energy CID fragmentations of α -solanine.

Figure 5.7 Low- and high-energy fragmentations of tomatine and α -solanine adapted from reference [9].

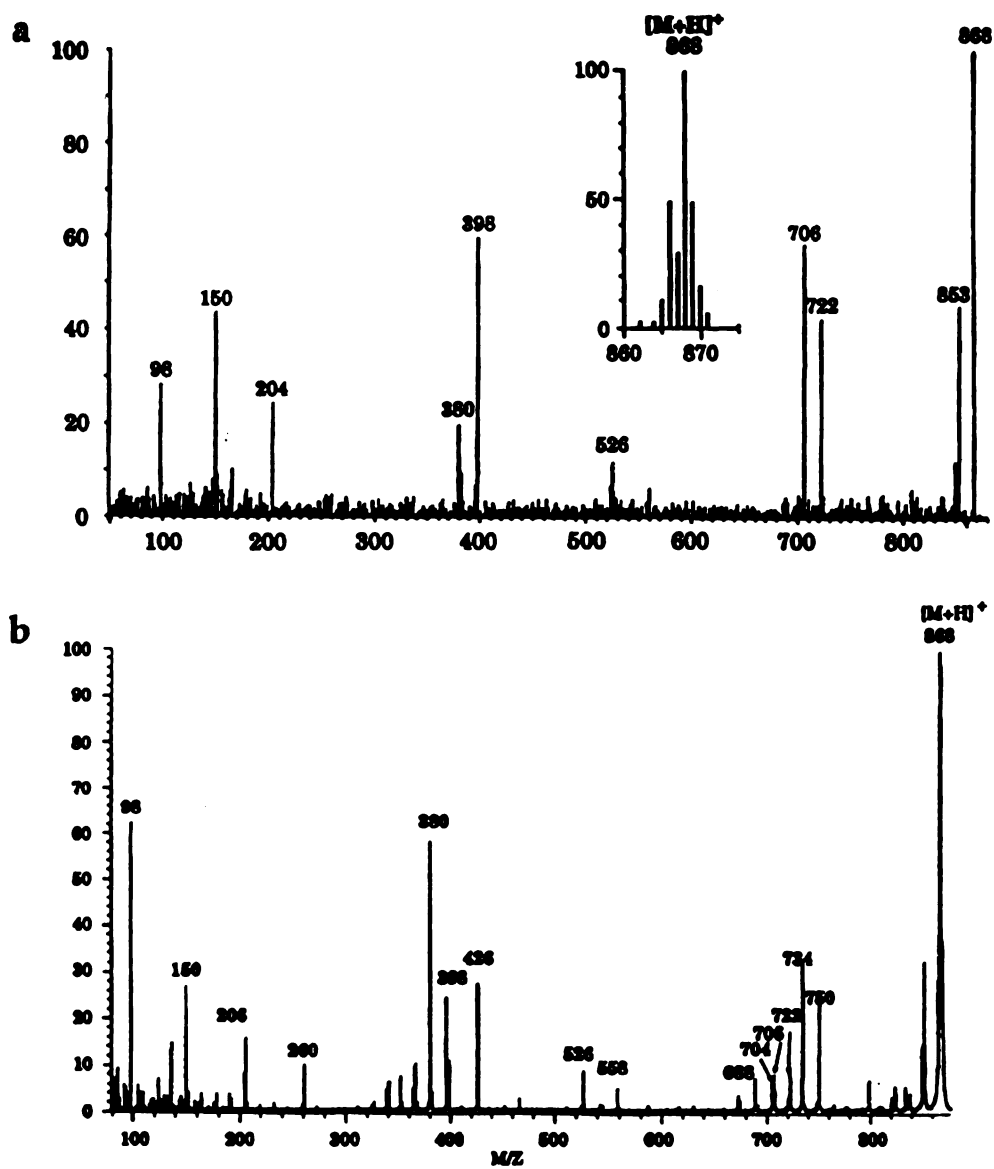


Figure 5.8a (a) Low-energy and (b) high-energy CAD spectra of α -solanine adapted from reference [9].

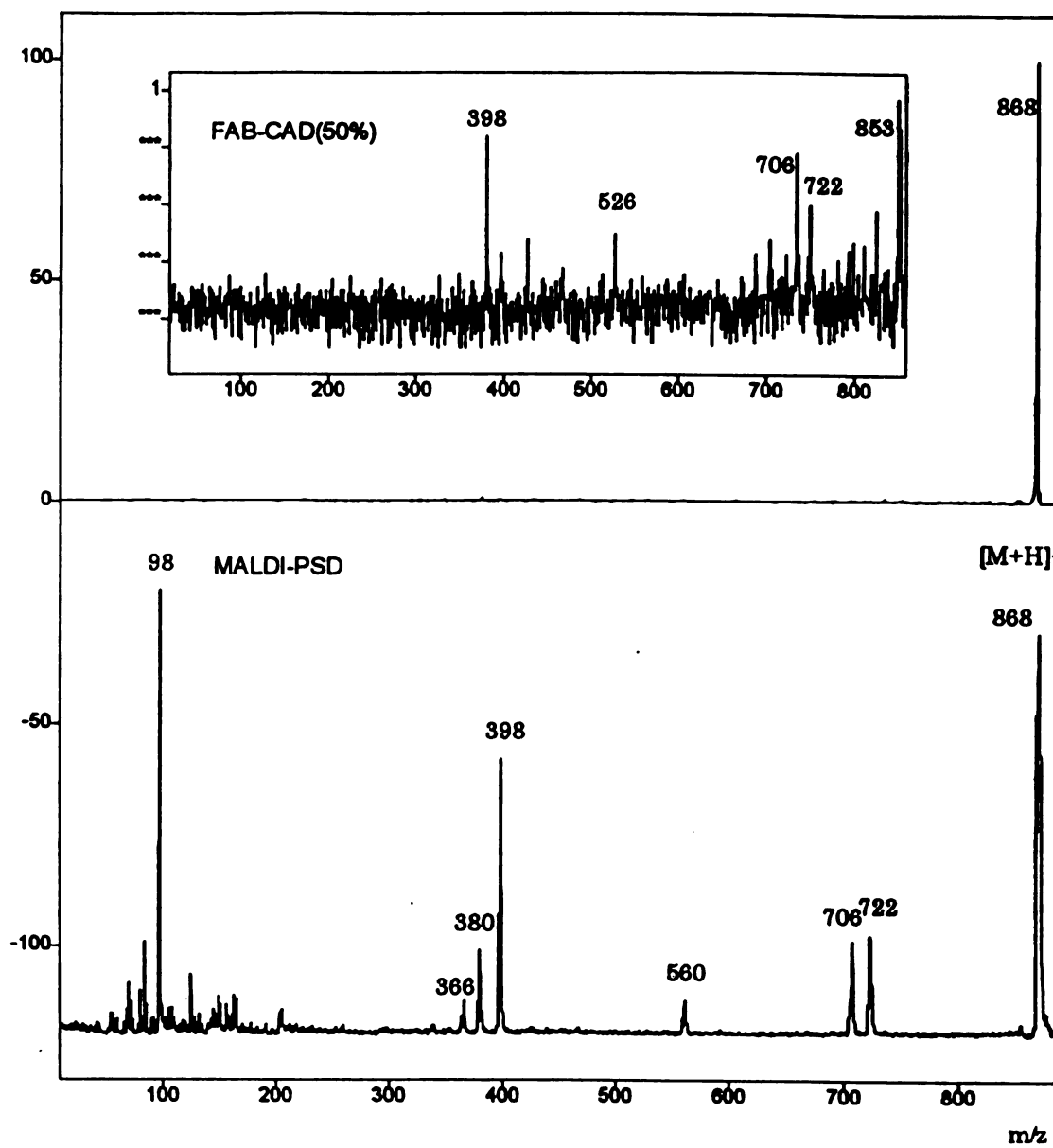


Figure 5.8b The FAB-CAD (top) and MALDI-PSD (bottom) spectra of α -solanine.

glycosidic oxygens. The ions characteristic of the high-energy fragmentation processes (m/z 426, 688, 704, 734, 750) are clearly missing from the PSD spectra.

The comparison of our spectra with the reported ones results in the conclusion that for the aglycone components the MALDI-PSD spectra resembles the low-energy CAD spectra, while for the glycoalkaloids the resemblance is not unambiguous. The MALDI-PSD spectra are different from the low- and high-energy CAD spectra. While they contain peaks representing ion currents resulting from low energy fragmentation processes and clearly lack the signature of high-energy fragmentation, they also show the appearance of new ions which have not been observed in the CAD spectra. However, the appearance of the MALDI-PSD spectra suggests the importance of low-energy activation.

It has been suggested that the activation mechanism of PSD is largely determined by collisional events (ion/neutral) occurring in the acceleration field during early plume expansion [26]. Is this in-plume activation model plausible? To answer this question let us consider the typical kinetic energy obtained by the ions formed at the target surface while they are accelerated out of the ion source and the possible number of collisions they undergo. It has been mentioned in the previous chapter that the MALDI ion source produces ions with a significant initial kinetic energy which is due to the fact that irradiation with the laser causes the evaporation and expansion of the sample with supersonic velocity [27]. Several research groups measured the initial velocities of the ions and neutrals produced by MALDI. Huth-Fehre *et al.*[28] determined a common velocity distribution for the desorbed neutrals in case of ferric acid matrix and gramicidine-S analyte, having a maximum between 300-400 m/s .

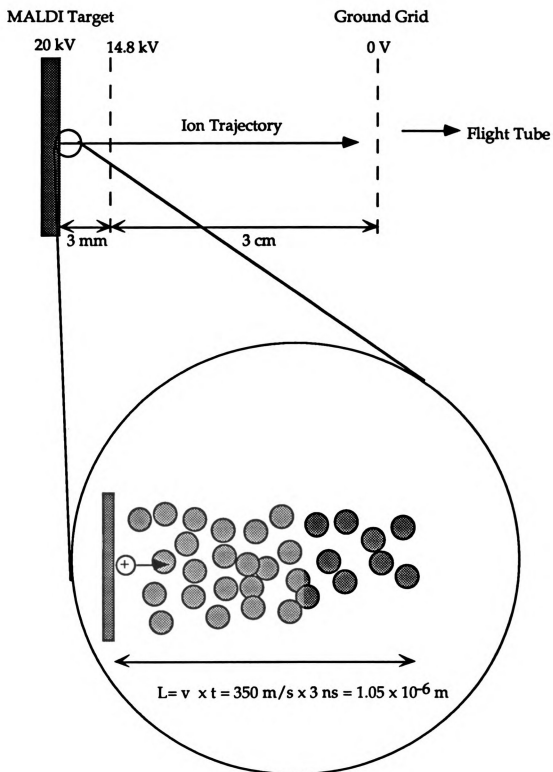


Figure 5.9. Schematic of the MALDI ion source. Assume that an ion formed at the sample plate has to travel through the dense cloud of neutrals ejected with a velocity of 350 m/s while it is accelerated out of the source.

This common velocity distribution suggests strong entrainment of the desorbed analyte molecules in the matrix. Beavis and Chait [29] measured the initial velocities of the ions. They found that sinapinic acid matrix ions had a maximum velocity of 1140 m/s, while polipeptide ions (1000-15600 Da) had velocities of around 750 m/s. Others also measured initial ion velocities within this range [30-32]. Imagine a situation that an ion is formed at the sample surface and it has to travel through the dense cloud of material, usually referred to as the plume. The plume mostly consists of matrix molecules because of the high matrix to analyte ratios (~ 10000:1) used in MALDI. The thickness of the expanded plume can be estimated as the ejection velocity times the laser pulse width. If, we assume an ejection velocity of 350 m/s for the neutrals [27] then for a 3 ns pulse laser this value is 1 μm . Using the higher ejection velocity of the ions 1140 m/s, the thickness of the plume is 3.4 μm . Figure 5.9 shows the schematic diagram of the MALDI ion source.

As was mentioned earlier, the Voyager Elite uses a two stage acceleration field. Next, we are going to show that the collisional events for an ion formed at the back of the plume (on the sample plate surface) take place within the first stage of the acceleration field. The time, it takes for a neutral matrix molecule ejected with a velocity between 350m/s and 1140 m/s, to travel to the grid placed at 3 mm from the sample plate, ranges between 8.5 μs - 2.6 μs . For the ions this time would be shorter because they are accelerated by the field. In the ion source of the Voyager Elite at 20 kV acceleration voltage and a grid voltage of 74 % in the first stage, an ion with a mass of 1000 Da undergoes an acceleration of

$$a = \frac{F}{m} = \frac{Eez}{m} = \frac{5,200 \text{ V} / 3 \times 10^{-3} \text{ m} \times 1.602 \times 10^{-19} \text{ C} \times 1}{1 \text{ kg/mole} / 6.02 \times 10^{23} \text{ 1/mol}} = 1.7 \times 10^{11} \text{ m/s}^2$$

The mean initial velocity of the desorbed ions of similar size was measured to be *ca.* 750 m/s [29]. Thus, for an ion of 1000 m/z, it would take 1.84×10^{-7} s to reach the grid, meaning that the ions would pass the neutrals within the first acceleration region. Considering the initial velocity and the acceleration field in our instrument (see. Figure 5.9) the velocity and the kinetic energy of an ion formed at the surface of the sample plate can be calculated at any time and at any distance from the surface, assuming that no collisions occur to change the velocity of the ion. These values are presented in Table 5.1

Table 5.1 The kinetic energy of an ion of m/z 1000 as a function of time and distance from the sample plate.

Time (μ s)	Distance above sample plate (μ m)	Kinetic energy (eV)
0	0	2.9
0.001	0.83	4.38
0.002	1.84	6.15
0.003	3.02	8.22
0.005	6.12	13.69
0.008	11.44	23.06
0.05	250	443
0.1	925	1632

In Figure 5.10 the situation is depicted as the packet of neutrals and ions travels in the ion source towards the field free region. According to our calculation an ion formed at the surface of the sample plate will reach the front of the plume after 5.15 ns at which point it has about 13.69 eV kinetic

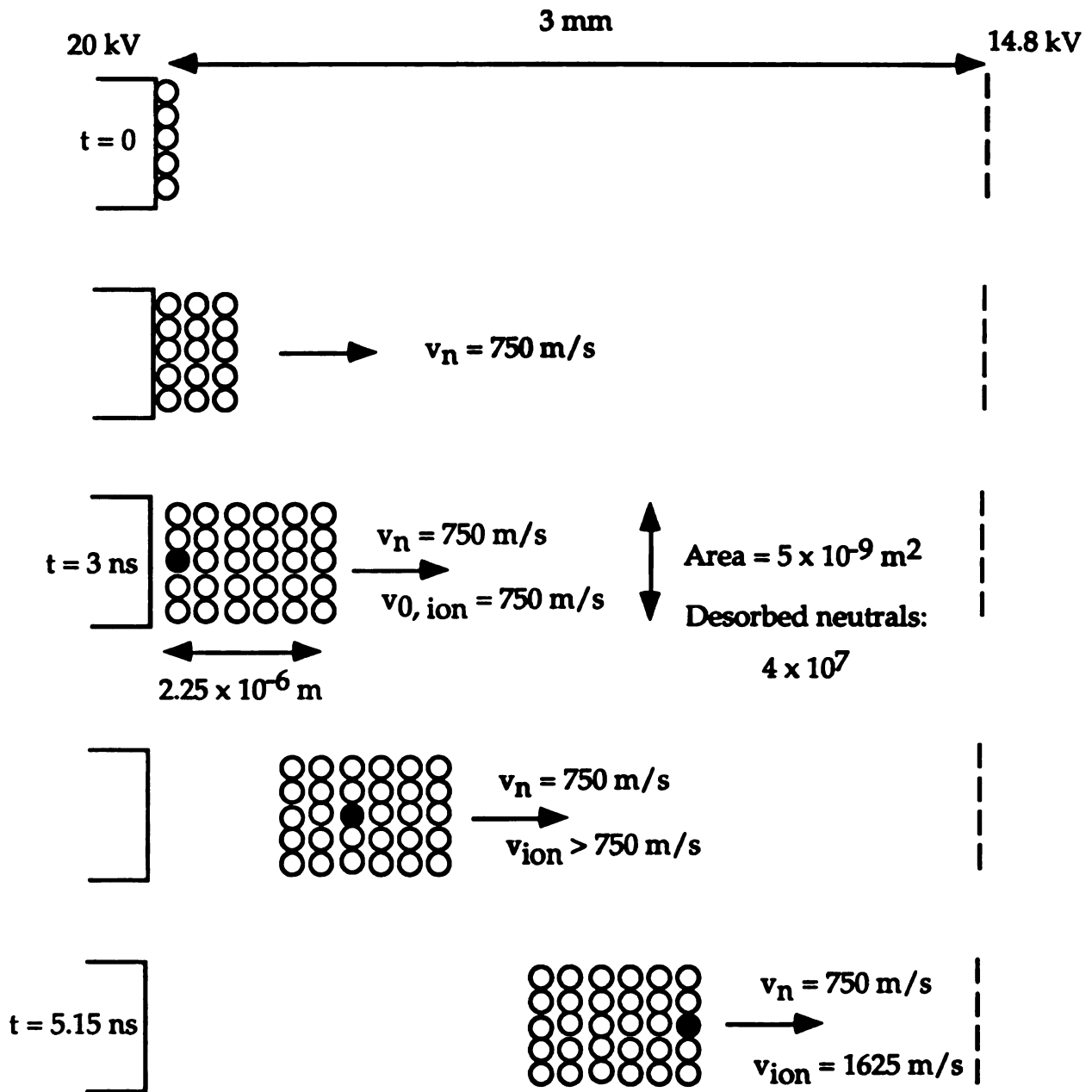


Figure 5.10 Schematic showing the desorbed packet of neutrals and ions as it travels through the ion source towards the field free region.

energy and it is about 6 μm above the target surface. In MALDI, the molar matrix to analyte ratio is generally 10,000:1. Thus, it is proposed that a dense plume consisting mostly of matrix molecules is formed upon irradiation. If the ion with an m/z value of 1000 and a kinetic energy of 13.69 eV collides with an α -cyano-4-hydroxycinnamic acid matrix molecule (M.W. 189) which has a kinetic energy of 0.3 eV, both velocity vectors are in the same direction, giving a relative kinetic energy of 13.39 eV. This is the maximum amount of available energy for collisional activation, which would correspond to low energy activation.

The number of collisions an ion undergoes while accelerated through the plume can be estimated by estimating the number density. *Ens et al.* [33] reported the ejection of 4×10^7 neutral molecules from an irradiated area of $5 \times 10^{-9} \text{ m}^2$ at threshold irradiance. Using an ejection velocity of 750 m/s (v), for the desorbed species and assuming that the same plume exists during the laser pulse, (τ), the thickness of the plume can be estimated as $v \times \tau$. For a 3 ns laser, this value is $2.25 \times 10^{-6} \text{ m}$ (see Figure). Thus, the volume of the plume is $11.25 \times 10^{-15} \text{ m}^3$. This gives a number density of $3.6 \times 10^{21} \text{ molecules/m}^3$. The number of collisions an ion undergoes while traveling through this dense plume can be calculated using the equation:

$$Z = \sigma_{\text{rel}} N$$

where σ is the collision cross section, c_{rel} is the relative velocity ($1625-750=875 \text{ m/s}$) and N is the number density. The collision cross section is estimated to be *ca.* $3 \times 10^{-18} \text{ m}^2$. The collision frequency calculated is, $Z \sim 1 \times 10^7 \text{ s}^{-1}$. It takes about 5.15 ns for the ion to get through the plume, which gives 0.05 for the number of collisions. This suggests single collision conditions in the plume, meaning that only about 5% of the ions undergoes collisions in the expanded plume. This may be consistent with the observation that using delayed

extraction did not significantly change the PSD spectra. In the continuous extraction mode, the precursor ion intensity is generally lower than in the delayed extraction mode, and the relative intensity of the product ions is higher than under delayed extraction conditions. This would be consistent with the in-plume activation model. In delayed extraction, before the acceleration field is switched on, the ions and the neutrals are travelling with the same initial drift velocities and the plume density decreases. When the field is switched on the ions are accelerated through the low-density plume where the probability of collisions is smaller, which explains the higher precursor ion yield.

As we saw, in the expanded plume the probability of collisions is rather low and such a low probability does not account for the very similar initial velocities observed for ionic and neutral species of a wide mass range. This suggests that the early stages of plume-expansion should be reconsidered. In the very early stages of the plume formation the number density in the plume can be approximated by the number density of the solid. For nicotinic acid matrix this value is 7.21×10^{27} molecules/m² [34]. The relative velocities of the desorbed species are smaller than at the time when the ionic species are accelerated considerably. Using an estimated relative velocity of 250 m/s, and the same collision cross section as before, the collision frequency calculated is, $Z = 5.8 \times 10^{12}$ s⁻¹. Assuming that this rather dense plume is maintained for 1/10 of the time an ion spends in the expanded plume, 5.15×10^{-10} s, the number of collisions an ion undergoes is about 2989. This implies multiple collision conditions in the early plume, however the available energy for collisional activation is small.

The possibility of high energy collisional activation with residual gas in the flight tube should also be considered. At 20 kV acceleration voltage, the

kinetic energy of the ions when they enter the field free region is 20 keV. For an ion with a mass of 1000 Da this corresponds to a velocity of 6.21×10^4 m/s. At a base pressure of 10^{-7} torr the number density in the instrument is 3.24×10^{15} molecules/m³. Using the same cross section and the velocity of the ion as the relative velocity the collision frequency is 648 molecules/s. The flight time of the ion in the flight tube of 1.2 m is 19.23 μ s. Thus, an ion can undergo about 0.012 collisions in the flight tube, that is only about 1 % of the quasi-molecular ions will undergo collisions. This explains, that unless the residual gas pressure is increased, high-energy collisional activation will not occur.

Conclusions

Compared to mass spectra obtained by FAB, MALDI mass spectra provide only limited structural information because of the low extent of fragmentation. In the second chapter of this dissertation, and in the published paper in Appendix One, mechanisms of ion formation in the case of FAB were considered. We have shown that FAB can be described as a glycerol chemical ionization experiment. Ions and neutral molecules are desorbed into a high pressure region called the selvedge, where they can undergo multiple collisions and participate in ion/molecule reactions. The average energy imparted by the fast atoms is high enough to induce fragmentation following bombardment, and the contribution of the gas phase ion/molecule reactions to the ion yield represented by the mass spectrum is also considerable. In this last chapter the possible activation mechanisms for the ions formed in a MALDI ion source were considered. Clearly, the MALDI ion source is different from the FAB source in terms of the nature of the gas

phase species above the target, electric fields, and ion kinetic energies. However, the possibility of ion/molecule reactions in the dense plume formed upon laser irradiation should still be considered. The estimated collision frequencies are much lower in the laser-desorbed plume than in the FAB selvedge region. Thus, the contribution of gas-phase ion/molecule reactions to the ions represented in the spectrum are expected to be smaller. The possibility of in-source collisional activation was also considered. Though the probability of collisions is low, if an encounter occurs, the available kinetic energy is in the range of 1-10 eV which is consistent with low-energy activation. To increase the fragment ion yield in MALDI-PSD, the desorption, ionization, and in-source activation mechanisms need further understanding. The effect of laser fluence should be studied. The fragmentation may potentially be increased by adjusting the number of matrix molecules ablated into the gas phase, through sample preparation, and/or by changing the acceleration field or applying delayed extraction. The continued studies on the mechanisms of desorption/ionization will hopefully lead to a unifying description of the different methods.

REFERENCES

1. M. Karas and F. Hillenkamp, *Anal. Chem.*, **60**, 2299-2301 (1988).
2. B. Spengler, D. Kirsch and R. Kaufmann, *Rapid Commun. Mass Spectrom.* **5**, 198-202 (1991).
3. B. Spengler, D. Kirsch, R. Kaufmann and E. Jaeger, *Rapid Commun. Mass Spectrom.* **6**, 105-108 (1992).
4. Ehring, H.; Karas, M.; Hillenkamp, F. *Org. Mass Spectrom.* **1992**, *27*, 472-480.
5. B. Spengler, D. Kirsch and R. Kaufmann, *J. Phys. Chem.* **96**, 9678-9684 (1992).
6. J.C. Rouse, W. Yu and S. A. Martin, *J. Am. Soc. Mass Spectrom.* **6**, 822-835 (1995).
7. T. Kosaka, T. Ishikawa and T. Kinoshita, *Rapid Commun. Mass Spectrom.* **9**, 1342-1344 (1995).
8. R. Kaufmann, B. Spengler and D. Kirsch, *Int. J. Mass Spectrom. Ion Proc.* **131**, 355-385 (1994).
9. M. Claeys, H. Van den Heuvel, S. Chen, P.J. Derrick, F. A. Mellon and K. R. Price, *J. Am. Soc. Mass Spectrom.* **7**, 173-181 (1996).
10. Barber, M.; Elliott, R. M. *Twelfth Annual Conference on Mass Spectrometry and Allied Topics 1964*, Montreal, Canada, June pp.150.
11. Jennings, K. R. *Int. J. Mass Spectrom. and Ion Phys.* **1968**, *1*, 227.
12. Haddon, W. F.; McLafferty, F. W. *J. Am. Chem. Soc.* **1968**, *90*, 4745.
13. Yost, Y. A.; Enke, C. G. *J. Am. Chem. Soc.* **1978**, *100*, 2274.
14. Durup, J. *Recent Developments in Mass Spectrometry*, K. Ogata and T. Hayakawa, eds., (University Park Press: Baltimore, 1970).
15. Loss, J. *Ber. Bunsenges. Phys. Chem.* **1973**, *77*, 640.
16. Cheng, M. H.; Chiang, M.; Gislason, E. A.; Mahan, B. H.; Tsao, C. W.; Werner, A. S. *J. Chem. Phys.* **1970**, *52*, 5518.

17. Herman, Z.; Futrell, J. H.; Fredrich, B. *Int. J. Mass Spectrom. Ion Processes*, 1984, 58, 181.
18. Singh, S.; Harris, F. M.; Boyd, R. K.; Beynon, J. H. *Int. J. Mass Spectrom. Ion Proc.* 1985, 66, 131.
19. Kim, M. S.; McLafferty, F. W. *J. Am. Chem. Soc.* 1978, 100, 3279.
20. Neumann, G. M.; Derrick, P. J. *Org. Mass Spectrom.* 1984, 19, 165.
21. Schwartz, R. N.; Slawsky, Z. I.; Hezfeld, K. F. *J. Chem. Phys.* 1952, 20, 1591.
22. Van Gelder, W. M. J. *Thesis*, Agricultural University of Wageningen, Wageningen, 1989, pp.9-23.
23. Jadhav, S. J.; Sharma, R. P. Salunkhe, D. K. *CRC. Crit. Rev. Toxicol.* 1981, 9, 21-101.
24. Friedman, M.; Dao, L. *J. Agric. Food Chem.* 1992, 40, 419-423.
25. Holmes, J. L. *Org. Mass Spectrom.* 1985, 20, 169.
26. Kaufmann, R.; Spengler, B.; Lutzenkirchen, F. *Rapid Commun. Mass Spectrom.* 1993, 7, 902-910.
27. Zhang, J-Y., Nagra, D. S.; Li, L. *Anal. Chem.* 1993, 65, 2812-2818.
28. Huth-Fehre, T; Becker, C. H. *Rapid Commun. Mass Spectrom.* 1991, 5, 378-382.
29. Beavis, R. C.; Chait, B. T. *Chem Phys. Lett.* 1991, 5 , 479.
30. Russon, L. M.; Whittal, R. M.; Li, L. *Proceedings of the 44th ASMS Conference on Mass Spectrometry and Allied Topics*, Portland, Oregon, 1996, pp. 731.
31. Juhasz, P.; Vestal, M. L.; Martin, S. A. *Proceedings of the 44th ASMS Conference on Mass Spectrometry and Allied Topics*, Portland, Oregon, 1996, pp. 730.
32. Schürenberg, M.; Schultz, T.; Dreisewerd, K.; Hillenkamp, F. *Rapid Commun. Mass Spectrom.* 1996, 10, 1873-1880.
33. Ens, W.; Mao, Y.; Mayer, F.; Standing, K. G. *Rapid Commun. Mass Spectrom.* 1991, 5, 117-123.

34. **CRC. Handbook of Chemistry and Physics; Weast, R. C.; Ed.; CRC Press: Boca Raton, Fl, 1983.**

Appendix I

If the Ionization Mechanism in Fast-Atom Bombardment Involves Ion / Molecule Reactions, What Are the Reagent Ions? The Time Dependence of Fast-Atom Bombardment Mass Spectra and Parallels to Chemical Ionization

Gabriella Székely and John Allison

Department of Chemistry, Michigan State University, East Lansing, Michigan, USA

The evaporation in vacuo of the matrices used and the particle-induced desorption of matrix molecules in fast-atom bombardment (FAB) contribute to a proposed high pressure region above the FAB matrix known as the selvedge region. If the neutral number density is sufficiently high, ions formed upon bombardment may undergo collisions with molecules, yielding matrix-related cluster ions and, in cases when the analyte is desorbed in neutral form, protonated and deprotonated analyte molecules. Similarities with the chemical ionization (CI) experiment have been pointed out previously and are further developed here. If FAB is similar to CI, then the response depends on the structures of the reagent ions—those ions that react with gas phase analyte molecules. We consider here the time dependence of positive and negative ion FAB spectra to attempt to identify the reagent ions of FAB. A model is suggested for the FAB ion source which evaluates similarities to a CI source, as well as spatial aspects that are unique to desorption/ionization techniques. (J Am Soc Mass Spectrom 1997, 8, 337–351) © 1997 American Society for Mass Spectrometry

Regardless of whether it is “an old maxim” or not, desorption/ionization methodology for mass spectrometry clearly *does* demonstrate that you “do not always need to know what you are doing to get useful information” [1]. Although several groups are currently investigating the details of the desorption and ionization steps in matrix-assisted laser desorption/ionization (MALDI), many of the same questions remain for fast-atom bombardment (FAB) and liquid secondary ion mass spectrometry (LSIMS). Nonetheless, each is used daily to solve chemical problems. Characterization of these systems continues with the promise that, once the physical and chemical aspects of the process are understood, the overall experiment can be optimized, for improved analytical capabilities.

In the case of FAB, a number of descriptions of the desorption aspect of particle bombardment have been put forth [2–6]. Details of this facet may be most closely related to the molecular weight limits of the technique. However, the response of analytes and the

fact that not all analytes yield detectable signals in FAB mass spectrometry may well be more closely related to the chemical aspects of the technique. *How are analytes ionized in the FAB process?*

In the development of FAB, its parallels with chemical ionization have been discussed [7]. Analyte responses appear to depend on gas phase proton affinities [8–11]. Protonated and deprotonated analytes are formed. With the introduction of the concept of a gas phase selvedge region existing above the liquid target [12], FAB could be described as essentially a glycerol chemical ionization experiment. Ions and analytes are desorbed not into the high vacuum, but into this region where collisions can occur. Although not incorporated into this model to date, the time dependence of FAB spectra could also be explained by invoking gas phase ion/molecule reactions.

More recently a very different mechanism has been developed in which the chemistry through which the observed ions are formed takes place in high pressure gas cavities, which constitute the initial *interfacial region* linking the distinct condensed and gas phases of the experiment [5] (see Figure 1). In these cavities, formed upon fast-atom impact as a result of the collision cascade, a variety of reactions can occur [5]. Of

Address reprint requests to Dr. John Allison, Department of Chemistry, Michigan State University, East Lansing, MI 48872-1322. E-mail: allison@cemvax.cem.msu.edu

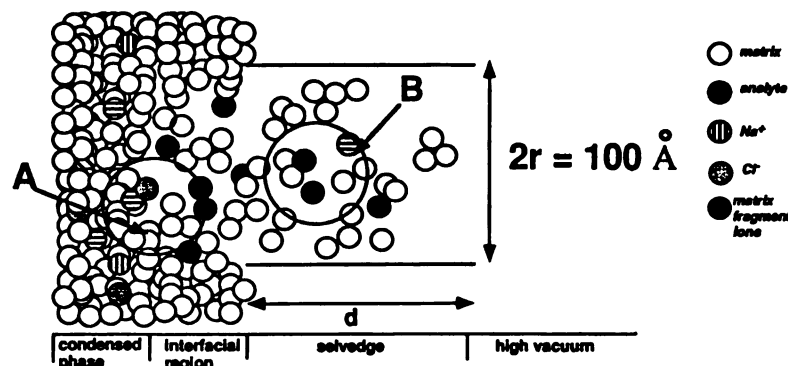
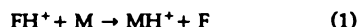
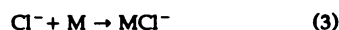


Figure 1. Schematic showing the site of fast-atom impact into a FAB target containing glycerol matrix, NaCl, and an analyte. The impact cavity is shown as well its contribution to the gas phase selvedge region. In the region labeled A, the interface between liquid and gas, ion/ion recombination reactions occur with high rates. Once desorbed from this region, analyte ions move into the "selvedge region," where ion/molecule reactions can occur, but not ion/ion recombinations. Dimensions indicated are discussed in the text.

particular importance are ion/molecule reactions, through which analytes acquire charge when the analyte (*M*) is present in the matrix in neutral form. In this discussion, the matrix is glycerol (*G*). These reactions include various kinds of proton transfer, such as

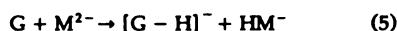


or anion/cation attachment, if salts such as NaCl are present:



In reaction 1, FH^+ represents any organic ion derived from glycerol that could protonate *M*.

When the analyte is ionic, introduced into the glycerol matrix as an Na_2M salt, for example, a variety of processes can occur to yield singly charged species, such as



Recombination reactions such as reaction 4 maybe the fastest in this interfacial region [5]. As desorption takes place, attractive ion/ion interactions overcome the influence of the solvent. When insufficient energy is available to desorb the multiply charged analytes proton abstraction involving matrix molecules is also an attractive option for M^{2-} [reaction (5)] because the desolvation energy is considerably less for species with lower overall charges [13].

Although chemistry in the interfacial region is clearly important, especially for charged analyte

species, there are aspects of FAB mass spectrometry that cannot be explained by the high pressure gas cavity alone. One is the time dependence of FAB, which will be the focus of this work. If all of the chemistry responsible for the ions observed takes place in very small microvolumes at fast-atom impact points, then FAB spectra would not be expected to have a substantial time dependence. The time-dependent spectra correlate with decreasing matrix/sample amounts, which could decrease the number of collisions in the gas phase, yielding fewer products of ion/molecule reactions. This concept will be developed and evaluated here, with a focus on the formation of the protonated matrix molecule and the higher mass proton-bound matrix clusters in positive ion mass spectra, as well as the analogous anions formed. The details of the time-dependent aspects of FAB will be discussed and the possibility of the contribution of gas phase ion/molecule reactions to the observed ions will be evaluated. We specifically attempt to define, if ion/molecule reactions are occurring, the reactant ions for the most common matrix—glycerol.

The "Chemical Ionization" Model of Fast-Atom Bombardment

If a situation is created in a portion of the FAB ion source that resembles a glycerol CI experiment, in which particle bombardment supplies reagent ions and desorbed neutral analyte molecules, then what are the reagent ions? Which ions are responsible for protonating desorbed analyte molecules *M*? Consider the similarities between the FAB experiment and methane chemical ionization (CI). In methane CI, CH_3^+ once

formed collides with many additional methane molecules, with little subsequent chemistry, allowing for the accumulation of large numbers of these reagent ions. In contrast, GH^+ reacts upon subsequent collisions with glycerol molecules, leading to proton-bound clusters as large as $(\text{G})_3\text{H}^+$ [14]. If one considers the high pressure ion source and the spectrum of methane alone, it is clear that most analyte molecules that collide with a gas phase ion will encounter CH_3^+ , and these are considered as the reagent ions (in addition, of course, to C_2H_5^+). In the FAB spectrum of glycerol, the most abundant cation is frequently m/z 93, GH^+ . Thus, one may consider glycerol CI as involving ionization of analytes through the following proton transfer reaction, as described by Kebarle et al. [8, 11],



and the response, or lack thereof, would depend on the relative proton affinities of the analyte and glycerol. This analysis is based on the assumption that many protonated matrix molecules are available for reaction because they are represented by one of the most intense peaks in the mass spectrum. Another possibility is that GH^+ ions are products of ion/molecule reactions as are MH^+ ions for neutral analytes M. One may also consider the various G_nH^+ ions as reagent ions, but these are expected to have high proton affinities, which makes them less likely to protonate analyte molecules than GH^+ [15].

Although FAB has many similarities with CI, there are critical differences. One that is most crucial to this discussion is the spatial aspects of the experiment (see Figure 2). When energetic particles collide with the glycerol target, primary ions are formed in the cavity created by the impact. Sunner et al. [16] refer to these ions as collision cascade ions. For simplicity, we will refer to them as reagent ions because, as the interface between the condensed phase and the vacuum breaks down forming the selvedge, the primary ions formed at the interface will pass through the selvedge and continue to react. The concentration of reagent ions and desorbed neutrals will be highest at this liquid/gas interface. As molecules diffuse away from the target, the CI model suggests that collisions occur and reagent ions are converted into ion/molecule reaction products, which react further, and so forth. At some point in space the average number density becomes sufficiently low that no additional chemistry occurs (the outer edge of the selvedge region) [12, 17], and it is the ionic species that exist at this point, after the chemistry is over, that are sampled and represented in a FAB mass spectrum. Although m/z 93, representing GH^+ , is the most intense low mass peak in the mass spectrum of glycerol, this does not mean that GH^+ is the reagent ion in this experiment [11]. In this model it would be a reaction product. When analyte molecules

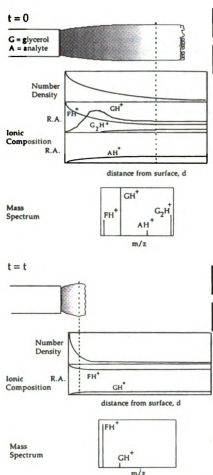


Figure 2. A schematic of aspects of the FAB ion source, for the CI model discussed, are shown at the beginning of the experiment, $t = 0$, and late in the experiment, many minutes after initiation of particle bombardment, at some $t = t$. The two figures show the relatively large liquid target (not to scale) at $t = 0$, the small remaining target at $t = t$, and the mass spectra for each point in time. The mass spectra represent the ions that leave the ion source, not the species initially formed at the target surface. In the upper figure, pressure decreases as d , the distance from the surface, increases. The pressure is due predominantly to neutral glycerol molecules. A variety of primary ions are formed at the surface; these are simply designated here as FH^+ (the figure focuses on the positive ion experiment). Their relative abundance decreases with increasing d as collisions lead to ion/molecule reaction products GH^+ and MH^+ . Subsequent collisions most apparently lead to glycerol clusters such as C_2H_5^+ . The dotted line represents some point in space that can be considered the edge of the high pressure selvedge region—that value of d where the pressure is reduced to a value where no additional chemistry occurs (no relative dimensions are meant to be implied in the figure). At long times, $t = t$, the sample size/area has been reduced to the point where it cannot maintain a “high” pressure selvedge region. Under such conditions, FH^+ ions, formed at the target surface, pass through the ion source essentially collision-free. It is at this point that, while total ion currents are reduced (because the total amount of matrix/analyte on the surface is very small), the ions detected are the nascent ions of particle bombardment of glycerol.

first desorb from the target, they encounter reagent ions. As they move away from the target and the ionic composition of the gas changes, they may be protonated by species such as GH^+ that will contribute to the MH^+ signal. However, both M and G are protonated in this model by the reagent ions generated from particle bombardment, and it is one purpose of this article to consider the identity of these ions.

In addition to GH^+ , G^+ is a reagent ion candidate, as are fragment ions, possibly similar to those observed in the electron ionization (EI) mass spectrum of glycerol [18]. When gas phase glycerol molecules are ionized by energetic electrons, there is essentially no molecular ion detected at m/z 92 ($\text{C}_3\text{H}_8\text{O}_3^+$): the four major fragment ions are m/z 61 ($\text{C}_2\text{H}_5\text{O}_2^+$), 43 ($\text{C}_2\text{H}_3\text{O}^+/\text{C}_3\text{H}_7^+$), 31 (CH_3O^+), and 29 ($\text{C}_2\text{H}_5^+/\text{CHO}^+$). These are all even-electron ions.

We propose that the identity of the reagent ions of FAB—those ions that play the role of primary reactant ions for subsequent gas phase ion/molecule reactions—can be experimentally determined. If a substantial fraction of the reagent ions are converted into product ions because of the high pressure selvedge region, then one need only to reduce the number density in this region, and the primary ions will be able to pass, unaltered, from the surface of the FAB probe to the mass analyzer. How might one remove the selvedge region? Remove/limit its source. The approach evaluated here involves decreasing the amount of glycerol present on the probe. With less glycerol surface area present, the contributions to the number density at points within the ion source decrease. As the number density decreases, there are fewer collisions—less conversion of reagent ions to reaction products. There are several ways to decrease the amount of glycerol present on the probe tip, and we propose that an informative way to do so is to begin with a typical amount of glycerol and let desorption in vacuo and particle bombardment deplete the sample to the amount desired. That is, the time-dependent spectra of glycerol should lead to a situation where very small amounts of glycerol remain (at long times), the spectrum of which could represent the reagent ions of FAB. This aspect of the model is summarized in Figure 2. It is well known that FAB spectra are time-dependent and that the ions from the matrix vary with time [19, 20]. As time passes in a FAB experiment, the most noticeable change is in the glycerol cluster ions. As the number of gas phase glycerol molecules in the source decreases, less clustering occurs, which would be consistent with having fewer collisions. Thus, for the G_nH^+ ions, the average value of n decreases as time increases, consistent with a gas phase clustering mechanism:



It also suggests that, at sufficiently long times, spectra can be obtained under conditions of reduced collision numbers. It is this proposal that we evaluate here, to identify the reagent ions, both positive and negative, formed in FAB from glycerol, realizing that we are evaluating a model, to determine the extent to which ion/molecule reactions could play a role in generating the ions observed.

Experimental

All experiments were performed on a JEOL HX-110 double-focusing mass spectrometer (JEOL, Ltd., Tokyo, Japan) of forward geometry with an accelerating voltage of 10 kV and a FAB gun voltage of 6 kV with 5 mA of emission current, by using xenon as the FAB gas. Resolution was set at 3000. The total cycle time for a single scan was set at 1 min. When data were acquired over a mass range of 0–400, each spectrum was acquired in 15.4 s with a reset time of 44.5 s. When the mass range of 0–800 was being studied, the time required to obtain each spectrum was 21.9 s, again with a reset time that allowed for the generation of one spectrum per minute.

The glycerol was mixed with an equal volume of methanol to allow for reproducible amounts of matrix to be transferred to the FAB probe tip. Typically, 1 μL was applied to the probe tip. The methanol was pumped away before the FAB experiment began. Separate studies were carried out with pure glycerol and were compared with the results of the experiments where the methanol:glycerol mixture was used, to be certain that residual amounts of methanol did not contribute to the mass spectra obtained.

The 1,1,2,3,3- d_5 -glycerol was obtained from Cambridge Isotope Laboratories (Woburn, MA). The extent of deuteration was reported to be 98%. The digoxin was purchased from Sigma Chemical Co. (St. Louis, MO). Both chemicals were used as received. Digoxin was dissolved in a 1:1 methanol:chloroform mixture to a concentration of 5 $\mu\text{g } \mu\text{L}^{-1}$. One microliter of this solution was mixed with the matrix on the FAB probe tip prior for insertion into the mass spectrometer.

Results and Discussion

The Chemical Ionization Model for Fast-Atom Bombardment

Results will be presented first for the positive ions formed by fast-atom bombardment of glycerol. Several studies have been reported on the ions formed from glycerol, which may be candidates for reagent ions [19–22]. In 1982, Field [19] discussed the time dependence of selected ions in the FAB spectrum and provided strong evidence for radiation damage to the matrix upon particle bombardment, wherein a fraction of the glycerol is converted into radicals, which react

to form larger molecules. These species appear in protonated form in the FAB mass spectrum (as does glycerol). According to Field, continuous bombardment leads to crystalline products from the viscous glycerol target. Ligon [21] also suggested the possibility of radical formation in glycerol. However, one of the major advantages of FAB that has been discussed is the constantly refreshed surface of the liquid matrix [1]. That is, any decomposition products are desorbed when formed. In 1994, Caldwell and Gross (referred to as CG) [22] reported a detailed study of the glycerol-derived ions. In their study, sufficient resolution was used to establish the ions' elemental compositions. They also report data that demonstrate that free radical chemistry occurs as particle bombardment takes place, leading to higher molecular weight species in the glycerol matrix, which contribute to the observed chemical background in FAB spectra. Proposed free radical reaction products were supported by both positive and negative ion spectra. We will use the CG data as the basis for a discussion of the possible reagent ions of FAB, keeping in mind the radiation damage model, and expand the information available by considering the time dependence of some of the dominant ions.

The Positive Ion System

Figure 3 shows six mass spectra obtained at various times when a glycerol sample is bombarded by fast xenon atoms. One mass spectrum was obtained per minute. Not shown is an example of the final, unchanging spectrum obtained when glycerol is completely depleted and the stainless steel surface is bombarded. In this case, the spectrum contains peaks representing Na^+ (m/z 23), K^+ (m/z 39), Cr^+ (m/z 52), and Fe^+ (m/z 56). Spectra undergo relatively small changes in early periods (in this particular experiment, the first 30 min), then begin to change more rapidly. First consider the protonated glycerol and proton-bound clusters m/z 93 (GH^+), 185 (G_2H^+), 277 (G_3H^+), and 369 (G_4H^+). If formed in the gas phase, their relative intensities are sensitive indicators of the mean number of collisions that ions undergo when passing from the target surface to the free vacuum of the mass spectrometer. As time passes, the peak representing m/z 369 first disappears from the spectra, then 277, then 185, and eventually, in spectrum 52, even m/z 93. This is consistent with a set of consecutive reactions 7-9. If one considers the relative intensities of the m/z 185, 277, and 369 peaks in spectra 1, 10, and 30, it appears that throughout the course of a FAB experiment the average collision number in the gas phase is *not* constantly decreasing. When the FAB beam is first turned on, the number density of glycerol molecules above the target is established by the desorption rate in vacuo. Particle bombardment increases the rate of desorption, resulting in an increase in aver-

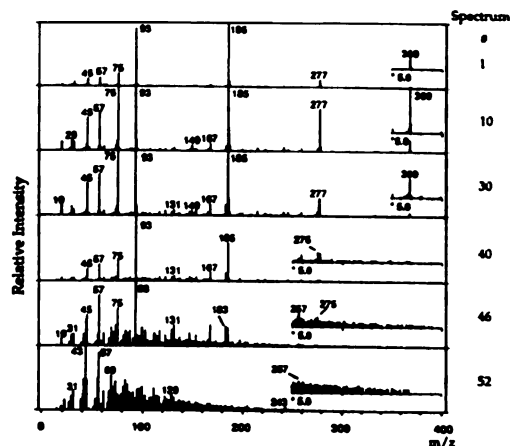
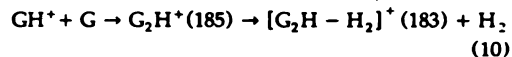


Figure 3. Positive ion FAB mass spectra of glycerol. The glycerol sample was bombarded continuously for 1 h, with one mass spectrum acquired each minute. The insets in spectra 40, 46, and 52 show the high mass portion of the mass spectra, magnified by a factor of 5.

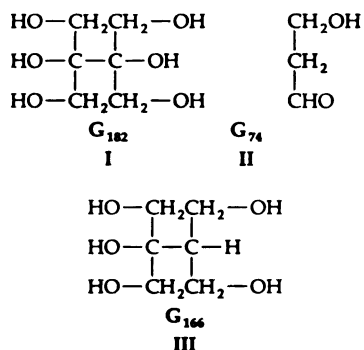
age number density until a tenuous steady state is achieved. This may also be influenced by a spreading of the glycerol, increasing the surface area, upon bombardment. That is, the data suggest that ions are undergoing more collisions to yield the ion distribution in spectrum 10 than in spectrum 1. From that point on, glycerol is depleted and its number density above the surface decreases.

Next, consider ions of intermediate mass, such as m/z 183. This ion could be a simple fragment ion of m/z 185, formed in a process such as

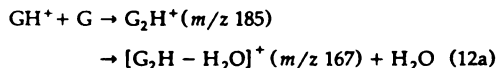
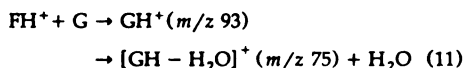


However, the m/z 183/185 ratio increases throughout the experiment. In the first spectrum of Figure 3, the ratio is zero, while in spectrum 46, the ratio is greater than 1. Field [19] and CG [22] are clearly correct in their discussions of radical formation and radical coupling. Compound I is formed upon particle bombardment, presumably due to radical chemistry. It accumulates to some extent in the matrix, being less volatile than glycerol. It is desorbed and protonated to yield the peak at m/z 183, which represents $(\text{G}_{182})\text{H}^+$. The time dependence is consistent with this mechanism. We will use here the designation for free radical chemistry products of glycerol that was employed by CG, in which the neutral molecule derived from glycerol with

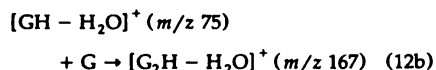
a molecular weight of 182 is designated as G_{182} :



Other ions are of note regarding proposed free radical mechanisms. Consider two pairs of ions that are observed: m/z 93 and 75 and m/z 185 and 167. Both pairs are separated by 18 u and could result from dehydration following protonation in the gas phase, as suggested in the reactions



Certainly water loss from protonated alcohols is a facile process [23]. However, it has been proposed that radical chemistry in the matrix leads to compounds II and III, with molecular weights of 74 and 166. Both then can appear in protonated form in the FAB spectrum. Which description is correct? Both probably contribute. If one compares spectra 46 and 52 in Figure 3, it appears that when m/z 93 vanishes, 75 does so as well, suggesting that a gas phase mechanism, process 11, links 93 and 75. However, the ratio of m/z 167 to 185 increases throughout the experiment, which would be most consistent with a buildup of the free radical coupling product G_{166} , with the m/z 167 peak representing this compound in protonated form. If pressure changes with time, the data also suggest that the direct protonation of G_{166} as a process leading to m/z 167 may be more important, at least at long analysis times, than other options such as a gas phase mechanism involving clustering of m/z 75 with glycerol:



In terms of the accumulation of products of radical chemistry in the matrix during FAB, the ions with m/z 75 and 167 may suggest that products with higher molecular weights (higher heats of vaporization, such

as III) accumulate more so than products such as II, with molecular weights less than that for glycerol. Now consider the low mass portion of the first spectrum in Figure 3. The intense fragment ions of glycerol are m/z 45, 57, and 75. These might be the primary ions of FAB, dominant at the surface, but attenuated as they pass through the selvedge region and are converted into GH^+ and its subsequent products. The first mass spectrum of Figure 3 may suggest



As time passes and the $G_n\text{H}^+$ ions decrease in abundance, the ions with mass-to-charge ratio values less than 92 increase in relative intensity, consistent with reaction 13; fewer collisions lead to less conversion of reactants to products. However, additional ions appear in the spectra acquired after many minutes of bombardment, such as m/z 31 and 43. These may be the most reactive reagent ions, as reflected by their low relative intensities in FAB spectra taken early in the experiment. Spectrum 52 suggests that when so little glycerol is present that a selvedge region cannot be established, the primary ions formed are m/z 31, 43, 45, and 57. Clearly many other low mass ions are formed in lower abundance; however, we will focus our discussion here on this set.

If these four ions constitute the primary "reagent ions" of FAB, then they must be consistent with reaction 13 representing exothermic processes. Can these ions protonate glycerol? First consider possible ion structures. CG [22] assigns the formula $\text{C}_3\text{H}_5\text{O}$ to the m/z 57 ion. In Table 1, possible structures are given. If m/z 57 is the product of multistep processes, it may be due to prompt fragmentation of m/z 75, upon elimination of water. Two pathways are shown in Figure 4, depending on whether the H that shifts in the process is from carbon or oxygen, to form an enol or epoxide ion. To assist in understanding ion structures, the FAB spectrum of d_5 -glycerol was obtained. The d_5 -glycerol has the structure $\text{CD}_2(\text{OH})\text{CD}(\text{OH})\text{CD}_2(\text{OH})$, with all deuteria on carbon atoms. With this modification, the peak at m/z 57 shifts to m/z 62. All five deuteria remain in this ion, which is consistent with the epoxide structure given in Table 1.

Next consider m/z 45. Caldwell and Gross [22] report an elemental composition of $\text{C}_2\text{H}_3\text{O}$. In Figure 4, a possible mechanism for its formation is shown, involving elimination of formaldehyde from m/z 75. In d_5 -glycerol, the mass-to-charge ratio value for this ion shifts to m/z 48. Two hydrogen atoms remain in the fragment, consistent with a mechanism involving formaldehyde elimination to form this 2-C fragment ion. The m/z 45 ion can eliminate H_2 to form the ion at m/z 43, consistent with one of CG's elemental assignments of $\text{C}_2\text{H}_3\text{O}$. At least two distinct species are represented by the peak at m/z 43; CG identified a second component with the formula C_3H_7 . It is not

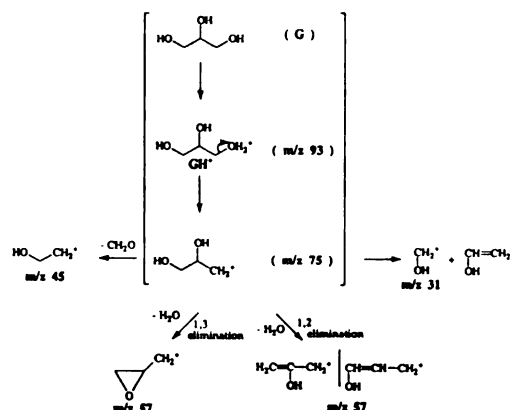


Figure 4. Possible mechanisms for formation of reagent cations. The observed ions can all be generated from a precursor of m/z 75, which could evolve chemically from protonated glycerol. The species in parentheses indicate possible precursors to the reagent ions observed.

unequivocally obvious what the mass shift is for m/z 43 in the deuterated glycerol experiment. The m/z 43 ions become dominant at long times, but while dominant, the ion currents for all species are low. It appears that the m/z 43 ion splits to yield two species, m/z 45 and 46, of approximate equal abundances, at long times in the d_5 -glycerol experiment, consistent with the indicated structures in Table 1.

The fourth ion to be considered is m/z 31, which CG [22] assign as CH_3O . When d_5 -glycerol is used, the peak splits, providing ion current at m/z 33 and 34. An inductive fragmentation of m/z 75, shown in Figure 4, would lead to formation of m/z 33 in the partially deuterated experiment, supporting a structure of $\text{HO}-\text{CD}_2^+$. The ratio of peak intensities for m/z 33:34 changes throughout the experiment.

It should be noted that this set of four ions is different from those formed by 70-eV electron impact ionization of glycerol, where the fragment ions evolve from the molecular ion. The four most intense EI fragments are m/z 31, 43, 45, and 61. We note that m/z 61 corresponds to loss of $\text{CH}_2\text{OH}^\cdot$ from the molecular ion, upon C-C bond cleavage. It may well be an intermediate, similar to m/z 75 proposed in Figure 4, for the ions observed in the FAB experiment. We note that m/z 75 is most easily formed not from G^+ , but from GH^+ , upon loss of water. Thus, the primary ions formed by particle bombardment of the matrix may evolve from prompt fragmentation of highly excited GH^+ . The primary ions from a liquid may resemble ion/molecule reaction products more than EI-like fragments, at least when mechanisms for their formation such as those shown in Figure 4 are considered. This parallels reports of the ionization of alcohol clusters in the gas phase [24].

With some candidate structures to consider, is proton transfer possible from these primary ion candidates to glycerol? Can they participate in reaction 13? To answer this question, proton affinities (PA) can be considered, as well as an additional, very useful fact. When d_5 -glycerol is used, protonated d_5 -glycerol ($\text{C}_3\text{D}_5\text{H}_3\text{O}_3$) H^+ is formed at m/z 98. The "reagent ions" that protonate the glycerol molecules, as well as analyte molecules, transfer protons, not deuterons. Actually, an analysis of the ratio of peak intensities for m/z 98 and 99 reveals that the m/z 99 peak does not only represent the ^{13}C isotopic variant of this ion, but ($\text{C}_3\text{D}_5\text{H}_3\text{O}_3$) D^+ as well. However, in the process, 95% of the glycerol is protonated, and only 5% is deuterated. A similar observation has been reported by Ligon [21]. This ratio persists in the G_nH^+ clusters as well, consistent with their formation via reactions 7-9.

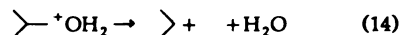
Can m/z 57 protonate glycerol? Its d_5 variant formed in the deuteration experiment does not appear to do so to any great extent, because the ion only

Table 1. Reagent cation candidates from glycerol

Mass-to-charge ratio and elemental composition		Proposed structures	
Glycerol	d_5 -Glycerol		
57	62	$\text{D}_2\text{C}-\text{O}-\text{CD}-\text{CD}_2^+$	$\rightleftharpoons [\text{D}_2\text{C}-\text{O}-\text{C}=\text{CD}_2]_{\text{D}}^+$
$\text{C}_3\text{H}_6\text{O}^+$	$\text{C}_3\text{D}_6\text{O}^+$		
45	48	$\begin{array}{c} \text{D} \quad \text{D} \\ \quad \\ \text{H}-\text{C}-\text{C}-\text{D} \\ \\ \text{OH} \end{array}$	$\rightleftharpoons [\text{DHC}-\text{O}-\text{CD}_2]_{\text{H}}^+$
$\text{C}_2\text{H}_6\text{O}^+$	$\text{C}_2\text{D}_5\text{H}_2\text{O}^+$		PA = 786 kJ mol $^{-1}$
43	(45, 46)	$\text{HO}-\text{C}=\text{CH}_2^+$	$\rightleftharpoons \text{O}^+$
$\text{C}_2\text{H}_3\text{O}^+$			
C_3H_7^+		$[\text{C}_3\text{H}_7]^+$	
31	33, 34	$^+\text{CD}_2\text{OH}$	
CH_3O^+	$\text{CHD}_2\text{O}^+, \text{CD}_3\text{O}^+$	CD_3O^+	$\rightleftharpoons [\text{CD}_2\text{O}]_{\text{H}}^+$
		$^+\text{CD}_2\text{OD}$	PA = 718 kJ mol $^{-1}$

contains deuteria, and protonation clearly dominates in the experiment. It is not clear which compound should be considered when evaluating the gas phase acidity of this ion, because it may rearrange as it protonates a neutral molecule. We do note that of the four candidates for primary ions, m/z 57 is the largest in the first FAB spectra formed, when the number of collisions occurring following ion desorption is presumably highest. This may reflect the fact that it is not efficiently converted into products, as are m/z 43 and 31.

Can m/z 45 and 31 protonate glycerol? The proton affinity of glycerol is 874 kJ mol^{-1} [9]. As m/z 45 is written in Table 1, the proton affinity of oxirane should be considered. $\text{PA}(\text{cyclo-C}_2\text{H}_4\text{O}) = 786 \text{ kJ mol}^{-1}$ [25]. Proton transfer can occur in an exothermic process. Also, as written, it would be expected that protonation, not deuteration, would occur in the d_5 -glycerol experiment. The reaction would be exothermic by approximately 88 kJ mol^{-1} for thermal energy reactants. Reaction 14, involving species for which heats of formation are known, involves elimination of water in an inductive cleavage from a protonated alcohol in an analogous process; it requires approximately 80 kJ mol^{-1} [25]:



Thus, it appears that m/z 45 can participate not only in reaction 13, but in reaction 11 as well. In considering m/z 31, the proton affinity of formaldehyde is relevant. $\text{PA}(\text{CH}_2=\text{O})$ is 718 kJ mol^{-1} . With a PA even lower than oxirane, obviously m/z 31 can also protonate glycerol and induce further fragmentation to some extent. No information is available on the structure of m/z 31. The $^+\text{CH}_2\text{OH}$ ion is estimated to be 139 kJ mol^{-1} more stable than CH_3O^+ [25]. If this ion is a direct fragment of ionized glycerol, then the $^+\text{CH}_2\text{OH}$ form could be formed easily via ionization of a nonbonding electron on an oxygen atom followed by an α -cleavage reaction. If this is the case, then the ion would protonate by using a hydrogen that initially resided on an oxygen atom.

Can m/z 43 protonate glycerol? In the "normal" FAB spectrum, high resolution analysis shows that two species are present. One is C_3H_7^+ . This is probably not a primary fragment of glycerol. It is the minor component of the m/z 43 peak; CG attribute it to a fragment of "various species higher in mass," that is, they suggest that it is a fragment of a radiation chemistry product. Thus, we will not consider it here, although protonated propene [$\text{PA}(\text{C}_3\text{H}_6) = 750.31 \text{ kJ mol}^{-1}$] would certainly transfer a proton to oxygen-containing molecules such as glycerol. The other species represented by the m/z 43 peak is $\text{C}_2\text{H}_3\text{O}^+$. Regardless of whether the hydrogen atom that is transferred in a

protonation reaction is initially bound to a C or O atom, proton transfer to glycerol should be exothermic.

Present in the spectra shown, but not listed in Table 1, is a peak representing H_3O^+ , which is formed in low abundance. The m/z 19 ion has been explained by CG as a degradation product of glycerol, although its evolution from small amounts of water in the glycerol is possible as well. Whereas $\text{PA}(\text{H}_2\text{O})$ is 697 kJ mol^{-1} [25], the H_3O^+ ion certainly would transfer a proton to glycerol or most analytes, although the low relative intensity of the peak at m/z 19 in all spectra would suggest that this ion would be a minor source of protons.

Thus, a consistent picture emerges. Low mass ions, with mass-to-charge ratio values less than 93, could act as the primary cations of FAB by using glycerol as a matrix if they emerge into a reactive gas phase environment—the selvedge region—where the number density is sufficiently high that ion/molecule reactions occur. They would protonate glycerol and analytes that desorb in neutral form. Certainly, under multiple collision conditions, GH^+ can protonate analytes as well. However, this model suggests that it is not the proton affinity of G that determines whether an analyte will be protonated in the gas phase. More specifically, if reaction 6 represents "the chemical ionization process" of FAB, then only analytes with PAs higher than glycerol would be ionized. With the model considered here, analytes with lower PAs could be ionized as well. The PAs relevant for the primary ions would then be what control the system thermochemistry, not $\text{PA}(\text{G})$.

The Negative Ion System

In negative ion FAB, deprotonated analyte and matrix molecules are usually observed. Multiple mechanisms for the desorption/ionization have been proposed that may each contribute. Again consider a mechanism involving gas phase ion/molecule reactions. The most intense low mass peak in the negative ion spectrum of glycerol is at m/z 91, representing deprotonated glycerol $[\text{G} - \text{H}]^-$. It could react with desorbed neutrals, ionizing them via proton transfer:



The time dependence of the negative ions formed by fast-atom bombardment of glycerol was studied and representative spectra from a single experiment are shown in Figure 5. In this experiment, spectra were acquired for approximately 1 h. Over that period of time, the total ion current decreased by more than an order of magnitude as the glycerol was depleted. (Not shown are spectra obtained at very long times when the glycerol is completely depleted.) Although bombardment of stainless steel yields iron and chromium cations, analogous anions are not observed. Instead, the

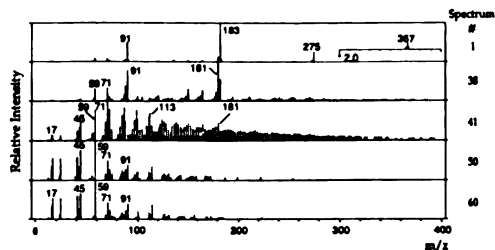


Figure 5. Negative ion FAB mass spectra of glycerol. The glycerol sample was bombarded continuously for 1 h, with one mass spectrum acquired each minute. The inset in spectrum 1 shows the high mass portion of the spectrum magnified by a factor of 2.

"clean" probe spectrum contains peaks representing Cl^- and fragment anions of pump oil at m/z 77, 89, 100, and so forth. As in the positive ion data, the spectra change as the glycerol is depleted and, in the model being considered, the number density of the neutral molecules in the source/selvedge region decreases. The set of ions that includes deprotonated glycerol $[\text{G} - \text{H}]^-$ at m/z 91 and its glycerol clusters $[(\text{G} - \text{H}) + \text{G}]^-$, m/z 183, $[(\text{G} - \text{H}) + 2\text{G}]^-$, m/z 275, and $[(\text{G} - \text{H}) + 3\text{G}]^-$, m/z 367, are shown in spectrum 1 of Figure 5. The relative intensities of these ions change with time, with the higher mass ions being lost first. In spectrum 1, m/z 183 is larger than 91. By the time spectrum 38 was obtained, the peak representing m/z 91 is larger and the higher clusters are no longer being formed. Spectrum 41 is typical in that moderately intense chemical noise (peaks at every mass) frequently appears at intermediate times; however, such signals make less of a contribution as bombardment continues.

In the cation spectra, we discussed the $[\text{M} + \text{H}]^+$ and $[\text{M} + \text{H} - \text{H}_2\text{O}]^+$ ions, suggesting that dehydration follows gas phase protonation—a common process for protonated alcohols that is known from the chemical ionization literature [23]. Obviously, although O-protonated alcohols can eliminate water in a facile process, there is no analogous mechanism for deprotonated molecules, and anionic analogs 18 u lower than some major peaks are not observed in the spectra of Figure 5. This further supports the premise that m/z 75 in positive ion FAB is more accurately written as $([\text{M} + \text{H}] - \text{H}_2\text{O})^+$ rather than $[\text{M} - \text{H}_2\text{O}]\text{H}^+$.

In the intermediate region of the spectra the peak at m/z 181 becomes larger than m/z 183 as bombardment time increases. Although 181 could be a fragment of 183, it is probably $[\text{G}_{182} - \text{H}]^-$, a deprotonated free radical coupling product, supporting evidence for G_{182} from the cation data. Although there is no direct description of the process leading to the m/z 113 ion, our data are consistent with the observation of CG that this

species grows with increasing time of particle bombardment.

The spectra taken at long times suggest that the following ions would be the primary anions of FAB, the glycerol negative reagent ions: m/z 17, 25, 43, 45, 59, 71, and 91. However, spectra taken after 60 min contain this set without m/z 91 present, so 91 will not be considered as a primary ion candidate. Could these ions act as reagent ions to deprotonate desorbed glycerol and analyte molecules? To answer this question, we will again consider possible ion structures, utilize data from FAB of d_5 -glycerol, and evaluate the thermochemistry. The "bond strength" between an anion A^- and a proton H^+ is reported as the gas phase basicity of the A^- ion. [Note that the gas phase acidity (GPA) of HA is equal to the gas phase basicity (GPB) of A^- .] For example, to evaluate reaction 15, one factor is the proton affinity of $[\text{G} - \text{H}]^-$, which is equal to the $\text{GPA}(\text{G}) = 1546 \text{ kJ mol}^{-1}$, the energy required to heterolytically cleave the RO-H bond.

Consider the anion with m/z 71. CG provided the elemental composition $\text{C}_3\text{H}_3\text{O}_2$ for this ion. The peak shifts to m/z 74 in the d_5 -glycerol spectrum, consistent with the structure shown in Table 2. We will at this point exclude m/z 71 as a candidate for the set of primary anions of FAB. Consider again Figure 3. We proposed that, at long times in the FAB experiment, sample size is depleted and the selvedge region is of sufficiently low number density that primary ions can pass through the source, experiencing few collisions, to the mass analyzer. From this standpoint, spectrum 50 in Figure 5 represents the ions formed at the matrix/vacuum interface (still, some reactions could be occurring in the gas phase to form m/z 91). However, it also is a spectrum taken after almost an hour of particle bombardment and is more likely to contain ions arising from bombardment of accumulating free radical chemistry products. Such ions will not dominate the primary ions formed early in a FAB experiment (short bombardment times). The m/z 71 ion may well fall into this category. CG suggest that m/z 71 is a deprotonated form of a degradation product, not a primary product of intact glycerol. It may come from two sources, because it is present in early spectra, although only in small abundances. While the relevant GPA is not known, we can suggest an approximate value of 1502 kJ mol^{-1} , based on data for a similar structure, $\text{CH}_2=\text{CH}-\text{OH}$ [25].

The ion with m/z 59 may have similar reactivity to m/z 71. The formula $\text{C}_2\text{H}_3\text{O}_2$ and the fact that the peak shifts to m/z 61 in the d_5 -glycerol experiment suggests the structure shown in Table 2. Again, it may have a GPB of approximately 1533 kJ mol^{-1} . However, when considering the proposed structure of the m/z 59 ion and that of vinyl alcohol (for which the GPA is given), one might expect m/z 59 to have a somewhat lower GPB. Hydrogen bonding in the ion, between the anionic oxygen and the adjacent hydroxyl group,

Table 2. Reagent anion candidates from glycerol

Mass-to-charge ratio and elemental composition		Proposed structures A ⁻	PA (A ⁻) (kJ mol ⁻¹)	AH (or analog)
Glycerol	d ₆ -Glycerol			
91 C ₂ H ₇ O ₃ ⁻	96 C ₃ D ₆ H ₂ O ₃ ⁻		1546	(<i>n</i> -propanol)
71 C ₃ H ₅ O ₂ ⁻	74 C ₃ D ₃ O ₂ ⁻		(1533)	
59 C ₂ H ₃ O ₂ ⁻	61 C ₂ D ₂ HO ₂ ⁻		(1533)	
45 CHO ₂ ⁻	46 CDO ₂ ⁻ (46)		1415	HCOOH
43 C ₂ H ₃ O ⁻	(26)		1533	CH ₂ CHOH
25 C ₂ H ⁻	18 OD ⁻		1576	C ₂ H ₂
17 OH ⁻			1635	H ₂ O

should lower its proton affinity. Obviously, fragment ions such as m/z 71 and 59 would deprotonate glycerol. Thus, all such reactions should be possible—slightly endothermic or exothermic depending on structural details such as hydrogen bonding that influence ion and neutral stabilities. Also, if the ions are formed with additional energy, this would be critical in inducing such chemistry.

The ion at m/z 45, observed in Figure 5, spectra 41, 50, and 60, is not observed early in the FAB experiment. It appears to yield an ion at m/z 46 at long times in the d_5 -glycerol experiment. CG [22] also report a peak at m/z 43 and assign it as C₂H₃O⁻. There is no m/z 43 in the d_5 -glycerol spectrum at long times; it may contribute to the ion current at m/z 46 in this case. The relevant GPB is 1502 kJ mol⁻¹ and it would deprotonate glycerol in an exothermic process:



The peak at m/z 25, again observed at long times, represents C₂H⁻. It appears in the d_5 -glycerol spectra at m/z 26. The relevant GPB is that for acetylene, 1576 kJ mol⁻¹. The last ion in question is m/z 17, OH⁻. Water has a high gas phase acidity, 1635 kJ mol⁻¹; thus as a primary ion it would deprotonate glycerol in a process that is exothermic by 89 kJ mol⁻¹.

Thus, low mass fragment ions are realistic reagent ions for the negative ion FAB (glycerol CI) experiment. The CI model would then support the proposal that

the primary ions cited contribute to the m/z 91 signal and form deprotonated glycerol clusters with subsequent glycerol molecules. When analytes are present in the glycerol and are desorbed in neutral form, they would first encounter the primary anions m/z 17, 43, 59, and so forth and would participate in ion/molecule reactions, most likely involving proton transfer to form [analyte - H]⁻ species.

Can Ions Emerging from the Fast-Atom Bombardment Target be Converted into Gas Phase Ion / Molecule Reaction Products?

Estimate of Collision Frequencies in the Selvege Region. The selvedge region has been defined as a region of space above the FAB target that extends to the point where chemistry/collision stops [12]. We use the term as shown in Figure 1 to represent a region of space separate from the interfacial region. Gas phase K⁺ ions have been injected into this region to show that gas phase analyte and matrix molecules are present and collisions can occur [26, 27]. Campana and co-workers [28-30] coupled CI with FAB to analyze desorbed molecules as well. Glycerol and analyte molecules are present in the gas phase: they desorb, pass through the ion source, and are pumped away by the mass spectrometer vacuum system. They also condense on ion source surfaces, to be desorbed at later times and again pass through the ion source. In addition to the contri-

butions of evaporation in vacuo, molecules are desorbed in the FAB process. At low ion fluxes, one might expect complex distributions of gas phase molecules—changing on a variety of time scales. Single desorption events send a collection of molecules and ions into the gas phase, in an expanding “packet.” As the number of collisions on the surface becomes large, these small “pressure pulses” contribute to the average number density in the gas phase above the surface.

Local pressures in the selvedge region encountered in FAB as high as 10^6 torr have been suggested [17], cited as sufficient to maintain CI-type conditions. If a selvedge region exists in which gas phase chemistry occurs, the question is not whether the region extends throughout the ion source or only a small distance above the surface. The important parameter is the number of collisions that a desorbed ion might experience. Whereas the ion is desorbed during a collision event, the desorption is accompanied by a “burst” of molecules. Consider the number of collisions that a desorbed, neutral glycerol molecule might experience as it leaves the FAB target surface and passes through the ion source. According to the kinetic theory of gases, the collision frequency Z in a gas can be calculated through the relation $Z = \sqrt{2} \sigma c N$, where σ is the collision cross section, c is the mean speed, and N is the number of particles per unit volume (n/V). Assume, that an incident fast Xe atom sputters 1000 glycerol molecules [31] from an area of πr^2 , where r is estimated to be 50 Å [17]. These molecules are present in some volume of the selvedge region, with a “thickness” d and a volume of $\pi r^2 d$. The glycerol molecule spends some time in this region, which depends on the dimension of the region and the speed of the molecule, $t = d/c$. Thus, the mean number of collisions a desorbing glycerol molecule will undergo is $z \times t = \sqrt{2} \sigma n / \pi r^2$. According to this simple model, the number of collisions depends only on the collision cross section and the number of particles sputtered per unit area. With an estimated molecular diameter of 6 Å [32], the hard sphere collision cross section for a glycerol molecule would be 113 \AA^2 , yielding a mean number of 20 collisions. Collision cross sections for reactions between ions and polar, polarizable molecules at thermal energies are usually an order of magnitude greater than for neutral-neutral collisions. Suppose the mean collision cross section for glycerol ions with glycerol molecules is 550 \AA^2 (the mean of 100 and 1000 \AA^2). In this case, the average number of collisions would be as large as 100. Although obviously a crude estimate, this calculation does show that multiple collision conditions are plausible. To keep the calculation simple and to avoid calculating speeds or the variable d , one assumption is that the set of molecules desorbed in a single collision event exists in essentially a cylindrical gas phase volume of $\pi(50)^2 d$. In fact, the “packet” diverges, lowering the number density with increasing distance from the surface. This leads to the

second contributor to the selvedge region—molecules desorbed from neighboring impact sites. The third contributor is the evaporation in vacuo of glycerol. If the selvedge is, as suggested by some, a gas phase region within 10–500 Å from the surface, then only the first and the third contributing factors may be significant. However, because all molecules, once desorbed, pass through the entire ion source, one can imagine a distribution of number density throughout the source, with all three processes contributing to the total number of collisions a desorbed molecule experiences. If the time-dependent aspects of FAB spectra are due to number density changes in the selvedge region, then the first contributor considered would not be a major contributor. Such considerations may be consistent with the observed temperature dependence of FAB spectra. FAB spectra of neat glycerol at a variety of temperatures have been reported [33, 34], with the relative intensities of the $G_n H^+$ cluster ions decreasing with decreasing temperature. Although changing viscosity and variations in hydrogen bonding are reasonable explanations, the changes in the spectra at reduced temperatures could also be due to the reduced number density in the selvedge region because thermal desorption no longer contributes.

Are the Ions Observed at Long Irradiation Times from Glycerol or Products of Radiation Chemistry?

Long Evaporation, Short Irradiation Experiments. We have developed a model that considers the ions formed at long times in the FAB experiment and evaluated the proposal that these are the primary ions of FAB. However, the sample was bombarded for a period of almost an hour to sufficiently deplete the glycerol and create the situation where the mean number density of neutrals above the target was minimal and primary ions could be identified. We also note that other species are formed upon particle bombardment, which have been proposed to accumulate and yield ions. Are the ions discussed here as primary ions of glycerol not that at all, but representative of accumulated radical chemistry products? This does not appear to be the case. If higher molecular weight species are formed and accumulate, then ions with higher mass-to-charge ratio values should be represented in the mass spectrum not the small fragment ions observed. Some candidates for primary ions can be ruled out on this basis. The question can also be addressed through analogous experiments *without* lengthy particle bombardment. It has been suggested that particle bombardment roughly doubles the rate of glycerol desorption [19]. Thus, if a glycerol sample is introduced into the low pressure ion source and the fast-atom beam is not initiated, then one should need to wait approximately twice the time to achieve the situation where the amount of glycerol on the probe is very small. These are difficult experiments. The time difference required between glycerol

introduction and initiation of the FAB process and data collection is difficult to establish, because one has to determine when there is just enough glycerol left on the probe so that the neutral number density in the source is low, but to do so without turning on the FAB beam. To determine when the sample is sufficiently depleted, we had to irradiate the sample for short periods of time (typically 5 s) to follow the course of evaporation. Representative results for these long time evaporation/short time irradiation experiments are shown in Figure 6. Pure glycerol was introduced on the FAB probe tip into the vacuum system of the mass spectrometer and was allowed to evaporate for up to an hour prior to the bombardment. It was then irradiated for 10 s while a mass spectrum was obtained (spectrum 60). In this spectrum, the most intense ions are m/z 93 and 185. The FAB beam was then turned off. In the spectra taken several minutes later (spectra 65 and 67 in Figure 6) these ions are no longer dominant and the relative intensities of the low mass fragment ions at m/z 45, 57, and 75 here increased. These results suggest that the low mass ions are formed from particle bombardment of glycerol and they are not the fragments of radiation damage products because the irradiation time in this data set was very short.

An interesting feature of these long evaporation/short irradiation experiments is the appearance of relatively intense ion currents at m/z 167 and 189. These ions are usually assigned as $[G_2 - H_2O + H]^+ = 167$ and $[G_2 - H_2O + Na]^+ = 189$. CG [22] however, suggest a different possible assignment for the ion at m/z 167 based on collision-activated dissociation spectra. Because no detectable loss of water can be observed from the tentative precursor ion $[G_2 + H]^+$, but consecutive losses of up to three water molecules can be observed for the ion at m/z 167, they propose that the possible structure is $[G_{166} + H]^+$; that is, this ion is formed by the protonation of a radical coupling product. In the experiment presented in Figure 6, the accumulation of radiation damage products is not expected. Instead, it seems that a compound with a molecular weight of 166 is originally present in the glycerol and its vapor pressure is lower than that of the glycerol; it becomes more concentrated as the glycerol evaporates from the probe. As the concentration of glycerol decreases, the rate of its protonation by the primary ions becomes lower than the rate at which the ion at m/z 167 is formed; thus this ion becomes more dominant in the mass spectrum. What is the origin of the ion at m/z 167? It is known that upon heating in vacuo glycerol forms diglycerol ether and this compound could be present in the glycerol [35]. We distilled the glycerol used but have not been able to completely separate out diglycerol ether. In addition to the ion at m/z 167, another ion appears at long times, m/z 189. This ion deserves to be discussed because it is formed by a different mechanism. It can be the sodium ion adduct of the diglycerol ether or can be formed via protonation of the sodium salt of the

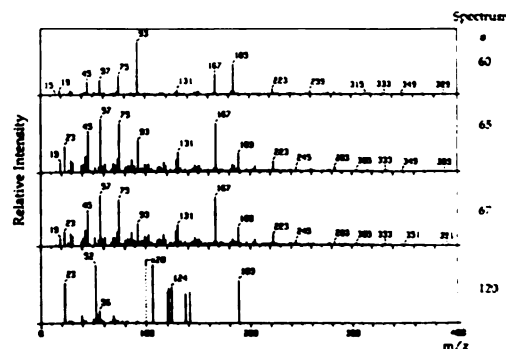


Figure 6. Positive ion FAB mass spectra of glycerol. The first mass spectrum was taken 60 min after sample introduction (spectrum 60); spectra 65 and 67 were taken at 7 min after introduction. Spectrum 120 shows the FAB mass spectrum of a target on which glycerol had been deposited and allowed to dry completely. The higher mass portion of the spectrum is magnified by a factor of 20.

diglycerol ether. The ion current representing the sodium ions is usually small in the FAB mass spectra of the system discussed here, but the relative intensity of the Na^+ peak increases in the long time evaporation experiments because the solution becomes more concentrated in contaminants that desorb more slowly. In Figure 6, spectrum 120 shows the result when glycerol was allowed to dry on the probe tip prior to analysis. The major ions in the mass spectrum are m/z 52 and 56 representing chromium and iron ions from the stainless steel and sodium and potassium ions at m/z 23 and 39. The glycerol is evaporated so there is no ion current at m/z 31, 45, 57, and 75. The ion at m/z 189 still can be seen when the environment is presumably not protonating, suggesting that the ion is a sodium adduct rather than a protonated sodium salt. The fact that this ion is still present when the glycerol has been evaporated also verifies that the compound from which this ion is formed is present originally in the glycerol.

Is There a Time Dependence of Analyte-Related Ions that Would be Consistent with the Chemical Ionization Mechanism for Fast-Atom Bombardment?

When Analytes Are Present. Relative intensities for the ions related to the neutral analyte molecules that are dissolved in the glycerol matrix also change with time. This is frequently not appreciated when "the FAB mass spectrum" of a compound is obtained. To demonstrate the behavior that can be observed, consider the cardiac glycoside digoxin (MW 780) [36]. The structure is shown in Figure 7, with spectra obtained at various times during the FAB analysis of a digoxin/glycerol mixture. Early in the analysis, a small peak representing the protonated molecule is present

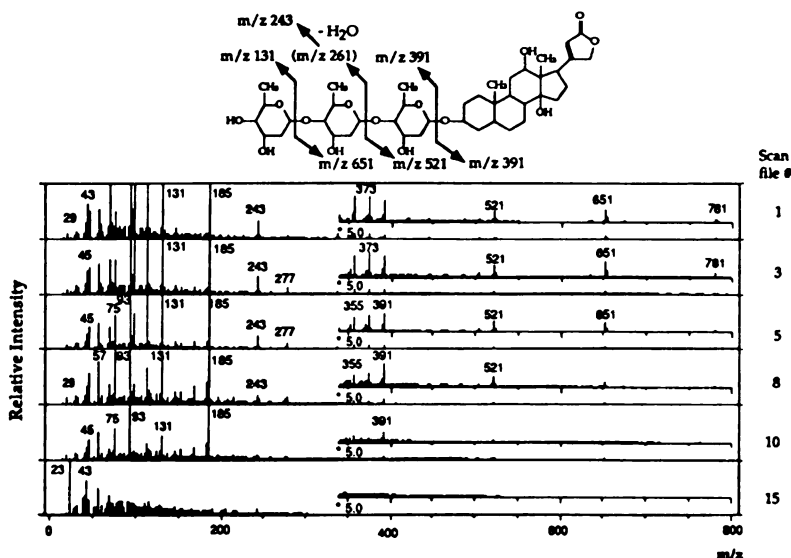
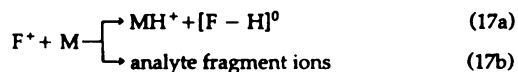


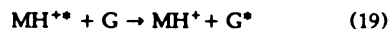
Figure 7. Positive ion FAB mass spectra of 1.5 nmol of digoxin in 0.5- μ L glycerol. The sample was continuously bombarded and one mass spectrum was acquired per minute. The protonated digoxin molecule has a mass-to-charge ratio value of 781. Fragment ions with m/z 651, 521, 391, and 131 are indicated in the figure. The m/z 391 species eliminate multiple water molecules to form the m/z 373 and 355 species. The species with m/z 261 is not observed, but its dehydration product m/z 243 is.

in the positive ion mass spectrum at m/z 781, and several fragment ions are observed throughout the mass range. At later times, fragment ions are observed while the $[M + H]^+$ peak is no longer present. Digoxin is a particularly interesting case. It appears to have some surface activity; thus it is depleted more quickly than compounds chemically more similar to the matrix. Would the time dependence of these analyte-related peaks be consistent with their formation via ion/molecule reactions in an experiment in which the average "pressure" changes in time? We believe this to be so. Early in the experiment when the number of collisions experienced by desorbed ions is large, a substantial fraction of the initially formed reagent ions (F^+) react to protonate glycerol and analyte. The relative abundance of the GH^+ ions is highest at this point, and these may react to protonate desorbed analytes as well. Thus, in addition to the reactions discussed to this point for glycerol, we have the reactions



Proton transfer from GH^+ to M is less exothermic than from F^+ , so the branching ratio between 17a, b may favor 17a, while processes 18a, b may favor 18b. Thus,

as the selvedge is depleted, a larger fraction of reaction products of F^+ are observed—fewer from MH^+ —favoring the formation of analyte fragment ions as opposed to the protonated molecule. Also, early in the experiment when collision frequencies are the highest, the opportunities for collisional deactivation of the protonated molecule would be most likely (reaction 19), again favoring MH^+ formation:



Similar trends are observed in the negative ion spectra of this system, again consistent with this mechanism. Practically, such observations suggest that if sufficient fragmentation is not observed for an analyte in the typical FAB spectrum, the spectrometrist should continue to acquire spectra; later data may provide additional structural information.

Conclusions

Developed here is a glycerol chemical ionization mechanism for the generation of ions from neutral analytes and the glycerol matrix, consistent with previous proposals and observed correlations between analyte responses and their proton affinities. CI and FAB have many aspects in common, such as the matrix (reagent gas):analyte ratios and the formation of protonated molecules rather than molecular ions. We have at-

tempted to refine this model by using time-dependent data in a number of ways, one being to identify possible reagent ions of the glycerol FAB experiment. The time-dependent nature of the species formed in FAB resembles data from an experiment in which ion/molecule reactions are under study—one in which the sample partial pressures are decreasing with time. With candidate reagent ions defined, formation of protonated analyte molecules via proton transfer reactions would be exothermic.

The dynamics of the system are complex, but molecules *are* present in the gas phase. Three processes contribute to the selvedge region and the number of collisions experienced by desorbed ions. At points in space above the target desorption from each unit area of the surface contributes. Second, discrete fast-atom collisions on the surface eject molecules into the gas phase. Third, ions desorb within a set of desorbed molecules. Ions can react with these molecules. Simple calculations suggest that multiple-collision conditions can exist. Thus, this model remains viable, consistent with many aspects of the experiment, and useful for predicting analyte response in many cases.

This does not in any way negate the importance of the interfacial region and chemistry in the short-lived cavities that are formed when a fast atom strikes the liquid surface. This *must* be where multiply charged analytes in solution are converted into singly charged gas phase ions, through recombination processes and reactions with matrix. Ion/molecule reactions must also occur in the interfacial region. However, after ions are formed, they must pass through a region of space in which desorbed molecules are present.

There may, of course, be other explanations for the time dependence of the spectra discussed here. Certainly, as bombardment time increases, one may expect the bulk temperature of the glycerol/analyte target to increase. The temperature increase has been calculated to be small [37]; however, we observe considerable warming of the probe upon bombardment. Although this may be the case, higher temperatures appear to favor more cluster formation, not less [34]. The data available for FAB seem to be consistent with a CI mechanism contributing to the ions observed and may be the dominant mechanism in some instances, depending on analyte, matrix, and the many variables associated with the ion source design.

Clearly, FAB is not currently receiving the attention of newer desorption/ionization techniques today, such as MALDI. We note that some discussions have appeared in the MALDI literature in which ions observed are cited as being formed in the selvedge region "similar to FAB." The nature of gas phase species above the target, electric fields, and ion kinetic energies in the MALDI ion source are clearly much different than in the FAB source. The continued discussion of mechanisms of desorption/ionization will hopefully lead to descriptions that involve all of these methods and the

time-dependent aspects of the spectra that are frequently overlooked.

Acknowledgments

This research was performed in the MSU Mass Spectrometry Facility, which is supported in part by grant no. RR-00480 from the Biotechnology Research Technology Program of the National Center for Research Resources of the NIH. G.S. gratefully acknowledges support from the Soros Foundation.

References

- Ligon, W. V., Jr.; Dorn, S. B. *Int. J. Mass Spectrom. Ion Processes* 1986, 78, 99.
- Sigmund, P. *Phys. Rev.* 1969, 184, 383.
- Benninghoven, A. *Surf. Sci.* 1973, 35, 427.
- Kelly, R. *Radiat. Eff.* 1977, 32, 91.
- Sunner, J. *Org. Mass Spectrom.* 1993, 28, 805.
- Pachuta, S. J.; Cooks, R. G. *Chem. Rev.* 1987, 87, 647.
- Schröder, E.; Münster, H.; Budzikiewicz, H. *Org. Mass Spectrom.* 1986, 21, 707.
- Sunner, J.; Morales, A.; Kebarle, P. *Anal. Chem.* 1987, 59, 1378.
- Sunner, J.; Kulatunga, R.; Kebarle, P. *Anal. Chem.* 1986, 58, 1312.
- Sunner, J.; Kulatunga, R.; Kebarle, P. *Anal. Chem.* 1986, 58, 2009.
- Sunner, J.; Morales, A.; Kebarle, P. *Anal. Chem.* 1988, 60, 98.
- Cooks, R. G.; Busch, K. L. *Int. J. Mass Spectrom. Ion Phys.* 1983, 53, 111.
- Huang, Z.-H.; Shyong, B.-J.; Gage, D. A.; Noon, K. R.; Allison, J. *J. Am. Soc. Mass Spectrom.* 1994, 5, 935.
- Barber, M.; Bordoli, R. S.; Elliott, G. J.; Sedgwick, R. D.; Tyler, A. N. *Anal. Chem.* 1982, 54, 645A.
- Feng, W. Y.; Goldenberg, M.; Lifshitz, C. *J. Am. Soc. Mass Spectrom.* 1994, 5, 695.
- Sunner, J.; Morales, A.; Kebarle, P. *Int. J. Mass Spectrom. Ion Processes* 1988, 86, 169.
- Pachuta, S. J.; Cooks, R. G. *Desorption Mass Spectrometry: Are SIMS and FAB the Same?*; American Chemical Society: Washington, DC, 1985; p 1.
- Heller, S. R.; Milne, G. W. A. *EPA / NIH Mass Spectral Data Base*; U.S. Government Printing Office: Washington, DC, 1978, 56.
- Field, F. H. *J. Phys. Chem.* 1982, 86, 5115.
- Kruger, M. S.; Cook, K. D.; Short, R. T.; Todd, P. J. *Anal. Chem.* 1992, 64, 3052.
- Ligon, W. V., Jr. *Int. J. Mass Spectrom. Ion Processes* 1983, 52, 189.
- Caldwell, K.; Gross, M. L. *J. Am. Soc. Mass Spectrom.* 1994, 5, 72.
- Harrison, A. G. *Chemical Ionization Mass Spectrometry*, 2nd ed.; CRC: Boca Raton, FL, 1992, 125.
- Shukla, A. K.; Stace, A. J. *J. Phys. Chem.* 1988, 92, 2579.
- Lias, S. G.; Bartmess, J. E.; Liebman, J. F.; Holmes, J. L.; Levin, R. D.; Marland, W. G. *J. Phys. Chem. Ref. Data*, 1988, 17, Suppl. 1.
- Rouse, J. C.; Allison, J. *J. Am. Soc. Mass Spectrom.* 1993, 4, 259.
- Rouse, J. C. Ph.D. Thesis, Michigan State University, 1993.
- Campana, J. E.; Freas, R. B. *J. Chem. Soc. Chem. Commun.* 1984, 1414.
- Freas, R. B.; Ross, M. M.; Campana, J. E. *J. Am. Chem. Soc.* 1985, 107, 6195.
- Campana, J. E.; Ross, M. M.; Callahan, J. H. *Int. J. Mass Spectrom. Ion Processes* 1987, 78, 195.

31. Wong, S. S.; Röhlgen, F. W.; Manz, I.; Przybylski, M. *Biomed. Mass Spectrom.* **1985**, *12*, 43.
32. Hirschfelder, J. O.; Curtiss, C. F.; Bird, R. B. *Molecular Theory of Gases and Liquids*; Wiley: New York, 1954; p 1112.
33. Katz, R. N.; Chaudhary, T.; Field, F. H. *Int. J. Mass Spectrom. Ion Processes* **1987**, *78*, 85.
34. Sunner, J.; Morales, A.; Kebarle, P. *Int. J. Mass Spectrom. Ion Processes* **1989**, *87*, 287.
35. Miner, C. S.; Dalton, N. N. *Glycerol*; American Chemical Society: Washington, DC, 1953; p 366.
36. Light, K. J.; Allison, J. *J. Am. Soc. Mass Spectrom.* **1990**, *1*, 455.
37. Todd, P. J.; Groenewold, G. S. *Anal. Chem.* **1986**, *58*, 895.